早稲田大学大学院 環境・エネルギー研究科

博士学位論文

# Optimization and Performance Analysis for Energy Storage System in an Island Power Grid

## 離島グリッドのエネルギー貯蔵システムに関する最適化と特性解析

2019 年 7 月

早稲田大学大学院環境・エネルギー研究科
環境エネルギーネットワーク研究

Nguyen Hong Nhung

# ABSTRACT

With thousands of small islands around the world, the investment of electrical systems for these islands has great potential and important social significance. A typical island power grid consists of the main source of diesel generators (DGs) and renewable energy sources (RES) such as wind generation (WG) or photovoltaic (PV). However, the expensive operating cost of DGs and the uncertainty in the primary energy sources of RES lead to many challenges in the operation of these systems. Therefore, energy storage systems (ESS) becomes to be an important component in the reliable and cost-effective operation of an island power system. With appropriate size, ESS can provide good support to these grids on both economic and technical side.

In this thesis, an optimal sizing problem of ESS employed in an island grid including DGs, WG is investigated. It is easy to see that during the lifetime of the project, the load will grow every year. Thus, accounting for the annual demand growth rate in optimal sizing problem is necessary. Besides, the uncertainty in wind speed is also considered. The optimal sizing problem of ESS is formulated as a two-stage stochastic optimization framework with scenarios tree built based on scenarios of load growth rate and wind speed. An efficient scenario reduction method is also proposed to reduce the computational burden. This algorithm is based on Maximum Entropy principle and K-means clustering approach, which preserves the statistical properties of the original scenarios.

Another issue solved in this thesis is the application of ESS in Fast Frequency Response (FFR) service to ensure the frequency criteria after the sudden loss of a generator. An optimal day-ahead scheduling problem is implemented to minimize the operating cost of the system and take full advantage of the available wind power when the wind power and demand are uncertain. Besides, the ESS is guaranteed to have enough energy for FFR in case of N-1 contingency event. This problem is formulated in terms of two-stage chance-constrained programming with the ON/OFF state and power output of DGs in the first stage and solved using a Modified Sample Average Approximation (MSAA) algorithm, a combination of the traditional Sample Average Approximation (SAA) algorithm and the k-means approach. The effects of the ESS size and its response time is analyzed. Results indicate that the proposed model should perform well under real-world conditions.

The second stage in the day-ahead scheduling issue is solved as a short-term scheduling problem. A multiparametric mixed integer linear programming is used to determine WG's power output and ESS charge/discharge power according to the very short-term forecasting results of wind and demand. Although the power output of DGs is decided in the day-ahead problem, an

adjustment from DGs is still considered to ensure power balance even if the long-term and short-term forecasting results are much different.

This thesis also considers the frequency quality after a small power disturbance. Due to the uncertainty of RES and demand, we cannot ensure the power balance at all times. When a small power imbalance happens, the inertia and primary frequency response start immediately to arrest and restore the frequency. Theoretically, the ESS can provide a part of the frequency regulation; however, if power imbalance is small enough, the ESS response may be not necessary. A probabilistic method is proposed to evaluate the steady-state frequency after a small power disturbance due to forecasting errors of RES or demand. This method can determine the steady-state frequency quickly, and then decide whether the ESS need to adjust the discharging/charging power.

In conclusion, some issues of the island power grid integrated ESS are considered in this thesis for the stable and economic performance of the system including the long-term and short-term operation of the system: Optimal sizing of ESS considering the demand growth rate during the project's lifetime and the optimal scheduling of the island grid taking into account FFR provided from the ESS. Also, this thesis focuses on the behavior of the ESS corresponding to the frequency deviation after a small power imbalance. The solution for each issue is proposed and applied to a small island grid in Vietnam. The results show the effectiveness of these solutions.

# Table of Contents

# List of Tables

# List of Figures

# Acronyms

| | |
|---|---|
| BESS | Battery Energy Storage System |
| CR | Critical Region |
| DPF | Dynamic Power Flow |
| ESS | Energy Storage System |
| FFR | Fast Frequency Response |
| IR | Inertial Response |
| LP | Liner Programming |
| MILP | Mixed Integer Linear Programming |
| mp-LP | Multi-Parametric Liner Programming |
| mp-MILP | Multi-Parametric Mixed Integer Liner Programming |
| MPP | Multi-Parametric Programming |
| MSAA | Modified Sample Average Approximation |
| PDPF | Probabilistic Dynamic Power Flow |
| PFR | Primary Frequency Response |
| PV | Photovoltaic |
| RES | Renewable Energy Source |
| RoCoF | Rate-of-Change-of-Frequency |
| RTUC | Real-time Unit Commitment |
| SAA | Sample Average Approximation |
| SRSM | Stochastic Response Surface Method |
| STUC | Short-term Unit Commitment |
| UC | Unit Commitment |
| WG | Wind Generator |
| WP | Wind Power |

# Chapter 1 Introduction

## 1.1 Background

Most power systems worldwide are large and interconnected systems, so that many studies focus on the economic and technical issues of these grids. With the development of renewable energy sources (RES) such as wind, solar, water sea, etc., there is an increasing interest in island system which is rich in RES. In this thesis, we focus on island systems that exhibit two specific features: small and isolated. They are not connected to and cannot receive support from other systems.

The authors of [1] show that there are more than two thousands of small islands over the world. In the past, these islands had no electricity or were powers by diesel generators (DGs) with expensive operating costs. This prevents the economic, social and educational development of these areas. Fortunately, these areas have great potential for RES [2]. It can be seen from the global map of the potential of wind and solar power in Figure 1.1. The installation of wind generators (WG) and photovoltaics (PV) in these areas has great significance in both economic and social viewpoints.

Although the installation of WG and PV into the remote grids helps to increase the electrification level and reduce the fuel cost of the DGs, the operation of these grids faces several challenges such as power quality, long-term and short-term operation planning, as well as power flow control. The important challenge is that the power balance must be guaranteed at all times. However, the primary energy source of RES is wind speed or solar radiation which is uncertain and dependent on the seasons and locations. This leads to not only RES cannot operate alone but also maintaining the power balance becomes more difficult. No matter what forecasting method is applied to determine these sources, the forecasting error is still available. Consequently, it cannot ensure that the RES output always meets demand. We can see that the higher penetration level of RES leads to a higher possibility of power imbalance.

Another significant issue in a small island system is frequency security. The main source in these systems is DGs which have small inertia and limited operating capability while the inverter-based generators such as WP or PV are less reliable in terms of providing frequency regulation. This makes the system inertia small; consequently, the frequency is more sensitive to any imbalance. Thus, to ensure the system inertia and load following reserve, we should keep a certain number of DG units in operating. This leads to the penetration level of RES is limited, or the RES output is curtailed during off-peak hours; thus, the economic efficiency of RES is decreased.

To overcome these technical issues, an energy storage system (ESS) such as flywheels or batteries is employed to compensate for the fluctuation of RES, consequently, to take full advantage of the RES' available power [3]–[8][9]–[14]. A system including RES, DGs, and ESS as illustrated in Figure 1.2 is a typical configuration for island power systems. In this system, the ESS can play several roles: improvement of system stability, improving the wind energy penetration level, providing primary frequency regulation service and voltage control [15]–[18]. The author of [19], [20] shows that there are many types of ESS technology with specific parameters such as efficiency factor, the discharge time at power rating or response time, etc. These parameters influence the application of ESS. For example, hydrogen systems including fuel cell, water electrolyze and hydrogen storage tanks have a significant long discharge duration. Therefore, they can store the excess power from RES to be utilized when it is beneficial from either an economic perspective [21]–[23]. The disadvantage of hydrogen systems is slow response time; thus, it cannot respond regarding the fluctuation of RES or load. In contrast, battery energy storage (BESS) and flywheels, which have a very small response time (milliseconds to seconds), can change their charge/discharge state very fast and immediately compensate the power imbalance due to the uncertainty in RES and load. Hence, the power system quality including frequency and voltage are ensured [24]–[32]. Besides, BESS can support load leveling or peak shaving to optimize the grid's operation to be economically [16], [30], [33] or energy management in a small system [19]. Although the role of the ESS is based on the technologies and its location in the grid (supply side or demand side), we do not need to consider the ESS location in the case of a small island grid. It can be explained that most of these systems are centralized controlled due to their small size.

## 1.2 Motivation of the Research

There are a large number of small islands that cannot connect to any power system and must use diesel generators to generate electricity at an expensive cost, all over the world. Therefore, the investment and installation of WP and PV in these areas have great potential. However, there are many aspects of this system that need to be considered such as optimal size, control method, frequency and voltage quality, etc.

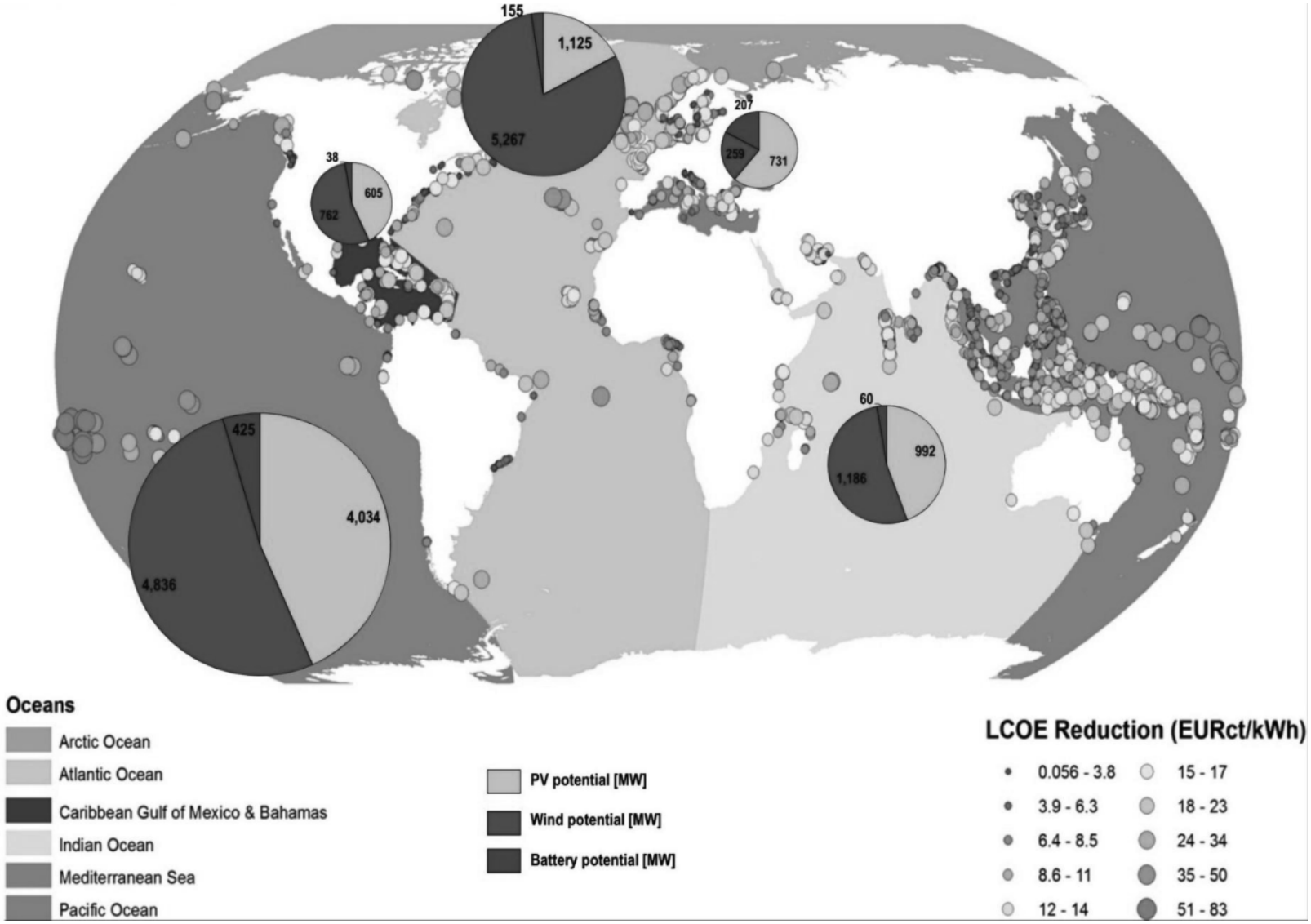


**Figure 1.1** Global map of islands: RES and ESS potential and LOCE reduction [1]

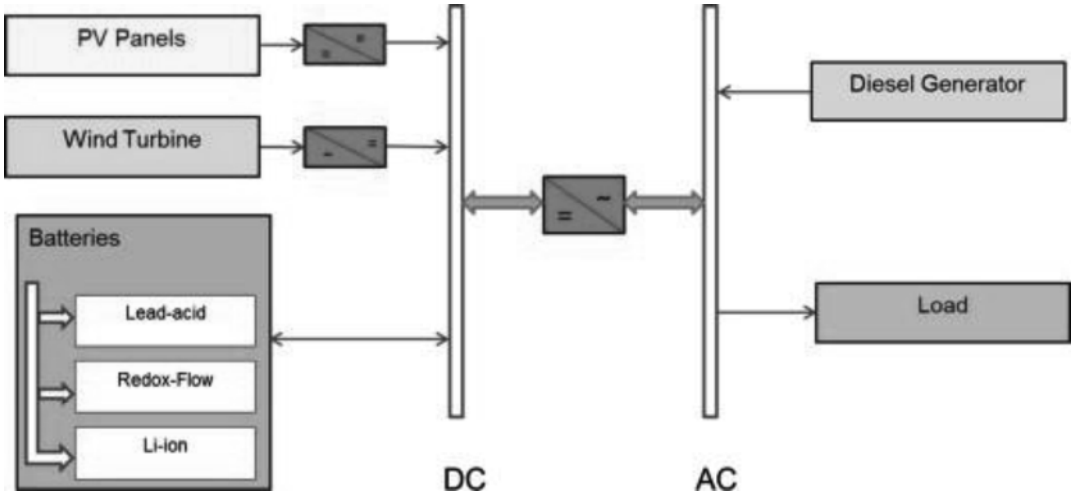


**Figure 1.2** A typical configuration in an island power system [34]

Note that the installation cost of both RES and ESS in these areas is very expensive, so an important issue of this system is to determine the optimal structure of the grid. There has been a considerable amount of research related to this issue with the objective function of minimizing investment costs or maximizing the grid's profit [5], [6], [33], [33], [35]–[39]. The uncertainty in wind and solar is considered in several studies [5], [38]. However, most articles do not consider the fact that the project's lifetime is several years and thus, ignore the annual growth rate of the load. Besides, the annual load growth rate is also an uncertain parameter.

Another problem motivated the researches is to ensure the system frequency quality in these systems. The authors of [40] show that contingencies as a loss of a generator are quite common and cause serious problems in non-interconnected grids. The RoCoF immediately after a contingency in these systems can excess 4Hz/s over the first 500ms due to the small inertia constant of DGs and the high penetration level of RES. Although there are many studies on the frequency control or primary reserve to ensure frequency after a contingency event and the role of ESS in frequency regulation [31], [32], [41]–[46], there is still little attention to small island grids [24], [28], [29], [47]–[49]. Besides, the case studies in these articles have a small RoCoF (0.2-0.5Hz/s) unlike the case of a small island grid.

On the other hand, the frequency quality after a small power disturbance is also an important problem. Due to the uncertainty of RES and demand, it is difficult to ensure the power balance at all times. After a small power imbalance, the inertia primary frequency response immediately to arrest and restore the frequency. Theoretically, the ESS can provide a part of the frequency regulation, however, is power imbalance is small enough, the ESS response may be not necessary.

Therefore, this thesis considers both technical and economic problems in an island power system including DGs, WP, and ESS. There are three main problems considered and solved:

- Optimal sizing of ESS considering the uncertainty in wind speed and annual load growth rate.
- Optimal scheduling of the island system considering FFR provided by ESS. Day-ahead and short-term scheduling problems are implemented.
- A method which can evaluate the system frequency after a small power imbalance and decide whether the ESS must provide the frequency regulation.

## 1.3 Statement of Objectives

The general objective of this thesis is the application of ESS in small island power systems with a high penetration level of RES. The primary goal of ESS in these systems is to compensate for the fluctuation of RES due to their primary energy source; consequently, help increase the energy produced from RES (rather than using curtailment). Besides, the ESS provides FFR as an ancillary service to ensure frequency stability after a significant disturbance such as a sudden loss of a generator. This thesis includes several small problems from choosing the optimal size for the ESS as well as the day-ahead or short-term operation planning considering FFR. Finally, this thesis evaluates the frequency quality and decides the BESS behavior after a small power imbalance in real-time operation.

Partial objectives of the thesis are also listed below.

- Investigate the optimization model to choose the optimal size of ESS. Determine uncertain parameters that effect on ESS sizing.
- Investigate a scenarios reduction method to increase calculation efficiency.
- Investigate the role of ESS in frequency stability service. Theoretical analysis of FFR. Review the application of FFR worldwide.
- Investigate the set of constraints which present not only the unit commitment and the power output of the main sources before the contingency but also the ESS behavior to make sure the frequency criteria after a significant disturbance, in order to apply to a day-ahead or short-term scheduling problem.
- Investigate a method which can evaluate the system frequency and decide the behavior of the ESS after a small power imbalance.

## 1.4 The Thesis Outline

Beyond the introduction, this thesis is organized in five chapters excluding **Chapter 1 Introduction**. The content of this thesis is written based on the author's publication shown in section 1.6.

**Chapter 2 Optimal Selection of Energy Storage System for the Small Island Power System**

This chapter presents the optimal sizing of ESS in a remote island power system. In this problem, the uncertainty in wind speed and load growth factor are considered. Section 2.2 details the optimization model for selecting the size of ESS. This model is formulated based on scenarios of wind speed and load growth rate each year. In addition, reserve requirements, as well as the minimum number of synchronous generators to be operated, are taken into account. Section 2.3 presents a scenario reduction approach that can easily adjust the number of scenarios after reducing while retaining statistical properties of uncertain parameters. Section 2.4 applies this approach to determine the optimal sizing of ESS in a realistic isolated island power system.

**Chapter 3 Day-Ahead Optimal Operation of the Small Island Power System Considering Fast Frequency Response**

In this chapter, the ESS, which is employed to keep power balance and take advantage of RES and can be determined by the optimization model in Chapter 2 , is considered to provide fast frequency response (FFR) to ensure the frequency criteria in the case of large frequency disturbances, such as loss of a generator. An optimal day-ahead UC problem is implemented to minimize the operating cost of the system, maximize the utilization of the available wind power, consider the uncertainty of the wind power and demand, and ensure that the ESS always has enough energy to provide FFR. In section 3.2, the fundamental of FFR is presented. A new constraint is proposed to show the relationship between the number of DGs in operation, the power output of each DG, the ESS charge/discharge power in each hour and the ESS' response time to ensure the frequency nadir criteria. In this constraint, the frequency dynamic is approximated using a first-order representation. The day-ahead optimal scheduling problem is formulated in terms of two-stage chance-constrained programming. Section 3.3 presents a Modified Sample Average Approximation (MSAA) algorithm to solve the UC model in section 3.2. The proposed method is tested with a realistic island power system in section 3.4. The effects of the ESS size and its response time is analyzed. Results indicate that the proposed model should perform well under real-world conditions.

**Chapter 4 Short-term Optimal Operation of the Small Island Power System Using a Multi-Parametric Programming Framework**

This chapter presents a short-term scheduling model, which solve the second stage problem of the day-ahead UC model presented in Chapter 3 . In this problem, the role of the ESS in FFR is still considered. The formulation of this problem is presented in section 4.2.2. Section 4.2.3 presents the theory of multiparametric mixed integer linear programming which is applied to solve this problem. The ESS charge/discharge power, the WG's power output, and DGs'

adjustment are determined as functions of uncertain input parameters. The impact of short-term forecasting errors is analyzed in section 4.3.

**Chapter 5 Probabilistic Dynamic Power Flow: A Method to Evaluate the Frequency Disturbance Caused by Forecast Errors and Decide the ESS Behavior**

This chapter proposes a probabilistic method to evaluate the steady-state frequency after a small power disturbance due to forecasting errors of RES or demand. Based on this probabilistic approach, we propose a method to determine the steady-state frequency quickly and then decide the ESS behavior. In section 5.2.1, a dynamic power flow model is presented while section 5.2.2 presents Stochastic Response Surface Method which can approximate the relationship between the output data and the input data by a Hermite polynomial chaos expansion. Section 5.2.3 presents the probabilistic dynamic power flow model, which is the combination of dynamic power flow and Stochastic Response Surface Method, and apply this model to evaluate the steady-state frequency for the 39-bus New England system in section 5.3.

**Chapter 6 Conclusions**

This chapter summarizes the main achievements of this thesis.

## 1.5 Main Contributions

The main contributions of this thesis are:

- The stochastic optimization problem to determine the optimal sizing of the ESS is proposed. This model takes into account the uncertain nature of wind speed and load growth rate**.** The effect of the project's length on the optimal sizing of ESS is analysed.
- The scenarios reduction algorithm based on Maximum Entropy principle and K-means clustering approach is proposed. This method preserves the statistical properties of the original scenarios. The reliability of the optimization model and the scenario reduction method is analysed with a varying number of reduced scenarios.
- A frequency stability-constrained UC model is proposed. The ESS, which is employed to keep power balance and take advantage of wind power, is considered to provide fast frequency response (FFR) in large frequency disturbances, such as loss of a generator. A new constraint related the FFR is presented, in which the frequency dynamic is approximated using a first-order representation.
- The proposed UC model is based on a two-stage stochastic programming framework which is suitable for the day-ahead planning of power systems with uncertain sources.

Chance constraints are also used in the proposed formulation to allow a certain risk level in the day-ahead scheduling.

- The Modified Sample Average Approximation (MSAA) method is presented and applied to solve the proposed optimization problem. The combination of SAA and k-means clustering approach is proven to be more effective than the original SAA approach.
- A short-term scheduling model is presented to determine the power output of WG and ESS as a function of uncertain parameters while the role of the ESS in FFR is also considered. This model ensures that the power balance in case the short-term forecast results are different from the long-term forecast value while still ensures that DGs adjustment is as small as possible.
- A probabilistic method is proposed to evaluate the system frequency and decide the behavior of the ESS after a small power imbalance.

## 1.6 Publications

### 1.6.1 Journal Articles

1. **N. Nguyen Hong** and Y. Nakanishi, "Optimal Scheduling of an Isolated Wind–Diesel–Energy Storage System Considering Fast Frequency Response and Forecast Error," *Energies*, 2019.

2. **N. Nguyen-Hong**, H. Nguyen-Duc, and Y. Nakanishi, "Optimal Sizing of Energy Storage Devices in Isolated Wind-Diesel Systems Considering Load Growth Uncertainty," *IEEE Trans. Ind. Appl.*, vol. 54, no. 3, pp. 1983–1991, May 2018.

### 1.6.2 Conference Papers/Oral Presentations

3. **N. Nguyen-Hong** and Y. Nakanishi, "Optimal Scheduling of an Isolated Wind-Diesel-Battery System considering Forecast Error and Frequency Response," in *2018 7th International Conference on Renewable Energy Research and Applications (ICRERA)*, 2018, pp. 464–468.

4. **N. Nguyen-Hong** and Y. Nakanishi, "Frequency-Constrained Unit Commitment Considering Battery Storage System and Forecast Error," in *2018 IEEE Innovative Smart Grid Technologies - Asia (ISGT Asia)*, 2018, pp. 1171–1176.

5. **N. Nguyen-Hong** and Y. Nakanishi, "Stochastic dynamic power flow analysis based on stochastic response surfarce method and ARMA-GARCH model," in *2017 IEEE Power & Energy Society Innovative Smart Grid Technologies Conference (ISGT)*, 2017, pp. 1–5.

6. **N. Nguyen-Hong** and H. Nguyen-Duc, "Optimal sizing of energy storage devices in wind-diesel systems considering load growth uncertainty," in *2016 IEEE International Conference on Sustainable Energy Technologies (ICSET)*, 2016, pp. 54–59.

7. H. Nguyen-Duc and **N. Nguyen-Hong**, "Chance Constrained Unit Commitment – A Comparative Study between Stochastic and Robust Optimization Approaches," in *The Vietnam – Japan Science and Technology Symposium 2019 (VJST2019)*.

8. **N. Nguyen-Hong** and Y. Nakanishi, "Unit Commitment considering Frequency Dynamic Constraint and Wind Power Forecast Uncertainties," in *IEEJ P&ES-IEEE PES Thailand Joint Symposium on Advanced Technology in Power Systems, Krabi, Thailand*, 2018.

# Chapter 2 Optimal Selection of Energy Storage System for the Small Island Power System

## 2.1 Introduction

In small island power systems, the main source is DGs which have a high cost of fuel. Thus, the development of wind and solar power generation is expected to replace DGs and reduce the system's operating cost. However, the operation of the hybrid DG-WG (or DG-PV) system faces several technical challenges. It can be seen that DGs have small inertia and limited operating capability while RES' inertia constants are almost zero. Thus, power system operators of island grids must ensure that a minimum number of diesel units online is online to guarantee frequency stability. They also keep a certain amount of spinning reserve to compensate for the sudden outage of any generator or load variations. This leads to not only the installation capacity of RES is limited, but also the power output of RES can be curtailed during off-peak hours. So, to take advantage of RES and reduce the system's operating cost, the installation of ESS is necessary.

In this chapter, we focus on determining the optimal sizing of the ESS in an island power system including DGs and WGs. The ESS is used to maximize utilize of wind power and provide a part of the spinning reserve, which in turn is expected to reduce DGs operating costs.

### 2.1.1 Literature review

In the literature, there are many studies on the role of ESS in the isolated grid. One interesting object is determining the required ESS capacity and its inverter rating [7], [38], [50], [51]. The objective function is minimizing the project life cycle cost or maximizing the project's profit [5], [37], [52], [53]. In several studies, the optimal sizing problem is formulated as two-stage stochastic optimization [38], [50] considering uncertain parameters such as wind power or demand. The first-stage variables that common to all scenarios are the ESS storage capacity ($E_{ESS}$) and its inverter rating ($P_{ESS}$). The second-stage variables include the active power of wind and diesel generators, charge/discharge power of ESS, the energy level of ESS, on/off state of generating units. These variables will take on different values in each scenario [38], [50]. A common method used to solve this problem is Stochastic Programming, in which each uncertain parameter is represented by discretized scenarios. The scenario trees, which is a combination of scenarios of all parameters, can be generated by using a Monte-Carlo based approach, as in [54], [55].

One important issue in an expansion problem is to ensure that the power system can operate stability for a long time. This means that the supply must match the demand at all times. However, the project lifetime of an ESS installation is usually 5 to 10 years, and during this planning horizon, the load can increase (or decrease) with an uncertain growth rate each year. Although there are some studies considering the load growth rate, most of them assume that the load growth rate is fixed (8% to 10%). As with other long-term capacity expansion planning studies, the load growth rate should be considered as an uncertain parameter.

As presented above, the stochastic optimization model is a common method to solve the optimal sizing problem considering uncertain parameters. In this method, each uncertain parameter is described as a finite number of scenarios. It is easy to see that the total number of scenarios to be considered for a realistic system is usually very large; in consequence, solving a stochastic capacity expansion problem becomes more difficult. Thus, we need an approach to reduce the number of scenarios. In the literature, several scenarios reduction algorithms have been developed [56], [57]. In these studies, the scenario tree is reduced based on minimizing the distance between the reduced and the original scenarios paths. This method is useful and has been used extensively in the literature. However, a required long computing time leads to this method is less useful when the number of stages of scenario tree increase. Another common method is using K-means clustering approach [58]. This method separates scenarios into groups and replaces each group by one new scenario having the smallest Euclidean distance to other scenarios in groups. The probability of the representative scenario is equal to the sum of all scenarios' probabilities in the group. This method is very fast, but it does not keep the statistical properties of the original scenarios. In our previous study [59], we used a simple method to reduce scenarios. Similar to the K-means clustering approach, this approach does not retain the statistical characteristics of the dataset. Note that the objective function of a stochastic optimization model is the expected value of the cost or the profit. Skipping the statistical characteristics when reducing the scenario tree will lead to the results less accurate.

To overcome the drawback of the above methods, the moment-matching approach presented in [60] reproduces accurately the first few moments of the original scenarios' distribution function. Therefore, the statistical properties of scenarios can be maintained. The authors of [61] also presented a method that is a combination of K-means and LP moment-matching approach. This method can overcome the drawback of K-means method but using LP moment-matching still takes considerable CPU time.

### 2.1.2 Research Objectives and Contribution

The study in this chapter proposes a two-stage stochastic optimization model to define the optimal sizing of ESS for an island power system including DGs and WGs. This ESS is used to take advantage of wind power and provide a part of the operating reserve. We identify these contributions of this work:

- The proposed model considers the growth of electricity consumption during the project's lifetime. The load growth rate and wind speed are assumed as uncertain parameters with finite scenarios.
- The scenarios reduction algorithm based on Maximum Entropy principle and K-means clustering approach is presented. This approach reduces the size of the scenarios tree while still preserves the statistical properties of the original scenarios. The reliability of the optimization model and the scenario reduction method is analyzed with varying number of reduced scenarios.

## 2.2 Proposed Optimization Framework

### 2.2.1 Nomenclature

**Indices and Sets**

$i \in I$ Diesel generators.

$s \in S$ The two-stage problem's scenarios.

$t \in T$ Time intervals (of variable duration).

$w \in W$ Wind generators.

**Constants**

$C_{diesel}$ Operation cost of diesel generator ($/kWh).

$C_{wind}$ Operation cost of wind generator ($/kWh).

$C_e$ Price of electrical energy ($/kWh).

$K_E$ Fixed cost of energy storage ($/kWh) .

$K_P$ Fixed cost of the inverter of the energy storage ($/kW).

$MRN$ Minimum required number of diesel generator online.

$\eta$ Charging/discharging efficiency of ESS

$R$ The required operating reserve.

$P_{load,s}^{t}$ Hourly load in scenario *s* at time *t* (kW).

$\pi_{s}^{t}$ Probability of the scenario *s* at time *t*.

**Variables**

$E_{ESS}$ Energy storage system's capacity (kWh).

$P_{ESS}$ Energy storage system's inverter rating (k ).

$P_{diesel,i,s}^{t}$ Power output of diesel generator *i* in scenario *s* at time *t* (kW).

$P_{wind,w,s}^{t}$ Power output of wind generator *w* in scenario *s* at time *t* (kW).

$P_{discharge,s}^{t}$ Discharging power of storage system in scenario *s* at time *t* (kW).

$P_{charge,s}^{t}$ Charging power of storage system in scenario *s* at time *t* (kW).

$u_{i,s}^{t}$ ON/OFF state of diesel generator *i* at time t, (binary variables).

$u_{w,s}^{t}$ ON/OFF state of wind generator *w* at time t, (binary variables).

$u_{ESS,s}^{t}$ Binary variable which equals to 1 if the storage system is being charged.

$e_{ESS,s}^{t}$ Energy stored in the storage system at time *t* in scenario *s* (kWh).

$e_{ESS,s}^{t=0}$ Initial energy stored in the storage system at $t = 0$, scenario *s* (kWh).

$e_{ESS,s}^{t=24}$ Energy stored in the storage system at the end of day ($t = 24$), scenario *s* (kWh).

### 2.2.2 Mathematical Formulation

This study analyzes the ESS sizing problem to minimize the total cost of the project including both operating cost and fixed cost in the island power system. The corresponding optimization framework is shown in Figure 2.1. In this problem, the ESS capacity and inverter rating are the first-stage variables while the dispatch schedule of the generators and the ESS are the second-stage variables which are dependent of each scenario of load demand and wind speed. The second-stage variables are indexed by time and by scenario.

*1. Objective Function*

The objective function is the expected value of the cost over the project lifetime, which is written as follow.

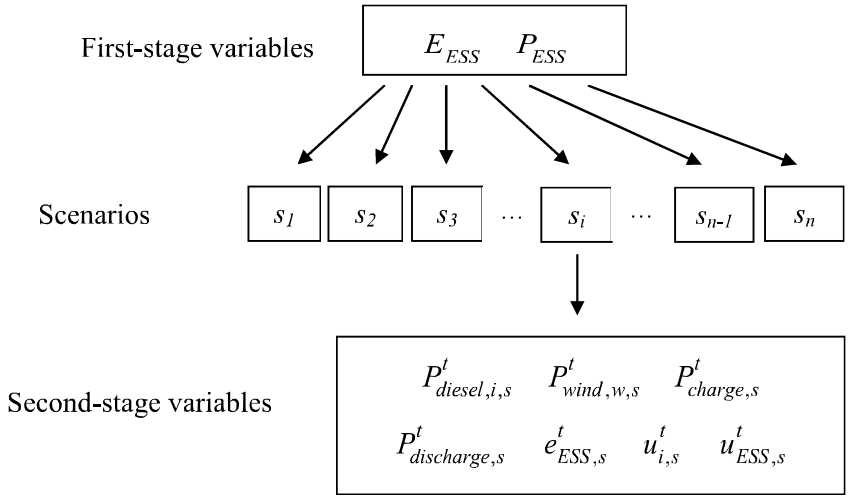


**Figure 2.1** Two-stage stochastic optimization of the energy storage capacity.

$$Minimize \sum_s \sum_t \pi_s^t \Bigg( (C_{diesel} - C_e) \sum_i P^t_{diesel,i,s} + (C_{wind} - C_e) \sum_w P^t_{wind,w,s} - C_e \sum_w P^t_{discharge,s} \Bigg) + K_E E_{ESS} + K_P P_{ESS} \tag{2-1}$$

*2. Constraints*

- Active Power Balance Constraint

The total active power output from the DGs, the WGs and the ESS must equal the total load in any scenario s at any time t.

$$\sum_i P^t_{diesel,i,s} + \sum_w P^t_{wind,w,s} + P^t_{discharge,s} = P^t_{load,s} + P^t_{charge,s} \tag{2-2}$$

- Operation Constraint of the DGs

The power output of each DG is limited by the following constraints:

$$P_{imin} u^t_{i,s} \le P^t_{diesel,i,s} \le P_{imax} u^t_{i,s} \tag{2-3}$$

The binary variables $u^t_{i,s}$ are used in (2-3) to make sure that that each DG output is zero if it is in shut down mode.

- Operation Constraint of the WGs

In this study, the WGs are assumed as the type 3 wind turbines which can regulate its power output by controlling the pitch angle. So that, the power output of WG can vary from $P_{wmin}$ to $P_{wmax}$.

$$P_{wmin}u_{w,s}^{t} \le P_{wind,w,s}^{t} \le P_{wmax}u_{w,s}^{t} \tag{2-4}$$

- Storage Constraint
  - The maximum charge / discharge power of energy storage: The ESS charging and discharging power must be smaller than the actual power rating of the storage device:

$$\begin{cases} 0 \le P_{charge,s}^{t} \le P_{ESS} \\ 0 \le P_{discharge,s}^{t} \le P_{ESS} \end{cases} \tag{2-5}$$

  - Charge/Discharge status constraint: $u_{ESS}^{t}$ is binary variable describing the charge/discharge situation of the ESS. The ESS can only in one state: charging or discharging state at all period *t*.

$$\begin{cases} P_{charge,s}^{t} - u_{ESS}^{t}M \le 0 \\ P_{discharge,s}^{t} + u_{ESS}^{t}M \le M \end{cases} \tag{2-6}$$

where *M* is a sufficiently large constant.

  - Energy capacity constraint: At all times, the state of charge of the battery storage $e_{ESS,s}^{t}$ should be smaller than its rated capacity:

$$0 \le e_{ESS,s}^{t} \le E_{ESS} \tag{2-7}$$

  - The process of charging/ discharging of the storage device: With an efficiency of $\eta$ for the charging and discharging process, we have the following constraint:

$$e_{ESS,s}^{t} = e_{ESS,s}^{t-1} + \eta P_{charge,s}^{t} - P_{discharge,s}^{t}/\eta \tag{2-8}$$

  - Energy daily balance: In each scenario, the energy stored in the ESS should be settled within one day.

$$e_{ESS,s}^{t=0} = e_{ESS,s}^{t=24} \tag{2-9}$$

- Operating reserve constraint

In this study, it is assumed that both the DGs and the ESS can take part in the operating reserve. Hence the following constraint can be imposed:

$$\sum_i (u_{i,s}^{t}P_{imax} - P_{diesel,i,s}^{t}) + P_{ESS} - (P_{discharge,s}^{t} - P_{charge,s}^{t}) \ge R \tag{2-10}$$

- Minimum required number of diesel generator online

As mentioned in section 2.1, DGs play an important role in the system's inertia which helps improve frequency stability. Hence, the system operators must keep a certain number of DGs online to guarantee the system inertia level:

$$\sum_i u_{i,s}^{t} \ge MRN \tag{2-11}$$

## 2.3 Scenarios Tree and Scenarios Reduction Method

In power system planning studies, the yearly load demand is considered an uncertain variable. Assume that there are $k$ possibilities of demand growth factor each year, and with an $m$-year project, we will have $k^{m-1}$ scenarios of the 24-hours load in the last year. It is easy to see that throughout the project duration, there is a large number of load scenarios, as shown in Figure 2.2.

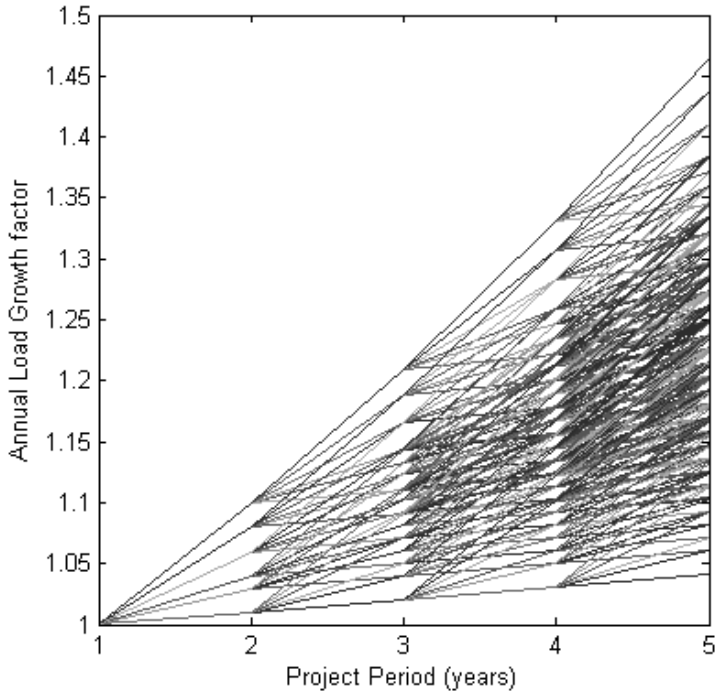


**Figure 2.2** Possibility tree of load scenarios with $k$ = 6 and $m$ = 5.

In this section, we propose a scenarios reduction approach that is a combination of K-means clustering approach and Maximum Entropy principle. Instead of generating and reducing scenario trees at the same time, the main ideas of our new algorithm are predetermining the outcomes in each stage of scenarios tree. In this study, they are $k^{m-1}$ scenarios of the load in the $m^{th}$ year. In the next step, their distribution function is approximated by a new finite set of scenarios.

The K-means clustering approach is used to obtain a new set of scenario nodes while the Maximum Entropy principle is applied to determine the probabilities of the new scenarios. The Maximum Entropy principle is a powerful approach for approximating density distribution function. Similar to the moment-matching approach presented in [60], the Maximum Entropy principle can keep the statistical properties of the original scenarios but is more computationally efficient [62], [63]. The details of Maximum Entropy principle to match moments were presented in [64], [65].

### 2.3.1 Discrete Approximation of Probability Distribution by Maximum Entropy Method

Suppose that we want to approximate a probability distribution function $f: \mathbb{R}^K \to \mathbb{R}$ by probabilities $\{p(x)|x \in D\}$ on a $N$-point finite discrete set $D = \{x_n|n = 1, \dots, N\} \subset \mathbb{R}^K$. The moments of true distribution need to be matched by the moments of approximated distribution [64].

Let $M(x)$: $\mathbb{R}^K \to \mathbb{R}^L$ be moments measured at each point in discrete set *D*, where *L* is number of elements of vector *M*(x). Let $\widehat{M} = \int M(x)f(x)dx$ be vector of the original distribution's moment. The probabilities $\{p(x)|x \in D\}$can be obtained by maximizing the Shannon Entropy:

$$Maximize - \sum_{x \in D} p(x) \log p(x) \tag{2-12}$$

Given the prior approximation $p_0(x)$, (2-12) can be interpreted as minimizing the Kullback-Leibler information, as follows:

$$Minimize \sum_{x \in D} p(x) \log \frac{p(x)}{p_0(x)} \tag{2-13}$$

S.t: $\sum_{x \in D} p(x)M(x) = \widehat{M}$

$\sum_{x \in D} p(x) = 1$

$p(x) \geq 0$

If the density function $f$ is unknown, the prior probabilities are set as a uniform distribution: $p_0(x) = 1/N$. If the density function *f* is known, we choose $\{ p_0(x) = f(x)|x \in D\}$.

The optimization problem (2-13) has a solution given by the following equation [64].

$$p(x) = \frac{p_0(x) \exp(\lambda^T M(x))}{\sum_{x \in D} p_0(x) \exp(\lambda^T M(x))} \tag{2-14}$$

$$\text{where: } \lambda = \arg\min\left(-\lambda^T \widehat{M} + \log\left(\sum_{x \in D} p_0(x) \exp(\lambda^T M(x))\right)\right) \tag{2-15}$$

and $\lambda$ is the Lagrange multipliers of the moment constraints $\sum_{x \in D} p(x)M(x) = \widehat{M}$

### 2.3.2 Proposed Scenarios Reduction Algorithm

For an m-year project, the proposed scenario reduction algorithm, which combines K-means clustering approach and Maximum Entropy principle, is described by the following steps. Besides, Figure 2.3 also shows this algorithm in detail.

STEP 1: For j = 1, 2, …, m

- Calculate the $k^{j-1}$ outcomes in the $j^{th}$ year.
- Choose the number of cluster $C_j$ each year. Group the outcomes in the $j^{th}$ year by the K-means method. The $k^{j-1}$ scenarios are replaced by centers of $C_j$ clusters.
- Choose the prior probabilities $p_0(x)$; compute the probabilities of $C_j$ new scenarios by using (2-14).

STEP 2: Collect the scenarios obtained in step 1 over the project's period. The final total number of scenarios can be adjusted by choosing the value of $C_j$.

The accuracy of this reduction method is estimated based on the total error $TE$ between the actual moments and those of the reduced scenarios:

$$TE = \sum_m \left\| \sum_{x \in D} p(x) M(x) - \widehat{M} \right\|_2 \quad (2\text{-}16)$$

In many decision problems, it is usually sufficient to create the reduced set of scenario which matches the first four moments [61].

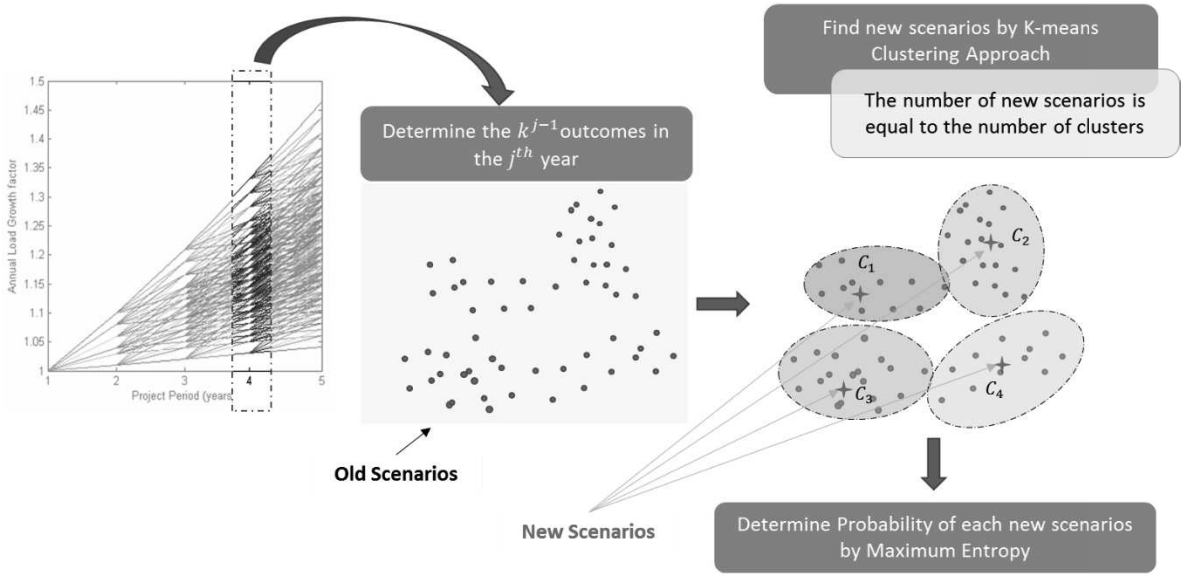


**Figure 2.3** Description of the proposed scenarios reduction algorithm

## 2.4 Numerical Examples

### 2.4.1 Study System and scenario reduction result

The data for this study is based on the actual power system in Phu Quy Island, Binh Thuan province, Vietnam. The medium voltage network has been installed since 1998, with six 500kW diesel generators. From 2016 until now, the electricity price for Phu Quy island residents is 8 US cent per kWh, which is the same as the electricity price on the mainland. Since the electricity is produced from diesel generators with relatively high fuel price, the installation of WGs and ESS is

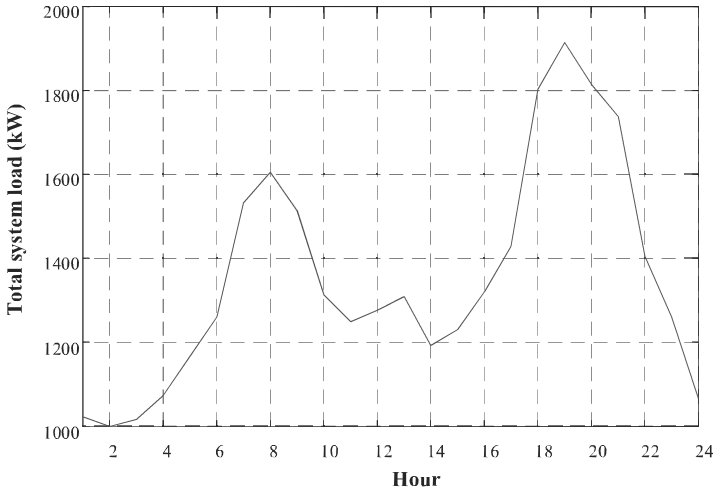


**Figure 2.4** Daily Load Profile of the Phu Quy island (2015).

**Table 2.1** Wind speed distribution data

| **Wind speed (m/s)** | 14 | 12 | 5.2 | 7 | 9 | 8 | 10 |
|---|---|---|---|---|---|---|---|
| **Probability (%)** | 16 | 19 | 25 | 10 | 10 | 10 | 10 |

**Table 2.2** Annual load growth factor

| **Load Growth factor** | 1.01 | 1.03 | 1.04 | 1.06 | 1.08 | 1.1 |
|---|---|---|---|---|---|---|
| **Probability** | 0.2 | 0.2 | 0.3 | 0.1 | 0.1 | 0.1 |

expected to reduce the operating cost. The typical daily load of this island and the wind speed profiles are shown in Figure 2.4 and Table 2.1, respectively. At present, there are two wind generators with a rated power of 1.8 MW. Since the ESS sizing study was carried out after the wind generators had been installed in 2012, the cost of installing wind generators was not included in the objective function (2-1). The cost data of ESS are taken from [50].

Each hourly scenario of the optimization problem is a combination of a load value and a wind speed value which is converted to an hourly wind power limit. Assume that there are possible 6 scenarios of load growth for each year with different probabilities (Table 2.2). This means that we have 1555 load scenarios for a 5-year project. After using the scenario reduction method in section 2.3, the total scenarios over five years can be reduced to 10 to 49 scenarios, depending on the value of $C_j$. The first four moments are exactly matched. The obtained scenarios after reducing process are shown in Figure 2.5 while Figure 2.6 presents the total error in moments over the project's duration. The error is greatest when there are 10 scenarios, but only approximately 0.8%.

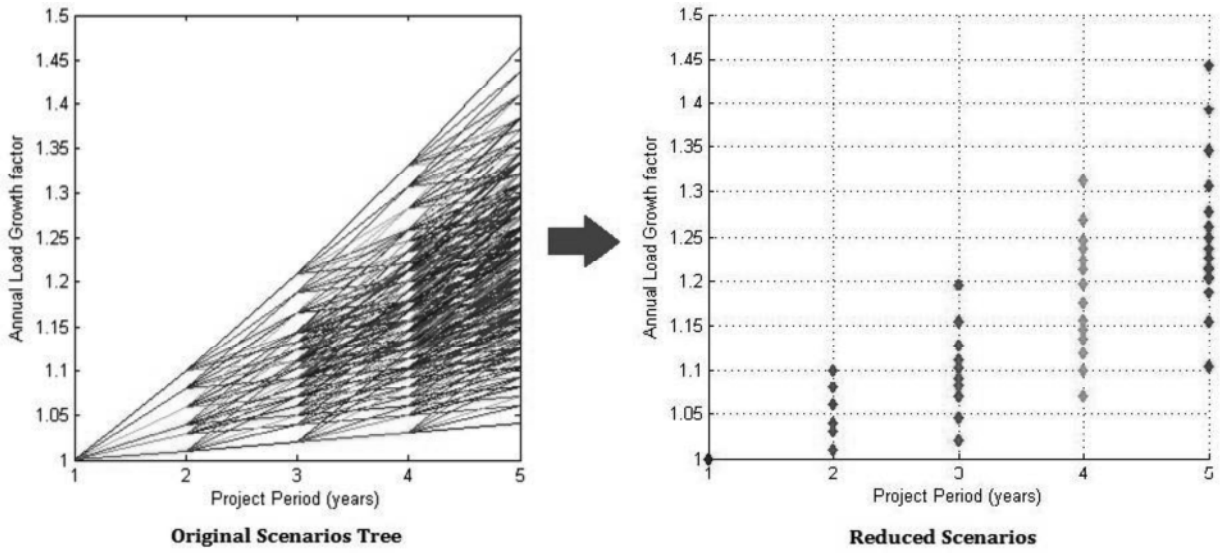


**Figure 2.5** Scenarios reduction result: 49 scenarios over five years.

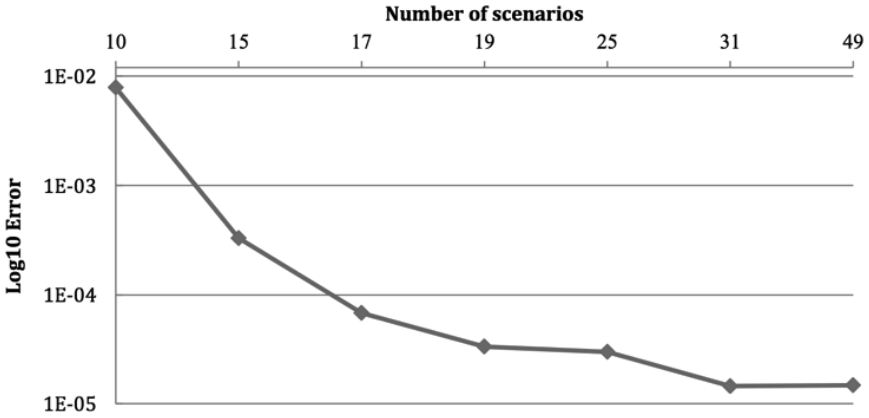


**Figure 2.6** Total moment errors of the reduced load scenarios in five years.

With 17 scenarios of load, 7 scenarios of wind speed (Table 2.1) and 24 values for hourly load demand, the total hourly scenarios are 2520. The corresponding optimization problem has 71419 variables, of which 19992 are binaries, 8681 equality constraints, and 87121 inequality constraints. The optimization problem is solved using CPLEX version 12.6. The CPU time to solve this MILP problem on a 2.6GHz Intel® Core ™ i5-3320M with 4GB RAM is roughly 25 minutes.

### 2.4.2 Optimization result

With the input data in section 2.4.1 and a project duration of five years, the optimal values for ESS capacity and inverter rating are 1808 kWh and 1719 KW, respectively. Figure 2.7 shows box plots of a typical daily commitment schedule for diesel generators, ESS and wind turbines in the fifth year. As discussed in section 2.2.2, a minimum of two diesel units should be online to provide the system inertia. Therefore, two diesel generators are run at minimum load ($2\times170$kW) at all times. With the ESS, wind turbines output can at times exceed the total load demand. The

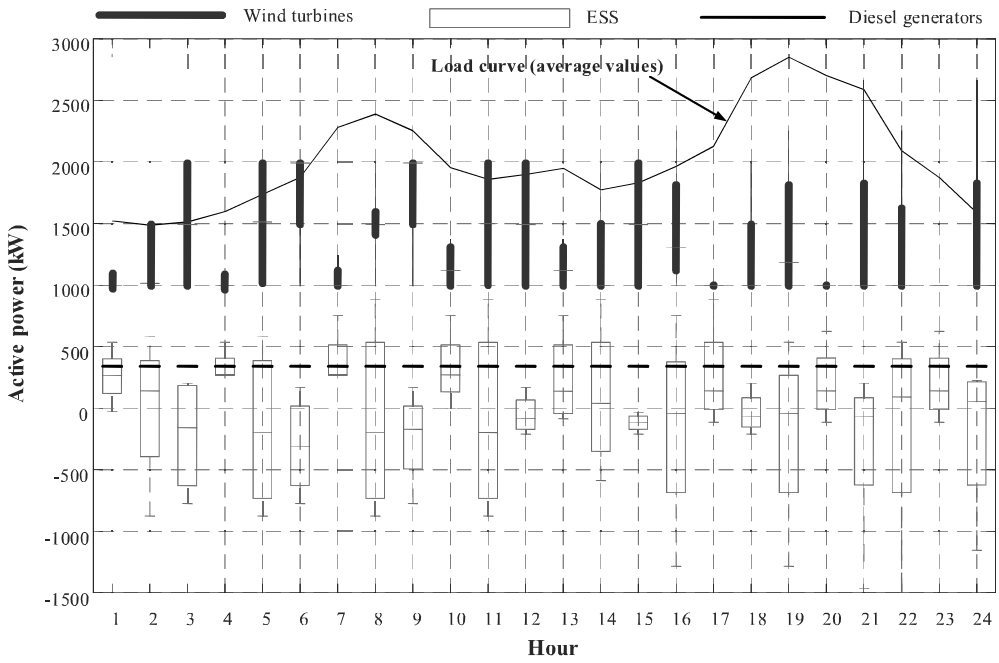


**Figure 2.7** Box plot of power outputs from wind turbines, ESS and diesel generators. A negative value of ESS means it is in charging mode.

**Table 2.3** Optimization results with a 5-year project, MRN=2, different wind turbine power ratings

| **Wind turbines** | 2×1.8MW (actual value) | 3×1MW | 4×700kW |
|---|---|---|---|
| **ESS capacity (kWh)** | 1808 | 1680 | 1665 |
| **Inverter rating (kW)** | 1719 | 839 | 832 |
| **Expected value of project cost (x $10^6$ USD)** | 11.14 | 7.06 | 6.21 |

ESS has a large variation of output power but tends to be in deep charging states at low load hours. Although the optimal inverter rating is 1719 kW, the ESS only occasionally operates at this output level (only when low load occurs at the same time with very high wind speed).

It should be noted that in this project, the problem of optimal ESS sizing is formulated after the wind turbines and diesel generators have already been installed. If the capacities of wind turbines and ESS are jointly optimized in a single planning study as in [38], [51], we can achieve a much better economic performance. As can be seen in Table 2.3, smaller wind turbines with lower minimum power output yield much lower cost, since they can be dispatched more flexible, which allows more efficient use of wind energy and requires smaller ESS capacity.

Besides the load growth factor and the wind speed which are included in the optimization problem as uncertain variables, the effects of other parameters are also considered in this work. In the following, we present the sensitivity analysis with respect to the project duration, the minimum number of diesel unit online, and the required operating reserve.

*1. Impact of the project duration*

In all cases, both ESS capacity and its inverter's rating increase when the project period is extended (Figure 2.8). Note that the installed generation capacity is much larger than the peak load at the first year. Therefore, if the project duration is short, there is not much difference in the optimized values for ESS capacity, because the available wind energy could not be fully used. When the project duration is extended beyond five years, the ESS capacity and its inverter power increase, which means more energy can be produced from wind power to serve the load demand in the later years, with the help of the energy storage device.

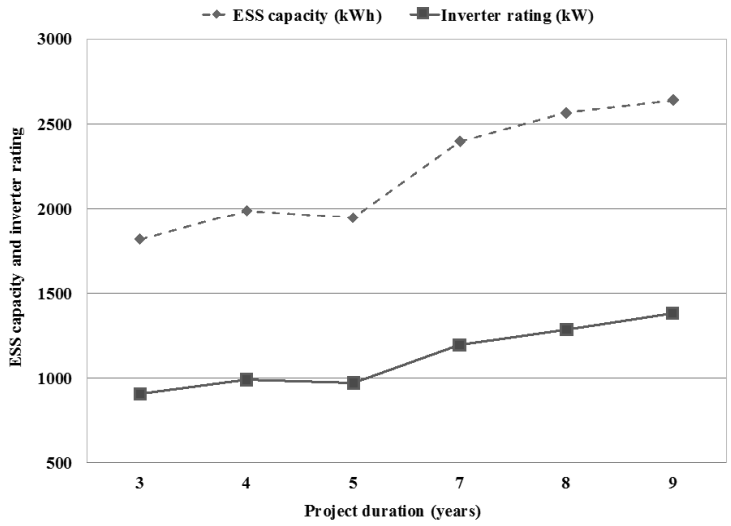


**Figure 2.8** ESS capacity and inverter rating with different project duration, operating reserve = 200kW, MRN = 1.

*2. Impact of the required operating reserve*

The results obtained with increasing reserve level from 100kW to 400kW show that the ESS capacity and inverter rating tend to increase when the operating reserve requirement is higher (Figure 2.9). In this study, it is assumed that both the diesel generator and the ESS are allowed to provide active power reserve. Therefore, if the required operating reserve is increased, the optimal size of ESS also increases.

Figure 2.10 shows the expected project cost versus the required operating reserve, for a planning period of five years. If the diesel generators are allowed to shut down, and the operating

reserve can be assumed by ESS, then the ESS capacity, and consequently the project cost increases with the required reserve. If diesel generators must be online, the required reserve does not have a significant impact on the project cost, since most of the time the diesel generators will run at minimum load and also provide the operating reserve.

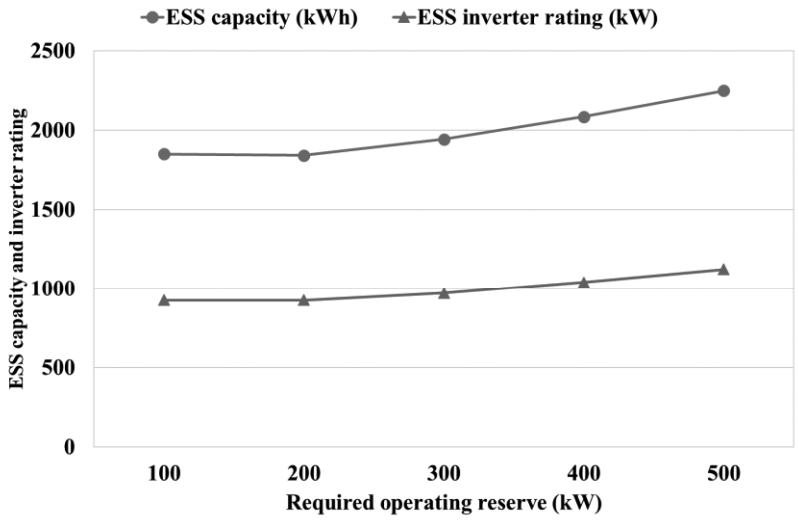


**Figure 2.9** ESS capacity with different operating reserve values, MRN = 1.

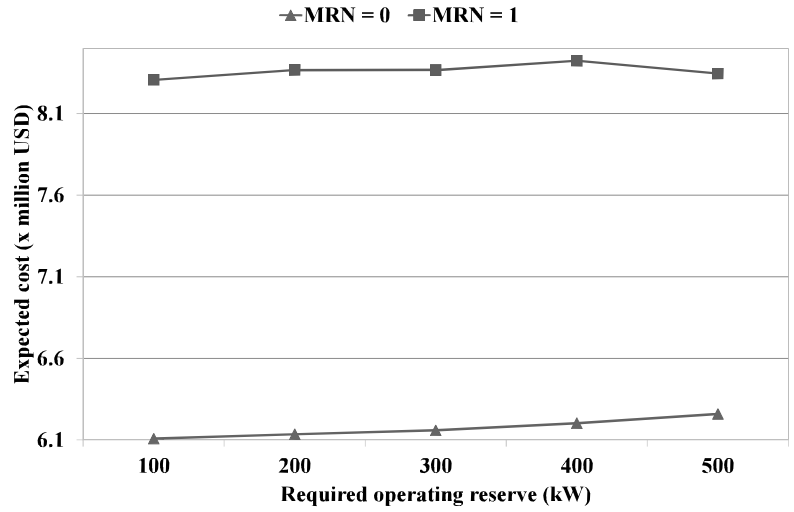


**Figure 2.10** Expected project cost with different operating reserve constraints.

*3. Impact of the minimum number of diesel units online*

The results presented in previous sections show that if the diesel generators can be shut down, the overall project cost can be greatly reduced. Thus, we study the effect of varying the MRN from 0 to 2 units. The optimal ESS capacity and inverter rating are summarized in Figure 2.11 and Figure 2.12. Conventional diesel generators have a minimum power output of about 30% of their rated capacity. Therefore, increasing the MRN will reduce the maximum wind

penetration level. As a consequence, the need for ESS is reduced. Besides, increasing the number of online diesel units limits the amount of energy that can be absorbed from wind generators. As can be seen in Figure 2.11, there is a consistent decline in ESS capacity with increasing MRN.

There is not much difference in optimal the inverter rating with MRN = 0 or 1 (Figure 2.12). On the other hand, it is interesting to note that when MRN = 2, the optimal inverter rating increases significantly. This result can be explained by the fact that increasing the minimum number of diesel generators to 2 units would strongly reduce the output from wind generators. Therefore, the power rating of the inverter should be increased for higher charging capacity at low load hours. The reduction of ESS capacity and the increase of inverter rating at MRN = 2 also means that this constraint makes it impossible to absorb all available wind energy, especially when the project duration is short.

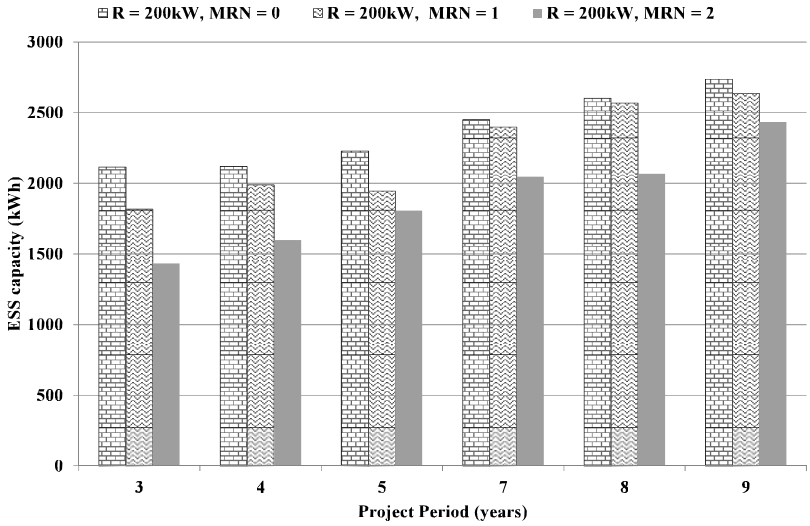


**Figure 2.11** Impact of MRN on ESS capacity.

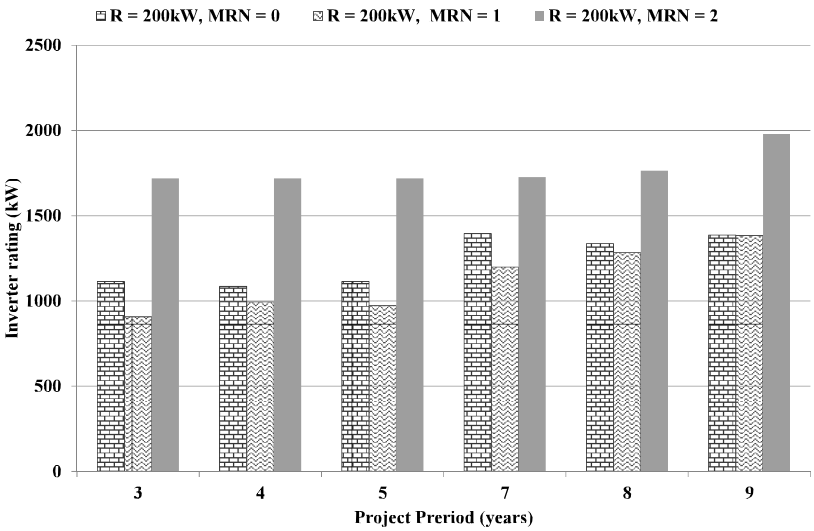


**Figure 2.12** Impact of MRN on inverter rating.

*4. Consistency of results with different reduced scenario sets*

In general, the optimization results in this work are close to those in our previous work [59], although a different approach to scenario reduction has been used. To investigate the efficiency of the proposed scenario reduction approach, the optimization problem is solved with different sets of reduced scenarios. Figure 2.13 and Figure 2.14 present the optimal ESS capacity and its inverter power rating with the number of reduced scenarios varying from 10 to 49. With more than 10 scenarios, the obtained optimal ESS capacity and the inverter power rating becomes consistent.

Regarding the objective function, the expected value of optimal project life cycle cost varies very slightly with the number of scenarios (less than 1%), as can be seen in Figure 2.15. These results show that the number of load scenarios can be reduced significantly without compromising the credibility of the optimal solution.

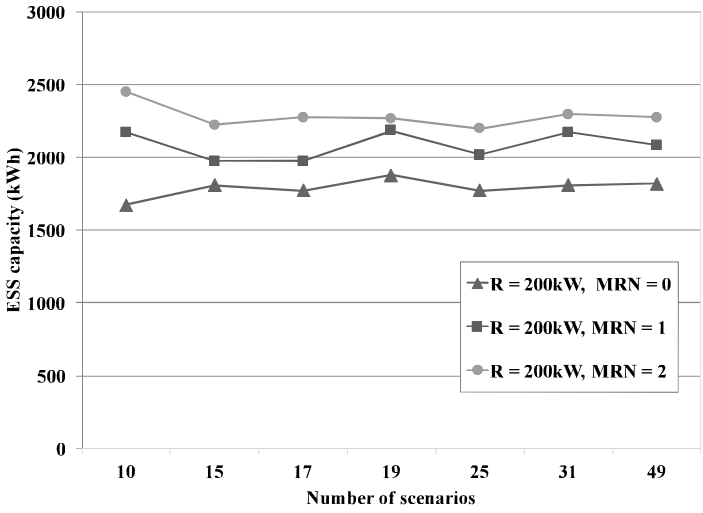


**Figure 2.13** Optimal ESS capacity vs. number of reduced scenarios.

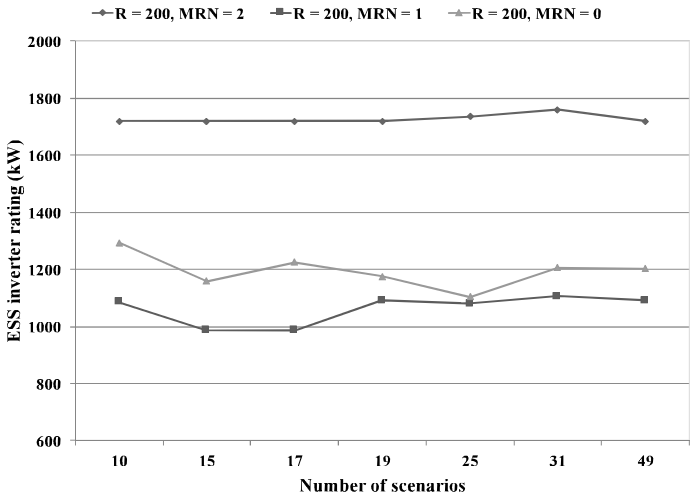


**Figure 2.14** Optimal ESS inverter rating vs. number of reduced scenarios.

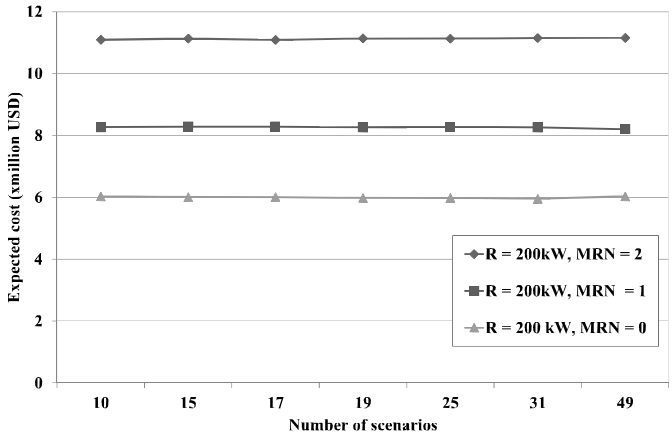


**Figure 2.15** Expected operating cost vs. number of reduced scenarios.

## 2.5 Summary

In this work, the problem of optimal ESS sizing in an isolated wind-diesel system is analyzed. The ESS sizing problem is formulated as a two-stage stochastic optimization framework, in which the load growth rate and the wind speed are two uncertain factors. The impact of the required operating reserve, the project duration, and the minimum number of online diesel generators on the optimal ESS parameters are analyzed.

Numerical results obtained using actual wind and load data of an island power system show that the optimal size for ESS and its inverter are quite stable when the project duration, the required reserve and the required minimum number of online diesel units are varied. This improves the confidence in investing in ESS. The proposed scenario reduction method is also shown to be very effective, which allows the determination of optimal ESS parameters with a substantially reduced scenario tree.

In the future work, the proposed approach can be extended to consider a larger number of stochastic variables such as fuel price, solar power generation, as well as other uncertain factors, such as equipment failures, etc.

# Chapter 3 Day-Ahead Optimal Operation of the Small Island Power System Considering Fast Frequency Response and Forecast Errors

## 3.1 Introduction

Integration of large share of RES increases the requirements for grid operations including frequency security. If a large power imbalance occurs, such as a sudden loss of a generator (or a large load is suddenly connected to power system), frequency regulation is necessary to maintain the frequency evolution within security boundaries and avoid emergency demand disconnections. Especially, in low-inertia power systems on isolated islands with small capacity and low inertia constant, the system frequency is more sensitive with any power imbalance.

This chapter presents Fast Frequency Response (FFR) – a method of frequency regulation – and the application of ESS for providing FFR. An optimal scheduling model of an island grid considering FFR after N-1 contingencies is also proposed.

### 3.1.1 Background

*1. Fundamental of Frequency Response*

Frequency is an important criterion in the power system's operation and is related to the instantaneous balance between supply and demand. To ensure stable operation of power systems, the balance between power demand and supply must be kept at all times; the system frequency is only allowed to vary in a tight band around the nominal value. Large frequency disturbances, caused by events such as the sudden loss of a generator, lead to serious active power imbalances and may lead to load shedding or partial or complete blackout. Fortunately, immediately after a frequency disturbance, the kinetic energy stored in the spinning masses of the generators is released into the power system in order to preserve the power balance, thereby reducing the rate of frequency change. This process is called the Inertial Response (IR) of the generator and shown as arresting period in Figure 3.1. At the same time, Primary Control Response (PFR) based on the characteristic of the conventional generators' governor also automatically starts to adjust the power output, thereby restore the frequency back to the stable level. This process is described by the rebound period in Figure 3.1. Normally, IR occurs within the first few seconds after the contingency while it takes up to ten seconds for PFR fully responds. For example, in operation standard of NEM, PFR almost fully respond after 6 seconds [66]. In a

conventional power system including synchronous generators with high inertia constant, the frequency decline can be arrested before reaching the minimum threshold.

In recent years, the penetration of renewable energy sources (RES) such as wind and solar into the power system is increasing rapidly and make frequency control challenging. RES power plants use inverter-based generators that do not have IR. Besides, the stochastic nature of wind and solar irradiation lead to the uncertainty in the reserved capacity for PFR from RES. Both of these factors contribute to the more complicated frequency control problem for power systems containing large fractions of wind and solar generation [67].

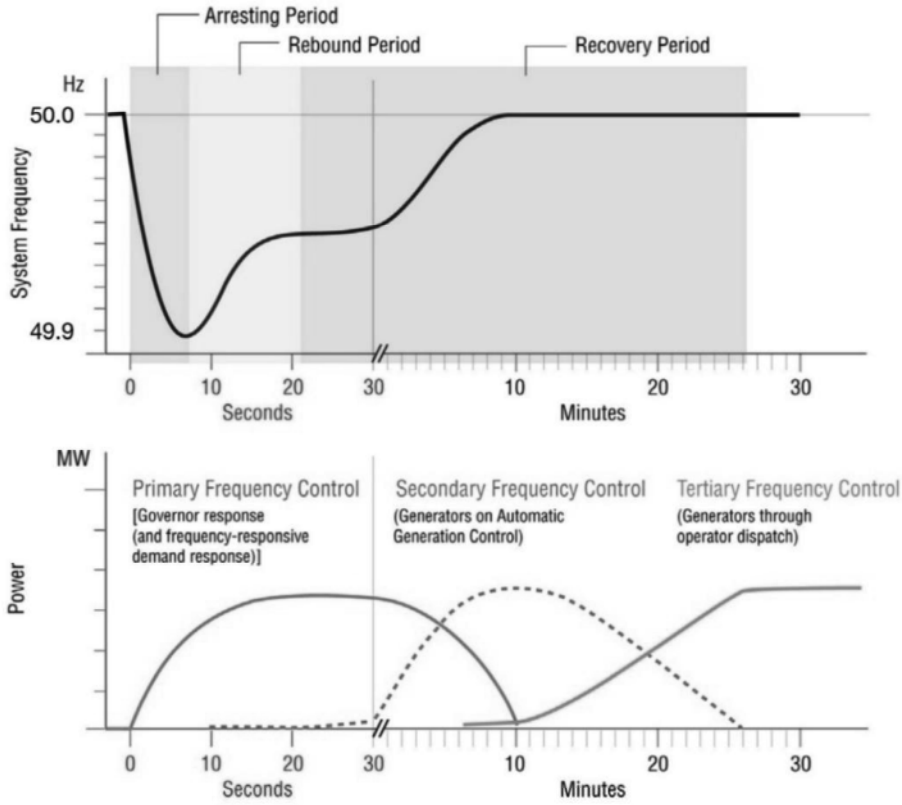


**Figure 3.1** The Sequential Actions of Frequency Responses after a Sudden Loss of a Generator [68]

To evaluate the post-contingency frequency, we use two important criteria including the rate-of-change-of-frequency (RoCoF) and the lowest frequency known as the frequency nadir $f_{nadir}$. The initial RoCoF immediately after the contingency event is defined as

$$RoCoF\left(\frac{\text{Hz}}{\text{s}}\right) = \frac{d\Delta f(\text{Hz})}{dt(\text{s})} = \frac{\text{Contingency size(MW)}}{\text{System inertia}\left(\text{MW}.\frac{\text{s}}{\text{Hz}}\right)} \tag{3-1}$$

It is easy to see that the higher penetration of RES, the lower system inertia, and then the higher RoCoF (Figure 3.2). The Australian electricity market has made a prediction about the increase of the RoCoF in the mainland (Figure 3.3). Meanwhile, [69] shows that the RoCoF can

reach to 1.7 Hz/s at 1 second after the contingency in New Zealand. Consequently, grid stability standard must be changed.

Report [66] shows that due to the increasing penetration of RES, the RoCoF standard is being changed around the world. In Great Britain (National Grid), the RoCoF standard was changed from 0.125 Hz/s to 1 Hz/s over 500ms for non-synchronous units recently. A RoCoF standard of 2.5 Hz/s over 200ms for wind and PV is applied in Denmark. The Australian National Electricity Market (NEM) requires the RoCoF lower than ±4 Hz/s for 250ms and ±1 Hz/s for 1 second. EirGrid/SONI in Ireland also increase their RoCoF standard from 0.5 Hz/s to 1 Hz/s over 500ms.

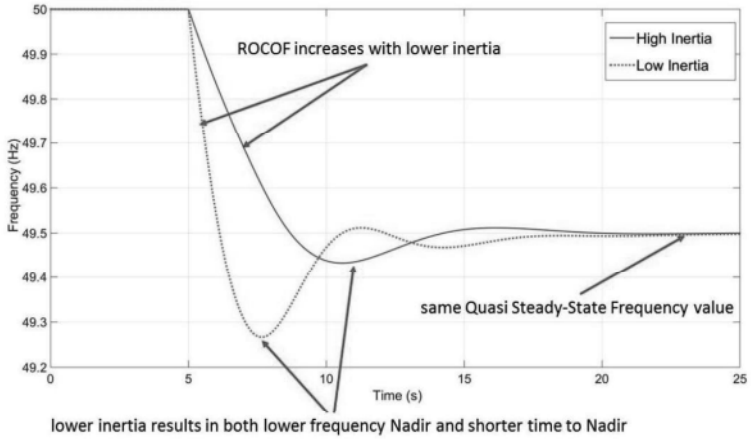


**Figure 3.2** The effect of the system inertia in system frequency response [70]

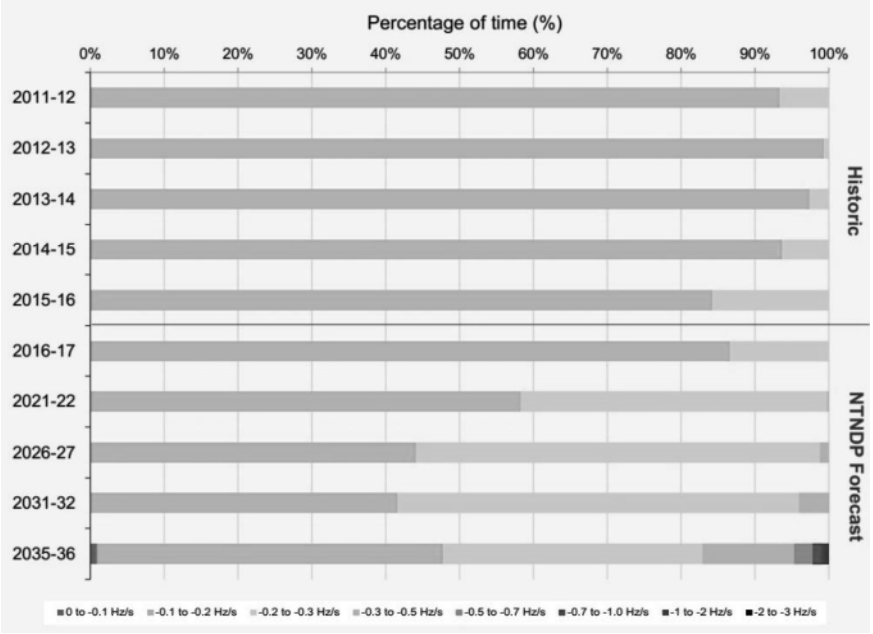


**Figure 3.3** Expected RoCoF in the mainland of Australia [71]

Especially, in island power systems, frequency control and regulation are even more challenging. The primary resources are diesel generators (DGs) or small synchronous generators

with low inertia and limited operating capability. While the inertia constant varies from 2.5 s to 10.0 s for a thermal unit or from 2.0 s to 4.0 s in the cases of a hydraulic unit [72], the inertia constant of a generator in a island system is less than 2.0 s, even in some cases this coefficient is only 0.5–0.8 s [73]. Also, these systems are not connected to other synchronous systems, so they do not have any support through transmission lines. Therefore, the overall system inertia of an island power system is also small and then the RoCoF after a contingency event can exceed these above standards. Noting that in case the nominal frequency is 50 Hz and the RoCoF is 4Hz/s, it takes only 250ms for the frequency drop to below the threshold of the UFLS relay (49Hz). Although DGs can increase their power output very quickly, even from a cold start condition (10–15 s), the UFLS relay will trigger to disconnect some customers before DGs active fully. Thus, Fast Frequency Response is applied as a measure to mitigate a high RoCoF.

*2. Overview of Fast Frequency Response*

Fast Frequency Response (FFR) method has been introduced as a measure to improve frequency stability in the context of rapidly increasing RES. Figure 3.4 shows the current situation of FFR application in the world. Although there are only a few power grids that apply FFR [74], this method is expected to grow widely.


**Figure 3.4** The current situation of FFR application in the world [74].

In the Australian electricity market, the definition of FFR is “
increase or decrease by generation or load, in a timeframe of less than two seconds, to correct supply- lances and assist with managing frequency” [71]. FFR can be considered simply as a measure to compensate for the “interval” between IR and PFR, during which the

frequency is too low and PFR is still not fully active. While IR slows down the RoCoF and PFR adjust each generator's power output based on the frequency deviation to restore the frequency back stable value, FFR injects active power into the system to compensate the power imbalance and arrest the frequency decline. If the FFR is sufficient, the frequency decay stops immediately, at which point the frequency nadir occurs.

There have been several studies of FFR encompassing a wide range of technologies [66], [75]–[78]. Report [66] carries out a global assessment and shows that ESS, wind turbines and demand response technologies are employed in several grids to provide FFR. Demand response in the grid PJM(USA) and New Zealand, which is based on interruptible loads, can provide FFR after 1 s and sustain for a period of at least 60 s. Another type of FFR technology is using the inertial response from wind turbines. The authors of [66] and [78] show that wind generators (WG) can provide IR for a very short duration (around 10 s). Although this method proved to be useful for frequency regulation, the kinetic energy provided by wind turbines is highly dependent on the wind speed; as a result, insufficient support is delivered in the case of low wind speed. Furthermore, in a low-inertia system, the frequency can drop below the threshold of the Under-Frequency Load Shedding (UFLS) relay within only 1 s, so the response of a WG is not effective. Presently, this technology is only employed in a few power systems such as Hydro-Québec, Ontario, and Brazil.

With a very short response time, energy storage systems (ESS) are able to instantly increase or decrease their power output to counteract a system power imbalance so ESS can be applied to FFR service. In fact, an ESS including batteries and flywheels is used to provide fast regulation in PJM with total capacities of 250MW. Meanwhile, Oahu, a typical island power system belong to Hawaii, has tested the BESS to provide frequency response in less than 1 second and put it into operation at the end of 2016 [66].

Note that FFR cannot completely replace PFR, it is only a support measure while waiting for the DGs to provide PFR. Thus, a long sustain duration is not necessary. In fact, FFR's sustain durations in real grids are not so long. Report [66] shows that in ERCOT (Texas), this duration is 10 minutes while EirGrid/SONI (Ireland) only requires an 8-seconds FFR.

An important requirement for FFR is fast response time. It is easy to that the systems having a higher RoCoF will require a faster response time. Assuming that the system has a nominal frequency of 50 Hz and a minimum frequency of 49 Hz, the relationship between the RoCoF level and the requirement of the response time can be shown in Table 3.1. For example, FFR must fully react within 250 ms in the case of a 4 Hz/s RoCoF. Table 3.2 summaries the times required to detect contingency and to send the control signal, as well as the reaction time and rise time of the ESS [75]. It can be seen that an ESS can respond fully after from 100 ms to 200 ms depending on

the contingency detection method and the ESS technology. Thus, the ESS is suitable for providing FFR.

**Table 3.1** Relationship between the RoCoF level and the required response time

| RoCoF (Hz/s) | Response Time |
|---|---|
| 0.5 | <2s |
| 1 | <1s |
| 2 | <500ms |
| 4 | <250ms |

**Table 3.2** Response times of various detection methods and types of ESS [75].

| | | Contingency event detection time | Control signal time | ESS reaction time + rise time |
|---|---|---|---|---|
| **Detection Method** | Direct detection | 40–60 ms | ≈20 ms | |
| | *RoCoF* detection/PMU | 40–60 ms | ≈20 ms | |
| | Local *RoCoF*/Frequency Measurement | ≈100 ms | ≈0 | |
| **Type of ESS** | Lithium Batteries | | | 10–20 ms |
| | Flow Batteries | | | 10–20 ms |
| | Lead-acid Batteries | | | ≤100 ms |
| | Flywheel | | | ≤4 ms |
| | Supercapacitor | | | 10–20 ms |

### 3.1.2 Literature Review

There are many previous studies focusing on the support of an ESS in frequency response such as [28], [32], [44], [49], [79], [80]. The authors of [28], [32], [44], [49] focused on the optimal sizing of the ESS, whereas [79], [80] propose control strategies for an ESS to provide virtual inertia. The results presented in these articles show the effectiveness of using an ESS for frequency response control. Besides, another interesting research approach in frequency regulation is to include frequency constraints in Unit Commitment (UC) models. Studies in this direction focus on predetermining power output of each generator per hour to ensure the

frequency criteria after a contingency event [41], [81]. The authors of [42] considered not only the constraints of frequency nadir and frequency at quasi-steady state but also load damping in the frequency response model. Reference [31] used an ESS to provide primary frequency response and found an optimal schedule of generators and ESS to take full advantage of wind power. Due to the high penetration of RES, the day-ahead optimal scheduling problem considering frequency-related constraints is necessary. Also, the results presented in these papers show the effectiveness of using an ESS for frequency response control. However, the following issues are still unresolved.

- Most of these works—with or without the support of ESS—focused on IR and PFR.
- Case studies are high-inertia power systems. Generators have inertia constant from 4s to 10s. The effect of the decline in the system inertia due to the increase in RES participation is not shown as clearly as a small island power system
- The rate-of-change-of-frequency (RoCoF) criteria in these papers are 0.2–0.5 Hz/s, which is very unlikely in the case of a small island system with the small inertia of DGs.

A problem that needs to be addressed in the frequency-constrained UC problem is how to handle the uncertainty in wind power and demand. The UC model in [41], [81] did not consider the uncertainty in the available wind power so the results are less accurate when applied to actual operations. Reference [42] solved the stochastic UC model based on a scenario tree, however, the scenario tree cannot include all possible scenarios. Therefore, although the results are significant when evaluating the expected value of the objective function, the obtained UC decisions do not guarantee the safety of any value of the uncertain parameter. The authors of [31] describe the wind power uncertainty by only three scenarios: the central forecast, the upper bound, and the lower bound. However, considering the boundary data as having the same probability characteristics as the central data may lead to higher operating costs.

A common method used to account for the uncertainty in wind power and demand is formulating the UC problem as a two-stage chance-constrained optimization model. The constraints related to uncertain parameters are written as probabilistic constraints with a chosen risk level [82], [83]. This method ensures that all possible values of the uncertain parameter will be taken into account. Considering the risk level of the constraints will make the result more meaningful in actual operation. To solve chance-constrained optimization problems, the authors of [84] developed an analytical method while a numerical approach known as the Sample Average Approximation (SAA) algorithm is applied in [85]–[89]. Although the method in [84] is useful and can consider the correlation of uncertain parameters, finding an inverse normal distribution is very complex, especially in the case of many uncertain parameters. On the other hand, the inverse normal distribution function may be nonconvex, so it is difficult to find an optimal solution. The

SAA algorithm in [85]–[89] involves Monte Carlo simulation to approximate the distribution function of a random vector using $N$ samples. Although this approach can solve a problem including many uncertain parameters, it requires a significantly long computing time.

### 3.1.3 Research Objectives and Contribution

The target of the study in this chapter is to develop a day-ahead scheduling model of the island power system including DGs, WG, and ESS. The ESS is used for power balancing and FFR after a single outage (N-1) contingency. The proposed model is expected to meet these purposes at the same time: to minimize the operating cost of DGs, take full advantages of the available wind power, consider the uncertainty of wind power and demand, and make sure that the ESS has enough energy to provide FFR after a contingency event.

On the other hand, we develop a Modified Sample Average Approximation (MSAA) algorithm which is a combination of the traditional SAA and a k-means approach. Although SAA is a simple and convenient method, all $N$ samples are considered to have the same probability regardless the true distribution of the random vector, so the number of samples must be large to ensure that a feasible solution is found. If there are many uncertain parameters, the size of the optimization problem increases, and a significantly longer computing time is required. The proposed MSAA algorithm is proven to be more effective than the original SAA approach.

## 3.2 Proposed Optimization Framework

### 3.2.1 Nomenclature

**Indices and Sets**

| | |
|---|---|
| $i \in I$ | Diesel generators |
| $t \in T$ | Time intervals (of variable duration) |
| $w \in W$ | Wind generators |
| $\xi$ | Random vector |

**Constants**

| | |
|---|---|
| $C_{su,i}$ | Start-up cost of diesel generator $i$ (\$/kWh) |
| $C_{sd,i}$ | Shutdown cost of diesel generator $i$ (\$/kWh) |
| $C_{0,i}$ | No-load cost of diesel generator $i$ (\$/kWh) |
| $C_i$ | Operating cost of diesel generator $i$ (\$/kWh) |

$C_{SSc}$ Charge cost of energy storage ($/kWh)

$C_{SSd}$ Discharge cost of energy storage ($/kWh)

$P_{maxi}$ Maximum power output of diesel generator *i* (kW)

$P_{mini}$ Minimum power output of diesel generator *i* (kW)

$\tau_{iON}$ Minimum uptime (hours)

$\tau_{iOFF}$ Minimum downtime (hours)

$P_{SSmax}$ Power rating of energy storage system (kW)

$E_{ssmax}$ Capacity of energy storage system (kWh)

$\eta$ Charging/discharging efficiency of energy storage system

$H_i$ Inertia constant of diesel generator *i* (s)

$f_{norm}$ Nominal frequency (Hz)

$f_{min}$ Minimum frequency threshold (Hz)

$f_{db}$ Dead band of governor (Hz)

$k_i$ Maximum governor ramp rate of generator *i* (kW/s)

$\Delta t_{FFR}$ The sustain duration of Fast Frequency Response provided by energy storage system (minutes)

**Semi-constants**

$P_{Wf}^t$ Forecasted wind power at time *t* (kW)

$P_{W-error}^t$ Forecast error of wind power at time *t* (%)

$P_{Wmax}^t$ Maximum possible wind power at time *t* (kW)

$P_{Df}^t$ Forecasted demand at time *t* (kW)

$P_{D-error}^t$ Forecast error of demand at time *t* (%)

$P_D^t$ Actual demand at time *t* (kW)

**Variables**

$u_i^t$ Start-up state of diesel generator *i* at time *t* (binary)

$v_i^t$ Shutdown state of diesel generator *i* at time *t* (binary)

$w_i^t$ ON/OFF state of diesel generator *i* at time *t* (binary)

$P_i^t$ Power output of diesel generator *i* at time *t* (kW)

$R_i^t$ Reserve of diesel generator *i* at time *t* (kW)

$u_w^t$ ON/OFF state of wind turbine at time *t* (binary)

$P_w^t$ Actual wind power at time *t* (kW)

$u_{SS}^t$ Charging state of energy storage system at time *t* (binary)

$P_{SS}^{ch,t}$ Charge power of energy storage system at time *t* (kW)

$P_{SS}^{disch,t}$ Discharge power of energy storage system at time *t* (kW)

$P_{dispost}^t$ Discharge power of energy storage system after a contingency event at time *t* (kW)

$E_{SS}^t$ Energy stored in the energy storage system at time *t* (kWh)

$E_{SS}^{t=0}$ Initial energy stored in the energy storage system at $t = 0$ (kWh)

$E_{SS}^{t=24}$ Energy stored in the energy storage system at the end of the day ($t = 24$) (kWh)

### 3.2.2 The Two-Stage Optimal Scheduling Model

The process of optimal scheduling comprises two stages, as illustrated in Figure 3.5. In the first stage, based on the forecasted values of wind power and demand, the deterministic day-ahead schedule of DGs is predetermined every hour for a 24-hour time horizon and sent to the grid operator; this process is illustrated by the solid blue arrows in Figure 3.5. In practical operation, the first-stage problem is a day-ahead UC problem that is implemented at least one day before the actual operation date based on the long-term forecast results of the wind and demand. Because long-term forecasting values normally have high errors, only the results of the unit commitment and the power output of DGs are reliable. The second-stage variables including the ESS charge/discharge power and WG's power output are be adjusted after wind power and demand are known with higher accuracy using a very short-term forecast. Because the short-term forecasting errors are very small, the forecast values can be treated as actual values.

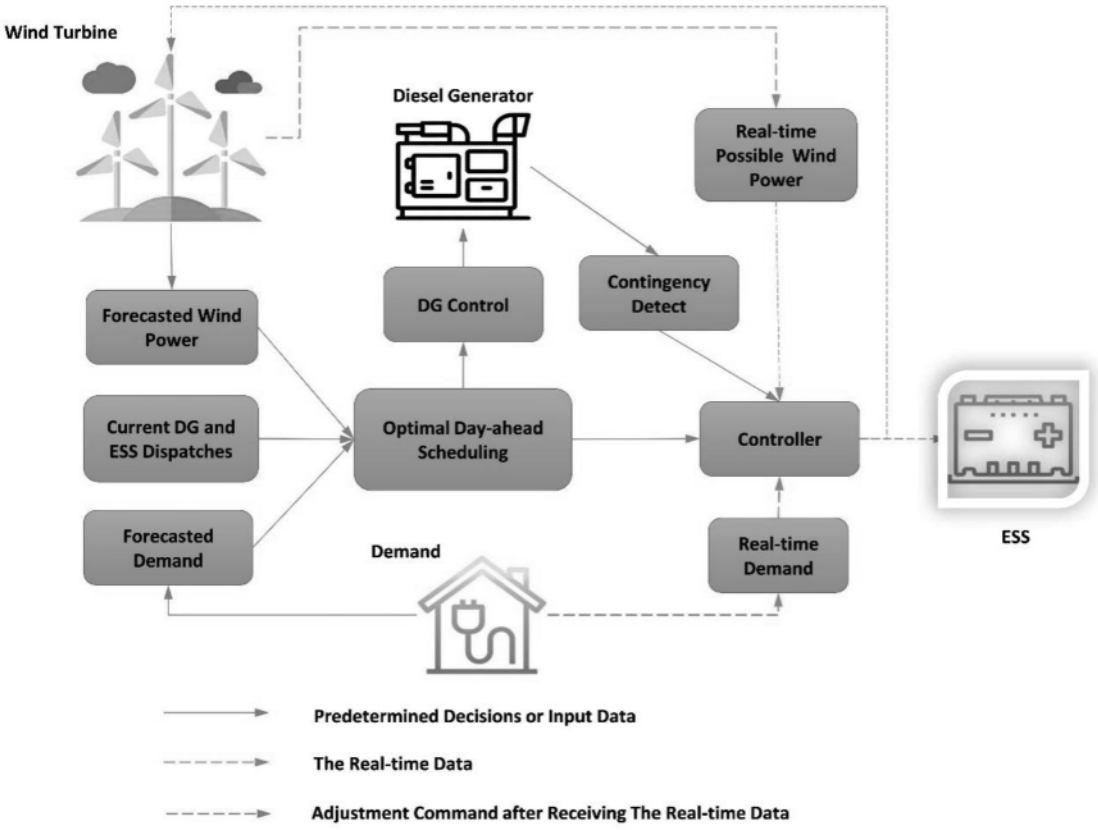


**Figure 3.5** Schematic illustrating the optimal scheduling problem for an island power system.

### 3.2.3 The Role of Energy Storage System in Fast Frequency Response

In this section, we outline the constraints on the power output of the DGs for each hour and the response of the ESS needed to satisfy the frequency criterion, $f_{min}$.

Consider, for example, a power system with $I$ generators. If at time $t$ generator $j$ with power output $P_j^t$ (kW) is lost, the *RoCoF* immediately after the contingency event is defined as

$$RoCoF = \frac{d\Delta f}{dt} = \frac{P_j^t}{M_H} \tag{3-2}$$

where $M$ is the system inertia (kW.s/Hz) after the loss of generation $j$ and is a function of the inertia of the online generators:

(3-3)

where $H_i$, $P_{maxi}$, and $w_i$ are the inertia constant, maximum capacity, and ON/OFF state of the remaining generators, respectively; $w_i$ is a binary variable that is equal to 1 if generator $i$ is online and 0 if it is offline.

The first-order model for a governor–prime mover presented in [81], [90] is applied to build an approximate model of the system's response after a sudden generation loss of amount $P_j^t$ and the application of ESS for FFR. After the governor's dead time $t_d$, which corresponds to the frequency dead band $f_{db}$, the power output of the DGs will change due to the governor's response with the system ramp rate $K = \sum_{i \neq j} k_i P_{maxi} / \sum_{i \neq j} P_{maxi}$. A control signal is also sent to the ESS to increase its output from $P_{ss}^{ch,t}$ or $P_{ss}^{disch,t}$ to $P_{dispost}^t$. Thus, the adjustment provided by the ESS is $P_{adjust}^t = P_{dispost}^t - \left(P_{SS}^{disch,t} - P_{SS}^{ch,t}\right)$ (Figure 3.6).

To simplify the model, we make two assumptions:

- The rise time of ESS is negligible
- The ESS can fully compensate for the power shortage. This means that the frequency decay stops immediately after the ESS fully responds, at which point the frequency nadir occurs.

The time evolution of the system frequency deviation after the contingency event can be described by

$$M_H \frac{d\Delta f(t)}{dt} = \Delta P_{DGs}(t) + \Delta P_{ESS}(t) - P_j^t \tag{3-4}$$

where $\Delta P_{DGs}(t)$ and $\Delta P_{ESS}(t)$ describe the additional power provided by DGs (due to the response of the governors) and ESS, respectively. $\Delta P_{DGs}(t)$ and $\Delta P_{ESS}(t)$ are formulated as follows:

$$\Delta P_{DGs}(t) = \begin{cases} 0 \ \ if \ t < t_{db} \\ K(t - t_{db}) \ if \ t_{db} \leq t \leq \ t_{nadir} \\ K(t_{nadir} - t_{db}) \ if \ t_{nadir} \leq t \end{cases} \tag{3-5}$$

$$\Delta P_{ESS}(t) = \begin{cases} 0 \ \ if \ t < t_{nadir} \\ P_{adjust}^t \ if \ t_{nadir} \leq t \end{cases} \tag{3-6}$$

Using the model presented in Figure 3.1, we can find the relationship between the adjustment power provided by the ESS and the time when the ESS can fully respond:

$$P_{adjust}^t = P_j^t - K(t_{nadir} - t_d) \tag{3-7}$$

Considering (3-5)–(3-7), the equation (3-4) can be integrated between $t = 0$ and $t = t_{nadir}$.

$$\int_0^{t_{nadir}} d\Delta f(t) = \frac{1}{M_H} \int_o^{t_d} \left(-P_j^t\right) dt + \frac{1}{M_H} \int_{t_d}^{t_{nadir}} \left(K(t - t_d) - P_j^t\right) dt$$

Assuming that before the contingency event, the system frequency is at the nominal value $f_{norm}$, we have:

$$f_{nadir} - f_{norm} = -\frac{1}{M_H} P_j^t t_d + \frac{1}{M_H}\left[\frac{1}{2}K(t_{nadir} - t_d)^2 - P_j^t(t_{nadir} - t_d)\right]$$
$$= -\frac{1}{M_H} P_j^t t_d + \frac{1}{M_H}\left[\frac{1}{2}K\frac{\left(P_j^t - P_{adjust}^t\right)^2}{K^2} - \frac{P_j^t\left(P_j^t - P_{adjust}^t\right)}{K}\right]$$
$$= -\frac{1}{M_H} P_j^t t_d - \frac{\left(P_j^t\right)^2 - \left(P_{adjust}^t\right)^2}{2KM_H}$$

The authors of [81] shows that the duration of $t_d$ is related with the governor dead-band $f_{db}$ (Hz) by equation $f_{db} = \frac{1}{M_H} P_j^t t_d$. Besides, noting that the frequency nadir should not be below the predefined threshold $f_{min}$, we obtain the frequency nadir' s requirement as follow.

$$f_{nadir} = f_{norm} - f_{db} - \frac{\left(P_j^t\right)^2 - \left(P_{adjust}^t\right)^2}{2KM_H} \geq f_{min} \tag{3-8}$$

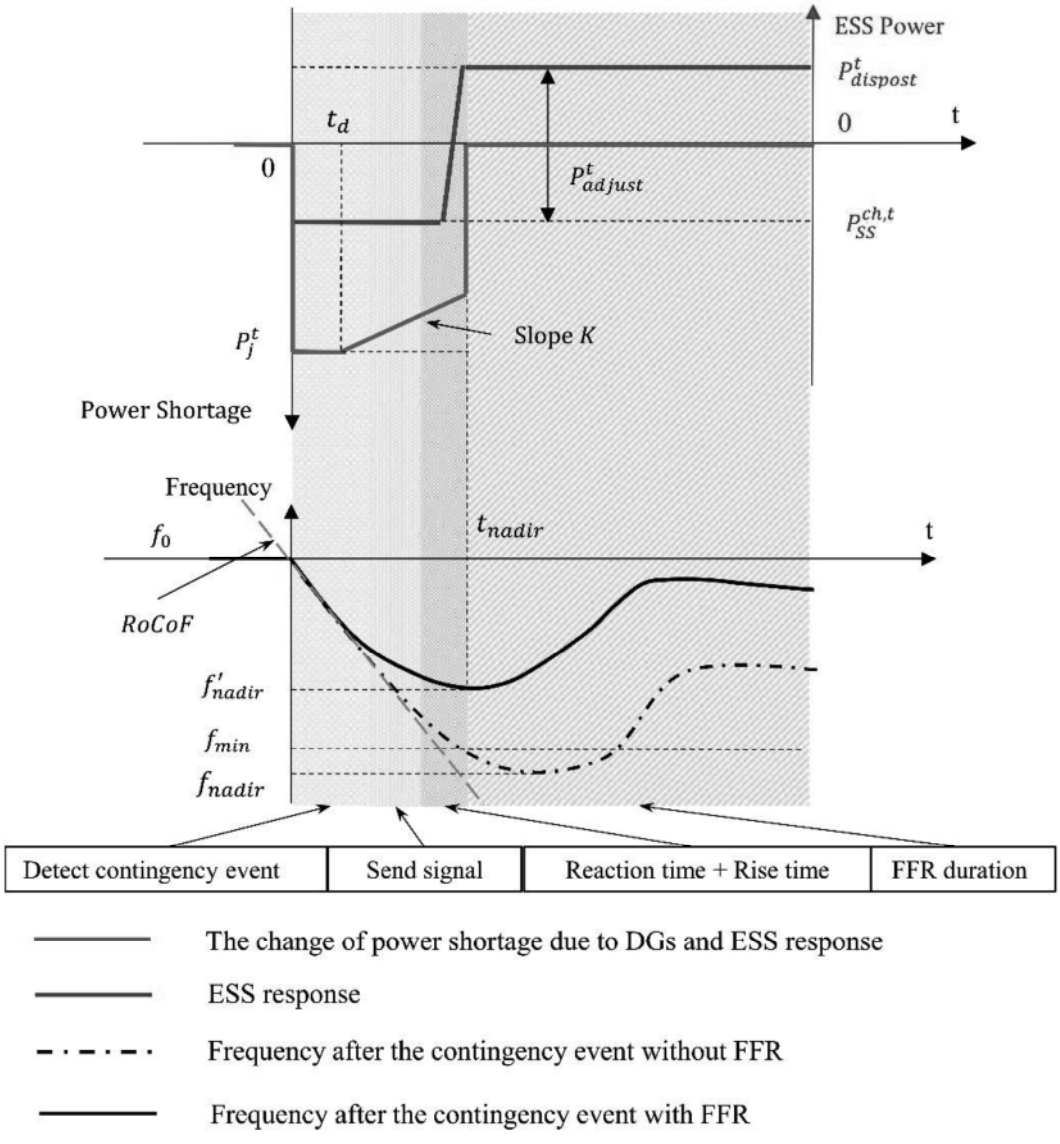


**Figure 3.6** Application of an energy storage system for fast frequency response

Substituting (3-7) into (3-8) and noting that $P_{adjust}^{t} = P_{dispost}^{t} - \left(P_{SS}^{disch,t} - P_{SS}^{ch,t}\right)$, we obtain the following constraint:

$$\begin{cases} 2M_H(f_{norm} - f_{db} - f_{min}) \geq \left(2P_j^t - K(t_{nadir} - t_d)\right)(t_{nadir} - t_d) \\ P_{dispost}^{t} - \left(P_{SS}^{disch,t} - P_{SS}^{ch,t}\right) = P_j^t - K(t_{nadir} - t_d) \end{cases} \tag{3-9}$$

Constraint (3-9) shows that the number of DGs in operation and their power output per hour is limited by the time taken for the ESS to fully react, and this will be used in the optimal scheduling formulation presented in next section.

### 3.2.4 Wind and Demand Models

A challenge in this problem is the uncertainty in the expected wind power and demand. Whatever prediction method is used to forecast wind speed and load, the results still contain errors. These errors will affect the operation of the system and must be taken into account in the optimal UC problem. The optimal scheduling problem will be formulated as a predictive optimization with results expressed as ranges of values that assure reliable operation of the system.

Both wind power and demand can be defined as the sum of the forecasted value and the forecasting error:

$$\begin{cases} P_{Wmax}^{t} = P_{Wf}^{t} + P_{W-error}^{t} P_{Wf}^{t} \\ P_{D}^{t} = P_{Df}^{t} + P_{D-error}^{t} P_{Df}^{t} \end{cases} \tag{3-10}$$

The errors $P_{W-error}^{t}$ and $P_{D-error}^{t}$ are assumed to follow a normal distribution with zero mean and the standard deviation $\sigma_W^t$ for wind power and $\sigma_D^t$ for demand. This means the maximum error would be $3\sigma_W^t$ for wind power and $3\sigma_D^t$ for demand in correspondence to the confidence level of 99.7%.

### 3.2.5 Mathematical Formulation

The optimal scheduling problem is formulated as a two-stage chance-constrained optimization model (Figure 3.7). The constraints in the first stage refer to the deterministic planning, and the second stage ensures that the power balance and frequency criteria after a contingency event are met with high probability for any values of demand and wind power drawn from distribution functions with the given standard deviation.

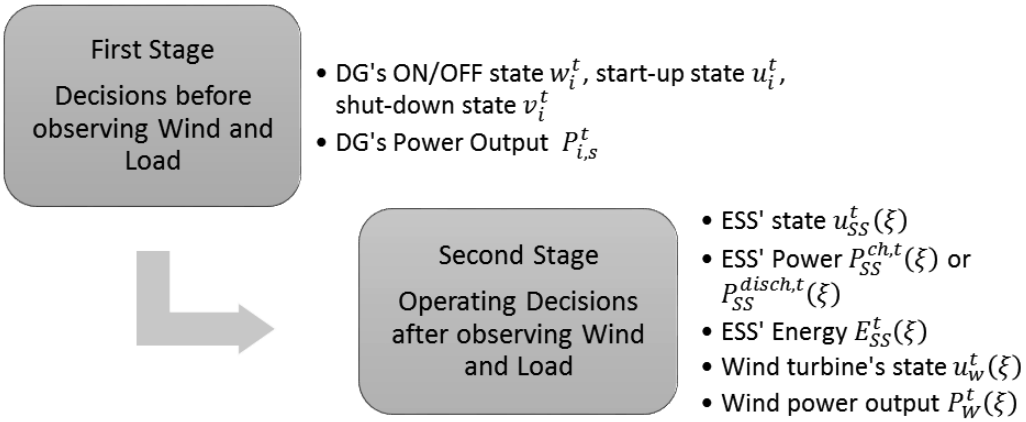


**Figure 3.7** The two-stage optimization model.

*1. Objective Function*

The objective function to be minimized comprises the first-stage operating cost and the expected value of the second-stage cost:

$$Minimize \sum_{t=1}^{24} \sum_{i} \left(C_{su,i} u_i^t + C_{sd,i} v_i^t + C_{0,i} w_i^t + C_i P_i^t\right) + \mathbb{E}\left(C_{SSc} P_{SS}^{ch,t}(\xi) - C_{SSd} P_{SS}^{disch,t}(\xi)\right) \quad (3\text{-}11)$$

where $\xi$ represents a random vector including wind and demand; $P_{SS}^{ch,t}(\xi)$ and $P_{SS}^{disch,t}(\xi)$ are the ESS charge/discharge powers, respectively, decided corresponding to the actual values or the very short-term forecast value of $\xi$.

*2. First-Stage Constraints*

The first stage is characterized by the following constraints:

- **Active power balance constraint.** The total active power output from the DGs $P$ , the wind plant , and the storage system ( $^{,t}$ and $P_{SS}^{ch,t}$ ) must equal the given forecasted load $P_{Df}^t$ at any time *t*:

$$\sum_i P_i^t + P_w^t + P_{SS}^{disch,t} - P_{SS}^{ch,t} = P_{Df}^t \quad (3\text{-}12)$$

- **DG operating constraints.** The power output of each DG must be in the operating range between $P_{\min i}$ and $P_{\max i}$, which are specified by the manufacturer. The binary variable $w_i^t$ in constraint (3-13) is used to keep the DG power output equal to zero if it is shut down. Constraints (3-14) and (3-15) describe the minimum uptime $\tau_{iON}$ and downtime $\tau_{iOFF}$ limitations of each DG.

$$P_{\min i} w_i^t \le P_i^t \le P_{\max i} w_i^t \tag{3-13}$$

$$w_i^t - w_i^{t-1} = u_i^t - v_i^t \tag{3-14}$$

$$\begin{cases} \sum_{k=t-\tau_{iON}}^{t} u_i^k \le w_i^t \\ \sum_{k=t-\tau_{iOFF}}^{t} v_i^k \le 1 - w_i^t \end{cases} \tag{3-15}$$

- **Primary reserve constraints for DGs.** This constraint shows that each DG can take part in the operating reserve.

$$\begin{cases} R_i^t \ge 0 \\ P_i^t + R_i^t \le w_i^t P_{imax} \end{cases} \tag{3-16}$$

- **WG operating constraint.** For a given forecasted wind power $P_{Wf}^t$, the power output of the WG must satisfy the following constraint, where $P_{Wmin}^t$ is the minimum wind power output:

$$u_w^t P_{Wmin}^t \le P_w^t \le u_w^t P_{Wf}^t \tag{3-17}$$

- **ESS constraints.** Constraint (3-18) states that the charging and discharging power of the ESS must be smaller than the actual power rating of the storage device $P_{SSmax}$. The process of charging/discharging the ESS is described by constraint (3-19). This constraint also imposes that the energy stored in the ESS should be smaller than its rated capacity at all times:

$$\begin{cases} 0 \le P_{SS}^{ch,t} \le u_{SS}^t P_{SSmax} \\ 0 \le P_{SS}^{disch,t} \le (1 - u\ \ ) P_{SSmax} \end{cases} \tag{3-18}$$

$$\begin{cases} 0 \le E_{SS}^t = E_{SS}^{t-1} + \eta P_{SS}^{ch,t} - P_{SS}^{disch,t}/\eta \le E_{ssmax} \\ E_{SS}^{t=0} = E_{SS}^{t=24} \end{cases} \tag{3-19}$$

- **Frequency nadir limit.** As presented in Section 3.2.3, to ensure that the frequency does not drop below the minimum allowable level, the following constraint must be satisfied:

$$\begin{cases} 2M_H(f_{norm} - f_{db} - f_{min}) \ge \left(2P_j^t - K(t_{nadir} - t_d)\right)(t_{nadir} - t_d) \\ P_{dispost}^t - \left(P_{SS}^{disch,t} - P_{SS}^{ch,t}\right) = P_j^t - K(t_{nadir} - t_d) \end{cases} \tag{3-20}$$

- **Post-contingency energy storage capacity constraint.** After providing FFR within $\Delta t_{FFR}$, the remaining energy in the ESS must satisfy the following constraint:

$$0 \le E_{SS}^t - P_{dispost}^t \Delta t_{FFR} \le E_{SSmax} \tag{3-21}$$

*3. Second-Stage Constraints*

In the second stage of the optimization model, uncertainties in wind power generation and load consumption are considered. The power output of the ESS and the WGs are re-dispatched as $P_{SS}^{disch,t}(\xi)$, $P_{SS}^{ch,t}(\xi)$, and $P_w^t(\xi)$, where $\xi$ represents a random vector. When a generator is lost, the ESS will discharge $P_{dispost}^t(\xi)$ to decrease the disturbance to $P \quad (\xi) = P_j^t - \left(P_{dispost}^t(\xi) - \left(P_{SS}^{disch,t}(\xi) - P_{SS}^{ch,t}(\xi)\right)\right)$. The second-stage constraints can be summarized as follows:

- **Active power balance constraint.**

$$\Pr\left(\sum_i P_i^t + P_w^t(\xi) + P_{SS}^{disch,t}(\xi) - P_{SS}^{ch,t}(\xi) = P_{Df}^t + P_{D-error}^t P_{Df}^t\right) \geq 1 - \varepsilon \qquad (3\text{-}22)$$

- **WG operating constraint.**

$$u_w^t P_{Wmin}^t \leq u_w^t P_w^t(\xi) \leq u_w^t\left(P_{Wf}^t + P_{W-error}^t P_{Wf}^t\right) \qquad (3\text{-}23)$$

- **ESS constraints.**

$$0 \leq P_{SS}^{ch,t}(\xi) \leq u_{SS}^t P_{SSmax} \qquad (3\text{-}24)$$

$$0 \leq P_{SS}^{disch,t}(\xi) \leq (1 - u \quad) P_{SSmax} \qquad (3\text{-}25)$$

$$0 \leq E_{SS}^t(\xi) = E_{SS}^{t-1}(\xi) + \eta P_{SS}^{ch,t}(\xi) - P_{SS}^{disch,t}(\xi)/\eta \ \leq E_{ssmax} \qquad (3\text{-}26)$$

- **Frequency nadir limit.**

$$\begin{cases} \Pr\left(2M_H(f_{norm} - f_{db} - f_{min}) \geq \left(P_j^t + P_{dispost}^t(\xi) - \left(P_{SS}^{disch,t}(\xi) - P_{SS}^{ch,t}(\xi)\right)\right)(t_{nadir} - t_d)\right) \\ \qquad\qquad \geq 1 - \varepsilon \\ P_{dispost}^t(\xi) - \left(P_{SS}^{disch,t}(\xi) - P_{SS}^{ch,t}(\xi)\right) = P_j^t - K(t_{nadir} - t_d) \end{cases} \qquad (3\text{-}27)$$

- **Post-contingency energy storage capacity constraint.**

$$0 \leq E_{SS}^t(\xi) - P_{dispost}^t(\xi)\Delta t_{FFR} \leq E_{SSmax} \qquad (3\text{-}28)$$

In the above constraints, constraint (3-22) guarantees that the ESS and WG will be adjusted so that the probability of power imbalance is less than a risk level $\varepsilon$. Similarly, constraint (3-27)ensures that the frequency criterion will be met after a contingency event with high probability, even if the ESS is re-dispatched.

## 3.3 The Modified Sample Average Approximation

In the literature, the SAA method is used widely to solve stochastic or chance-constrained optimization [85]–[89].

To present SAA method in detail, we consider a simple two-stage chance-constrained optimization model as follow

$$V = \min\{f(x) + \mathbb{E}(Q(y,\xi))\} \tag{3-29}$$

subject to

$$\Pr(G(x,y,\xi) \le 0) \ge 1-\varepsilon \tag{3-30}$$

where $x$ is the first-stage variable, $y$ is the second-stage variable, and $\xi$ is random input data..

In this method, Monte Carlo simulation is used to approximate the distribution function of the random vector $\xi$ by $N$ samples. The optimization formulation (3-29) then becomes

$$V = \min\left\{f(x) + \frac{1}{N}\sum_{n=1}^{N} Q(y_n,\xi_n)\right\} \tag{3-31}$$

subject to

$$\frac{1}{N}\sum_{n=1}^{N} \mathbf{1}_{(0,\infty)}(G(x,y_n,\xi_n)) \ge 1-\varepsilon \tag{3-32}$$

where $\mathbf{1}_{(0,\infty)}(G(x,y_n,\xi_n))$ is an indicator function that is equal to one if $G(x,y_n,\xi_n) \le 0$ and zero otherwise.

It is seen from equation (3-32) that the $N$ samples are handled with the same probability $(1/N)$. This helps to simplify the formulation of the optimization; however, a large number of samples are required to guarantee accuracy, which means the CPU time required to solve it increases accordingly.

In the present study, we propose a modified approach to the SAA is proposed, by using a k-means clustering approach to reform the samples. Instead of directly using $N$ samples, the k-means clustering divides the samples into $M$ clusters. The probability of each cluster is the sum of the probabilities of the constituent samples. The $M$ centroids of the clusters will be used as the input samples, with the probability of each centroid being equal to the probability of the cluster that it represents. Figure 3.8 illustrates a small example: 1000 samples generated from the standard normal distribution N(0,1) are replaced by 10 centroids.

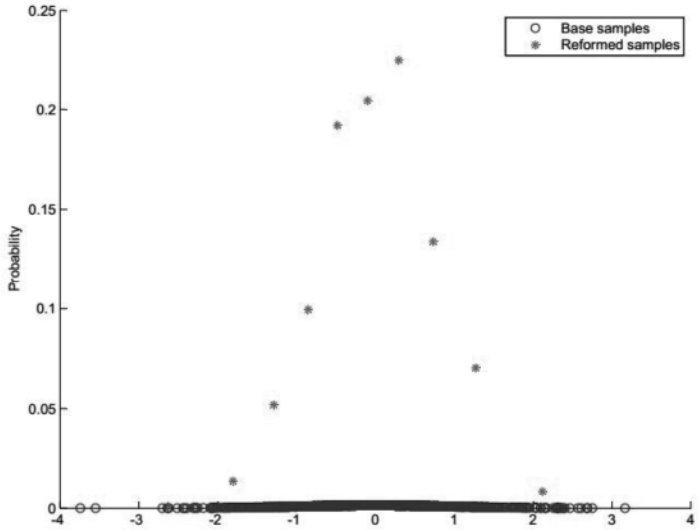


**Figure 3.8** Example of using k-means clustering to reform samples.

For $M$ centroids and their corresponding probabilities, the above chance-constrained model is reformulated as

$$V = \min\left\{f(x) + \sum_{m=1}^{M} p_m Q(y_m, \xi_m)\right\} \tag{3-33}$$

subject to

$$\sum_{m=1}^{M} p_m \mathbf{1}_{(0,\infty)}\big(G(x, y_m, \xi_m)\big) \geq 1 - \varepsilon \tag{3-34}$$

where $p_m$ is the probability of each centroid ($m = 1,2, \dots M$).

Now let $\bar{x}$ and $\bar{V}$, respectively, be the optimal solution and value of the optimal problem in (3-33) and (3-34)and check whether this solution is feasible or not. In next step, a new set of $N'$ samples is generated with $N'$ is much larger than $N$, we find the value of the probability constraint (3-32) with solution $\bar{x}$ is

$$g(\bar{x}) = \Pr(G(\bar{x}, y, \xi) \leq 0) = \frac{1}{N'} \sum_{n=1}^{N'} \mathbf{1}_{(0,\infty)}\big(G(\bar{x}, y_n, \xi_n)\big) \tag{3-35}$$

The (1–ε)-confidence lower bound on $g(\bar{x})$ is then computed using

$$L(\bar{x}) = g(\bar{x}) - \Phi^{-1}(1-\varepsilon)\sqrt{\frac{g(\bar{x})\big(1 - g(\bar{x})\big)}{N'}} \tag{3-36}$$

where $\Phi^{-1}$is the inverse normal distribution function. $\bar{x}$ is a feasible solution of the original problem only if $L(\bar{x}) \geq 1 - \varepsilon$. Repeat this process K times according to the flow chart illustrated

in Figure 3.9 and find the maximum value $\overline{U}$ and minimum value $\overline{L}$ of the optimal value $\overline{V}$. If the optimality gap given by $(\overline{U} - \overline{L})/\overline{U} \times 100\%$ is smaller than a predetermined threshold, the algorithm terminates, and we obtain the optimal solution of the original problem.

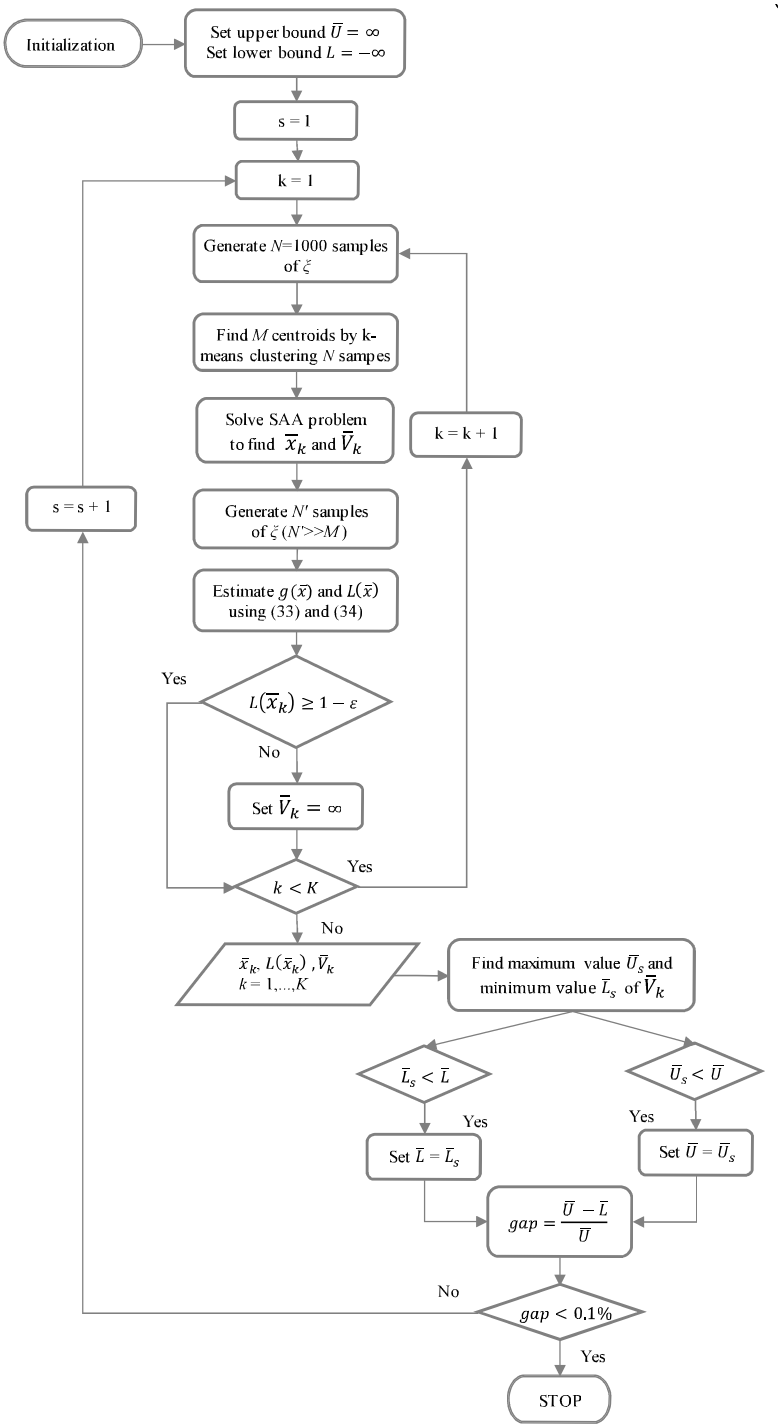


**Figure 3.9** Flow chart of the MSAA algorithm.

## 3.4 Numerical Examples

### 3.4.1 Data and Cases

The proposed method in Section 3.2 is tested on the actual power system on Phu Quy Island, Binh Thuan province, Vietnam. The risk level of the probability constraints in the second stage is 5%, which means these constraints should be met with a probability of greater than 95%. The other parameters are presented in Table 3.3.

The UC problem is implemented with wind power and demand as described in Figure 3.10. The maximum possible instantaneous penetration of wind power is approximately 45% during the first hour and highest in the fifth hour (49%). However, this ratio is only 15% when the load is highest at the 19th hour. The forecasting errors is assumed that they follow a normal distribution with zero mean and the standard deviations of 0.05 for both wind power and demand. This means that the maximum forecasting error in the values each hour can be considered to be 15% corresponding the confidence interval of 99.7%.

**Table 3.3** Input data.

| | |
|---|---|
| **Diesel generator** | $P_{max} = 500$ kW; $P_{min} = 170$ kW; $H = 0.8$ s |
| **ESS** | $\eta = 90\%$; $SoC_{min} = 10\%$; $SoC_{max} = 90\%$ |
| **Frequency criteria** | $f_{norm} = 50$ Hz ; $f_{min} = 49.2$ Hz; $f_{db} = 0.02$ Hz |

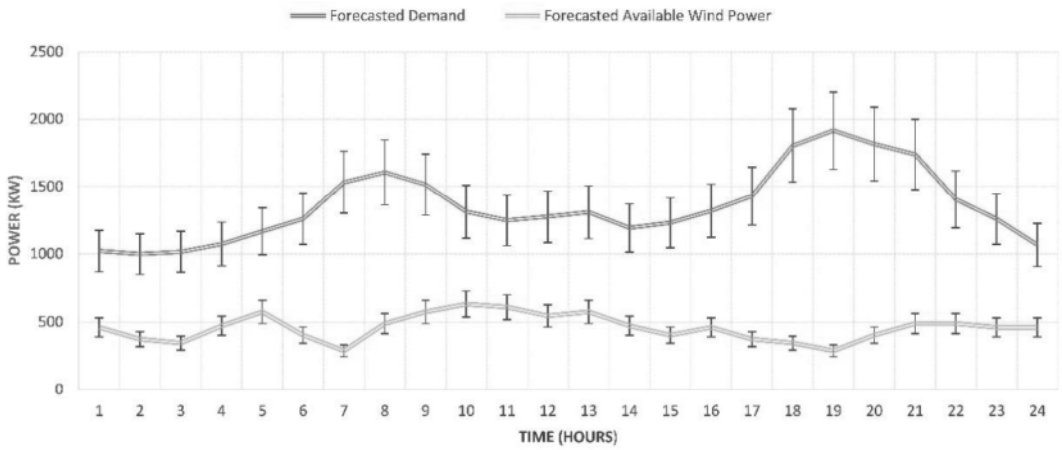


**Figure 3.10** Forecasted wind power and demand.

We evaluate the effectiveness of using ESS to provide FFR by comparing the frequency criteria after contingency and the optimal operating cost in the following cases:

- **Case 1a.** This case simulates the original UC problem without frequency constraints. The ESS is used to take advantage of wind power and compensate for the uncertainty in wind speed and demand.
- **Case 1b.** The original UC problem with frequency constraints. The ESS is not used to provide FFR.
- **Case 2.** UC problem with frequency constraints. The ESS is used to provide FFR.

Besides comparing the frequency criteria $f_{nadir}$ after a contingency event in these cases, the effects of other parameters such as ESS size are also considered. The optimization problem is solved using the MSAA approach presented in Section 3.3 with CPLEX version 12.6 and the YALMIP toolbox [91].

### 3.4.2 Results

*1. Case 1a: Original Optimal Scheduling Model Without Frequency Criteria*

With an ESS rating of 400 kW/800 kWh and the other input data given in Section 5.1, the optimal daily schedule for DGs in Case 1 is presented in Figure 3.11. Figure 3.12 shows the actual wind power and ESS charge/discharge power using box plots. It can be seen that, although the possible wind capacity and demand are uncertain, the available wind power is still fully utilized most of the time; this is undoubtedly due to the involvement of the ESS in the grid.

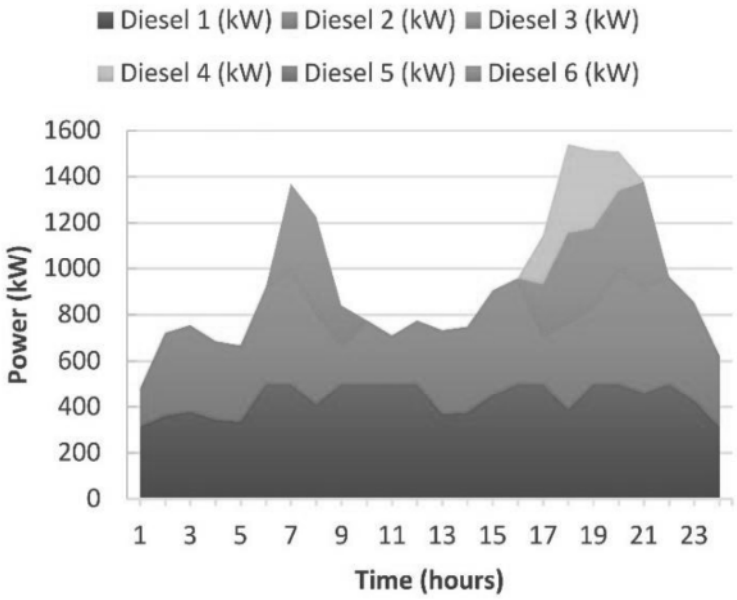


**Figure 3.11** Case 1a (frequency criteria not considered): Optimal daily schedule for the DGs

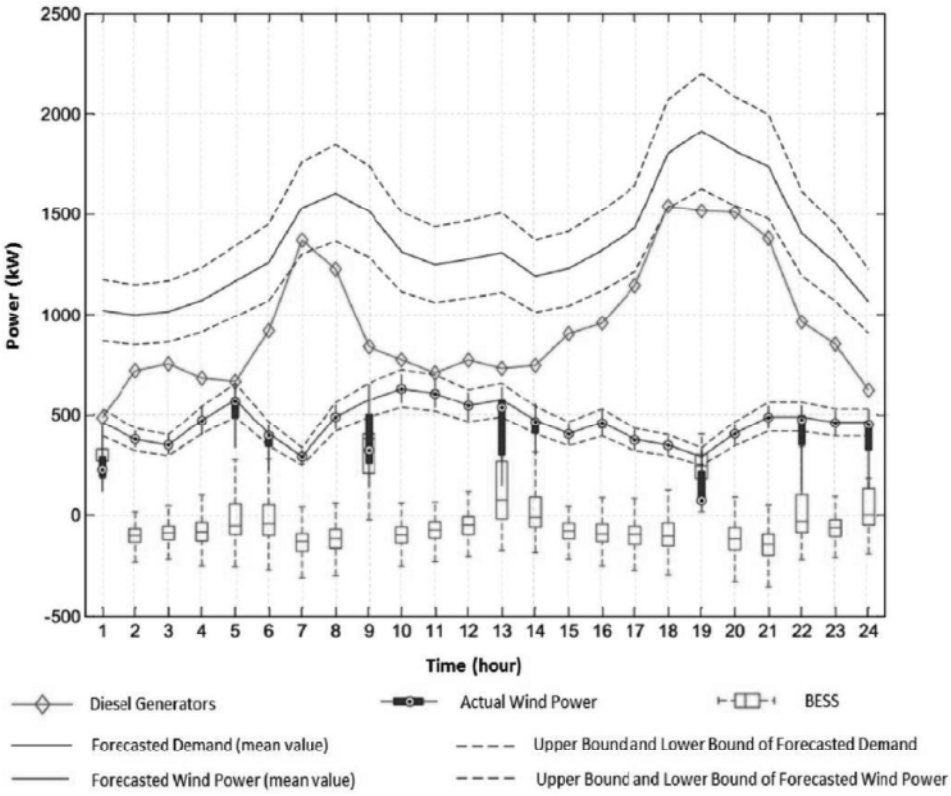


**Figure 3.12** Case 1a (frequency criteria not considered): Box plots of wind power and ESS power, DG power and forecasted demand.

The *RoCoF* immediately after a contingency event in which the DG having the largest power output is lost is presented in Figure 3.13. During the period from the 17th to the 20th hour, demand is at its highest, whereas available wind power is quite low, so four DGs are online. This means that the stored kinetic energy in this period is higher than that in the rest of the day. However, the *RoCoF* is still approximately 10 Hz/s. Although DGs can increase their power output very quickly, even from a cold start condition (10–15 s), the frequency declines rapidly to below the minimum threshold. This can be explained by the inertia constant of the DGs being small (H = 0.8), which means the total inertia of the system is also small.

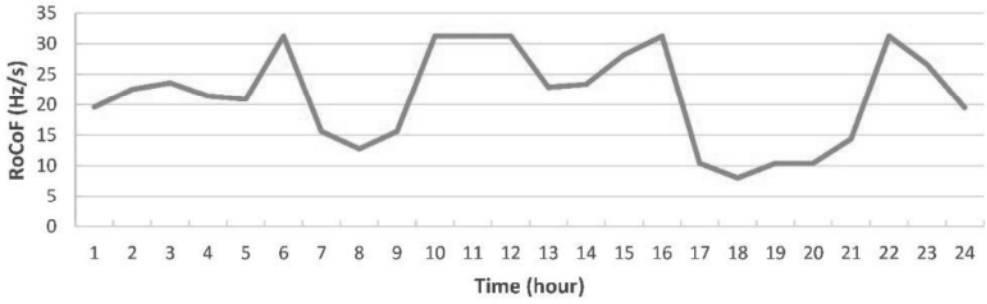


**Figure 3.13** *RoCoF* after a contingency event in Case 1a.

*2. Case 1b: Optimal Scheduling Problem Considering Frequency Criteria*

Accounting for the frequency criteria in the optimal scheduling problem, as many DGs as possible are kept online while keeping their power output at a low level (Figure 3.14 and Figure 3.15). For example, during peak load hours, there are six DGs in operation even though only four DGs are needed in Case 1a. This helps to increase the inertia of the system and reduce the *RoCoF*. The reduction of the *RoCoF* can be seen by comparing the results in Figure 3.13 and Figure 3.16. However, the frequency nadir $f_{nadir}$ at almost all hours is still much smaller than the minimum threshold $f_{min}$ (49.2 Hz). Moreover, increasing the power output of the DGs leads to higher operating costs (Table 3.4).

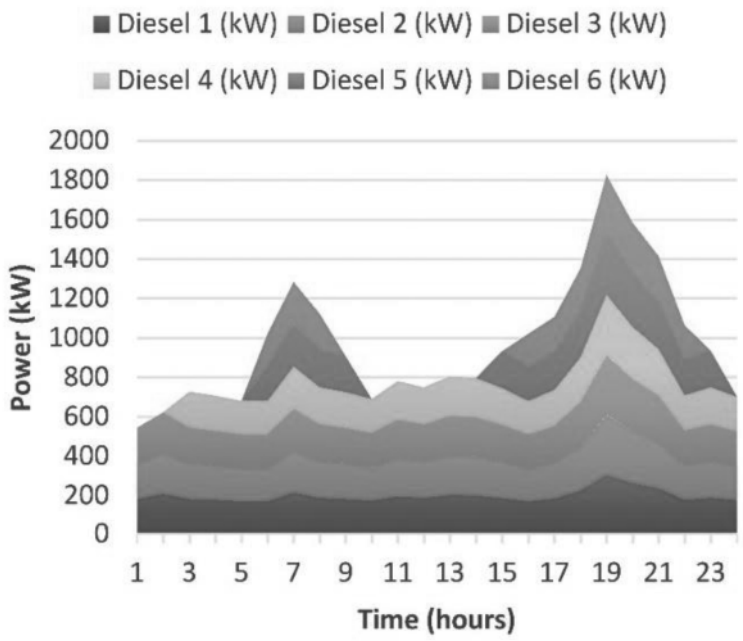


**Figure 3.14** Case 1b results (frequency criteria considered): Optimal daily schedule for the DGs

**Table 3.4** Comparison of optimal costs between Cases 1 and 2.

| | **Case 1a** | **Case 1b** | **Case 2** |
|---|---|---|---|
| **The optimal cost (USD)** | 11103 | 11376 | 11120 |

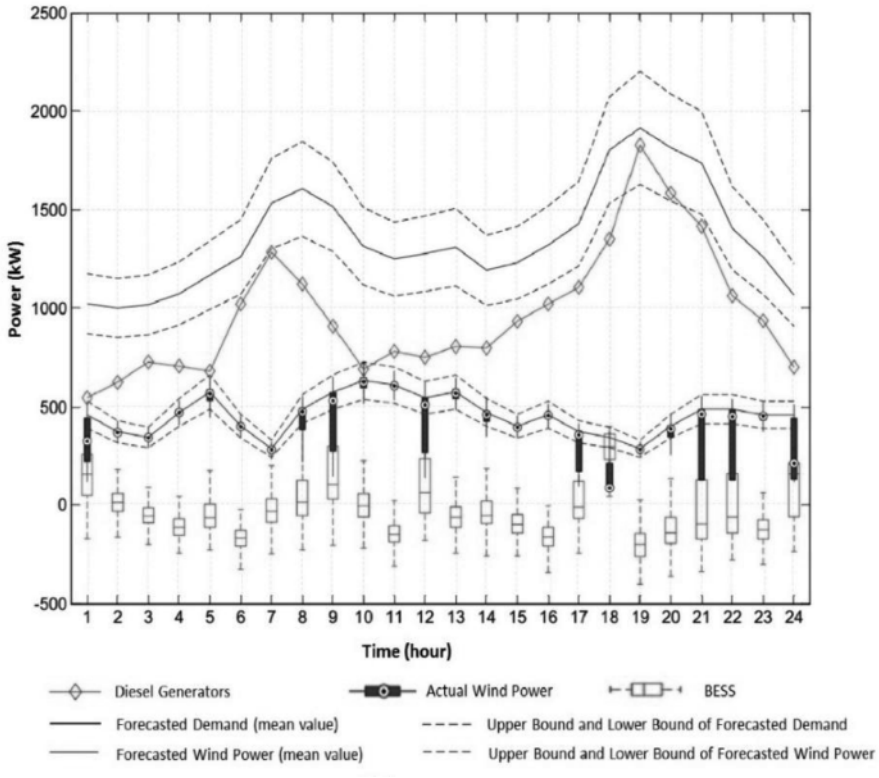


**Figure 3.15** Case 1b results (frequency criteria considered): Box plots of wind power, ESS power, DG power and forecasted demand.

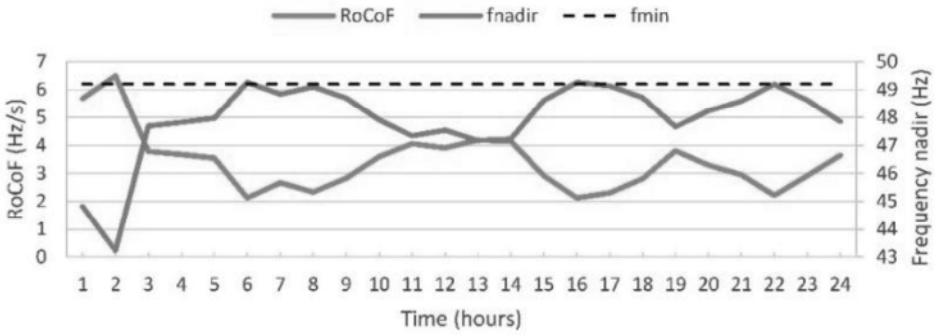


**Figure 3.16** *RoCoF* and frequency nadir for Case 1b.

*3. Case 2: Optimal Scheduling Problem Considering Frequency Criteria with FFR Provided by ESS*

As in Cases 1a and 1b, an ESS rated at 400 kW/800 kWh is used in this case. However, the ESS is not only used to maintain the power balance but also provide FFR. The optimal schedule of the DGs and box plots of the ESS and wind power for this case are presented in Figure 3.17 and Figure 3.18.

As discussed in Section 2, if the DG with the largest power output is lost, the frequency deviation will activate the ESS response, and here we assume that the total response time for FFR is 100 ms. Based on the state of the ESS before the contingency event, the charge/discharge power

of the ESS post-contingency at each hour can be in a range, as shown by the box plot in Figure 3.19. The frequency nadir values for each hour are obtained using Equation (3-8), as shown in Figure 3.20.

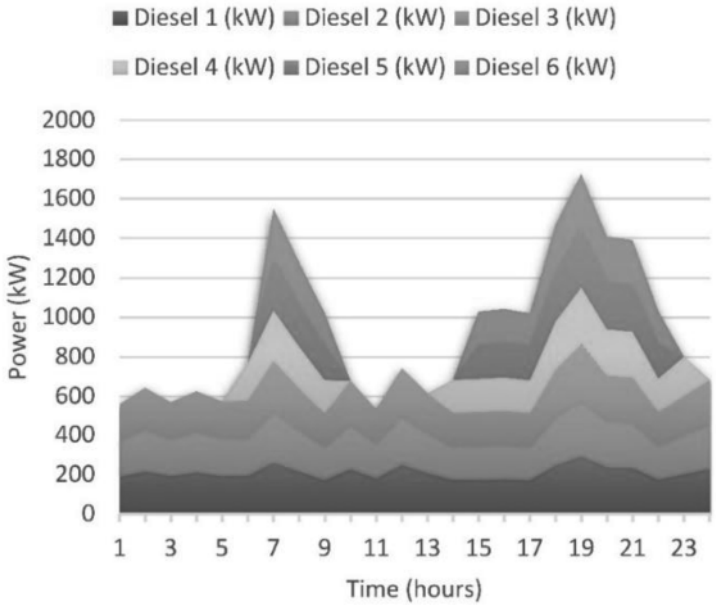


**Figure 3.17** Case 2 results: Optimal daily schedule for the DGs

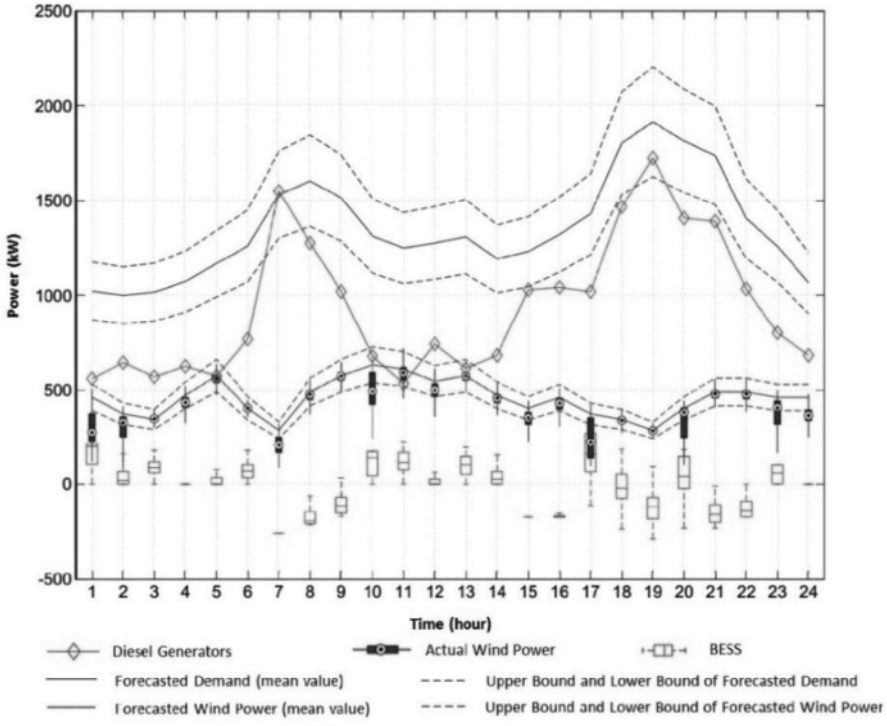


**Figure 3.18** Case 2 results: Box plots of wind power and ESS power, DG power and forecasted demand.

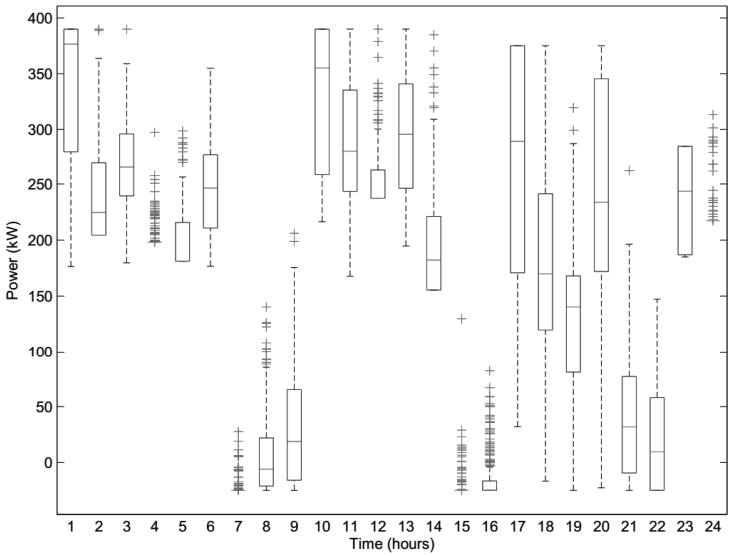


**Figure 3.19** Box plot of the ESS charge/discharge power after contingency event for Case 2.

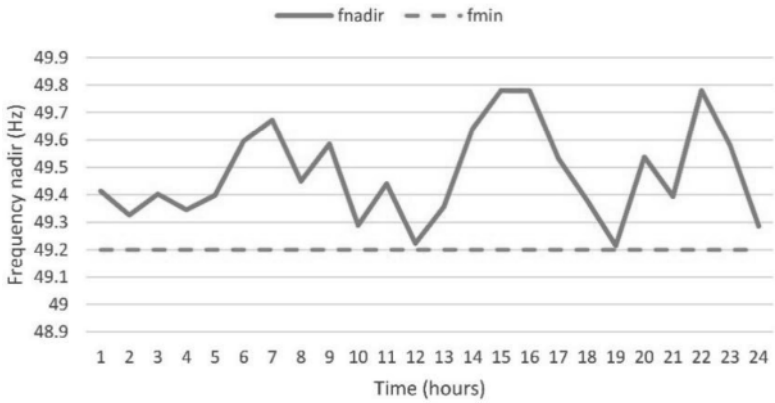


**Figure 3.20** Frequency nadir with ESS providing FFR for Case 2.

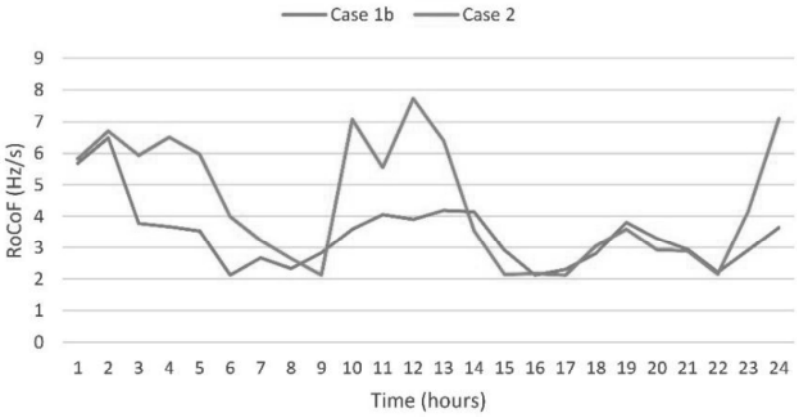


**Figure 3.21** Comparison of *RoCoF* between Cases 1b and 2.

To evaluate the effect of the ESS on FFR, we compare the *RoCoF* immediately after the contingency event for Cases 2 and 1b. Figure 3.21 shows that the *RoCoF* in Case 2 is higher than in Case 1b in a few hours. However, the frequency nadir in Case 2 is ensured, while it is violated in several hours in Case 1b.

Note that constraints (3-20) and (3-27) in the optimization formulation limit the power output of each DG. This explains why the number of hours with six DGs in operation in Case 2 is more than that in Case 1b. In contrast, when the demand is low, the ESS support in Case 2 helps to ensure the frequency criteria after a contingency event even when the number of online DGs is less than in Case 1, thus ensuring maximum utilization of the available wind power. This can be seen by comparing the box plots of wind power in Figure 3.15 and Figure 3.18. It is interesting to note that, when the ESS is able to provide FFR, the UC solution will reduce DGs uptime and increase the wind power/ESS output, which in turn reduces the operating cost. The op timal cost of Case 2 is smaller than that of Case 1b and is not significantly higher than the non-constrained optimal cost (Table 3.4).

*4. Impact of ESS Size and Response Time*

In this section, we consider the effect of the ESS size and the total response time from the moment the contingency event occurs until the ESS fully responds. Table 3.5 shows the smallest possible value of the frequency nadir for two total response times, 100 ms and 200 ms, and several ESS sizes, which are defined by the charge/discharge power rating $P_{SSmax}$ and the full charge or discharge duration $E_{SSmax}/P_{SSmax}$ (from 0.5 h to 4 h). It can be seen that the ESS size must be larger than 200 kW/400 kWh to ensure the problem has a feasible solution. It should also be noted that the forecast errors are assumed to be ±15%, so too small an ESS will not be able to compensate for the mismatch between the predicted and actual values of the load and wind power. However, even if the optimization problem has a feasible solution, depending on the size of the ESS, there will still be a nonzero probability that the frequency nadir is lower than the minimum threshold (these values are shown in red in Table 3.5). The reason for this is that the frequency nadir constraint (3-27) is formulated as a probabilistic constraint with a risk level of 5%. On the other hand, constraint (3-27)shows that a longer response time requires a lower power output from each DG or more DGs in operation to provide enough kinetic energy; consequently, increasing the ESS power rating is necessary. It can be seen from the results in Table 3.5 that when the response time is 200 ms, the power rating of the ESS must be larger than 600 kW to maintain the frequency nadir above 49.2 Hz, whereas an ESS with rated power 400 kW is acceptable if the response time is 100 ms.

**Table 3.5** Summary of frequency nadir for different ESS sizes and response times.

| **Response time** | **ESS Parameters** | | **Lowest possible value of frequency nadir (Hz)** | | | | |
|---|---|---|---|---|---|---|---|
| **100 ms** | $P_{SSmax}$ | | **200 kW** | **400 kW** | **600 kW** | **800 kW** | **1000 kW** |
| | $\frac{E_{SSmax}}{P_{SSmax}}$ | **0.5 h** | x | 48.91 | 49.22 | 49.22 | 49.22 |
| | | **1 h** | x | 49.09 | 49.22 | 49.22 | 49.22 |
| | | **2 h** | x | 49.21 | 49.23 | 49.22 | 49.22 |
| | | **3 h** | 49.08 | 49.22 | 49.22 | 49.23 | 49.22 |
| | | 4 h | 49.09 | 49.14 | 49.35 | 49.22 | 49.22 |
| **200 ms** | $P_{SSmax}$ | | **200 kW** | **400 kW** | **600 kW** | **800 kW** | **1000 kW** |
| | $\frac{E_{SSmax}}{P_{SSmax}}$ | **0.5 h** | x | 48.67 | 48.69 | 48.69 | 49.27 |
| | | **1 h** | x | 48.67 | 48.97 | 49.20 | 49.27 |
| | | **2 h** | x | 48.99 | 49.01 | 49.25 | 49.22 |
| | | **3 h** | 48.77 | 48.85 | 49.15 | 49.22 | 49.30 |
| | | **4 h** | 48.79 | 48.89 | 49.27 | 49.26 | 49.27 |
| x: Infeasible | | | | | | | |

*5. Comparison Between the MSAA, SAA, and the Robust Chance-Constrained Algorithms*

Case 2 was solved by the traditional SAA algorithm and the MSAA algorithm to compare their computational efficiency. We realize that to solve Case 2, the SAA algorithm must be repeated at least 50 times per loop (K = 50) and needs at least 100 samples per loop (N = 100). On the other hand, the original set of 1000 samples can be replaced with five centroids, and the MSAA algorithm must be repeated 50 times to obtain the results. Interestingly, five centroids in the MSAA algorithm are equivalent to five samples in the SAA algorithm; thus, it is easy to see that the computing time required for the MSAA algorithm is much smaller than that required for the SAA algorithm (Table 3.6), which demonstrates the efficiency of the MSAA algorithm.

The performance of the proposed MSAA is also compared with that of the Robust chance-constrained formulation, which is also a popular approach. In this comparison, a two-stage robust

chance-constrained model, solved by column-and-constraint generation algorithm (CCG) [92]–[94], is implemented. The constraints related to power balance and frequency criteria are also formulated as probability constraints with the same risk level. Besides, the results obtained with a two-stage robust model is also shown. The results in Table 3.6 clearly demonstrate the compromise between CPU time and economic performance: although the required CPU time for MSAA is longer than the robust method, the optimal cost obtained by MSAA is significantly lower than both robust models—with or without chance constraints.

**Table 3.6** Comparison of computing time between the MSAA, SAA, and the robust method

| Method | N | M | N' | K | S | CPU Time (s) | Optimal cost (USD) |
|---|---|---|---|---|---|---|---|
| **SAA** | 100 | - | 1000 | 50 | 1 | 2950 | 11154 |
| **MSAA** | 1000 | 5 | 1000 | 50 | 1 | 853 | 11120 |
| **Robust chance constrained UC** | - | - | - | - | - | 8 | 12196 |
| **Robust UC** | - | - | - | - | - | 8 | 14435 |

## 3.5 Summary

In this chapter, an optimal day-ahead scheduling problem concerning the application of ESS for FFR is considered and analyzed in detail. The optimization problem is formulated within a two-stage chance-constrained framework, in which the load and the maximum possible wind power are uncertain. The relationships between the power output of each DG, the ESS charge/discharge power, and the response time are studied. The impact of the size and response time of the ESS on the frequency nadir after the sudden loss of a DG is also analyzed. It is also noteworthy that an MSAA approach was proposed in the present study to solve a chance-constrained problem, and the effectiveness of this method was demonstrated.

The results obtained in two cases—with and without FFR provided by ESS—demonstrate the effectiveness of FFR in arresting frequency deviations after a contingency event. The proposed method ensures that the minimum frequency threshold is not violated, even when the actual values of wind power and demand are different from the predicted values incorporating the predetermined maximum errors. The results also show that a slower FFR requires a larger ESS to ensure frequency criteria.

The proposed approach can be extended to consider multiple contingencies such as line outages or load interruptions as well as equipment failures. The model can also be readily

adapted to include other uncertain factors, such as solar power generation or electricity prices. These topics are left for future work.

# Chapter 4 Short-term Optimal Operation of the Small Island Power System Using a Multi-Parametric Programming Framework

## 4.1 Introduction

As mentioned in Chapter 3, to account for the uncertainty in demand and RES, the UC problem is commonly formulated as a two-stage optimization model. In this model, the first variables such as the commitment of generators are decisions predetermined before the uncertainty is revealed and the solution has a unique value for each first-stage variable. In contrast, the second-stage variables including ESS and RES power are expressed as ranges of values because they are decided after the actual demand and available RES power are known. The authors of [95] surveyed the methods of solving the UC problem considering the uncertainty and found that although this problem is addressed in many previous studies, most of them only determine and fix the solution of first-stage variables. Therefore, only the value of the first variables is meaningful in the actual operation.

Noting that the day-ahead scheduling problem is based on the day-ahead forecast of demand and RES power. It is easy to see that a longer prediction horizon leads to less accurate forecasting results. Thus, although the day-ahead UC is a common problem in the power system operation, its results still have limited significance in practice. In fact, to solve the above issues, the UC problem is combined with a rolling horizon approach and implemented on different time frames [96]–[99]. The concepts of this approach are to repeat the UC problem periodically and get the latest updated forecasted value of the demand and RES as the input parameters. The time interval of the UC problem depends on the prediction horizon of the uncertain parameters [100]. The authors of [101] show that there are five time-scale horizons used in the actual California system (Figure 4.1). In this system, the day-ahead UC for 1-hour intervals on an operating day must be implemented before 10:00 a.m on the previous day. Besides, the short-term/real-time schedules (STUC/RTUC) is taken for 15-minute interval based on 8 hours-ahead wind forecast. The real-time dispatch (RTED) is repeated every 5 minutes and based on 1 hour-ahead wind forecast. The last problem is regulation REG that is taken every 4 seconds and belongs to control issues. The second variables in the day-ahead UC will be determined in the STUC/RTUC or RTED.

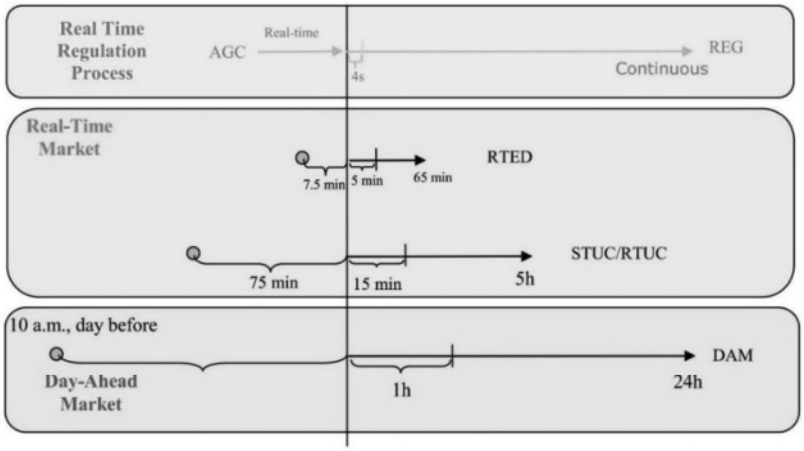


**Figure 4.1** The scheduling process in the California grid with different time intervals [101]

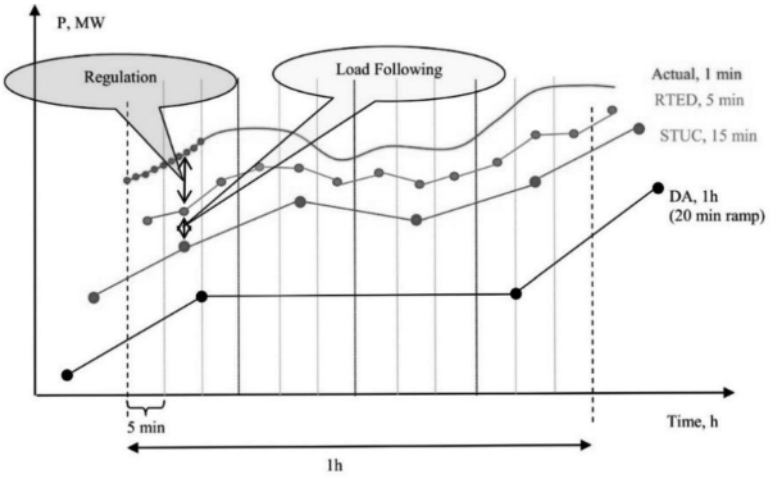


**Figure 4.2** Generation Dispatch Components with different time intervals [101]

On the other hand, there are two kinds of forecasting results: point forecast and interval forecast. Some previous studies used the point forecast of RES and demand to solve the scheduling problem [99], [102]. The deterministic UC problems with different time intervals are implemented and then sent an adjustment control signal to generators, RES or ESS. This means that 75 minutes ago, the system is expected to be set up in the first state (the blue line in Figure 4.2); up to 8 minutes ago, the system is set up again in the second state (the green line) and when the system operates in real time, the system is in the third state (the red line). It is easy to see that if the prediction error is high, the distance between the real-time operating state and the planned operating state becomes wide and leads to a possible power imbalance due to insufficient reserve capacity.

In order to avoid power imbalance in real-time operation, recent studies have considered uncertainty parameters in short-term problems as STUC/RTUC or RTED. The authors of [96], [103] formulated the wind power forecast model as a Markov decision process which considers the state-transition matrix from wind power at time t to wind power at time t+1. In this method,

the wind power at each time step is approximated by a number of states. The advantage of this method is to account for the correlation between two states of wind power at two steps. However, to increase the accuracy of the result, we need to use more states at each time step so that the computing time will be longer.

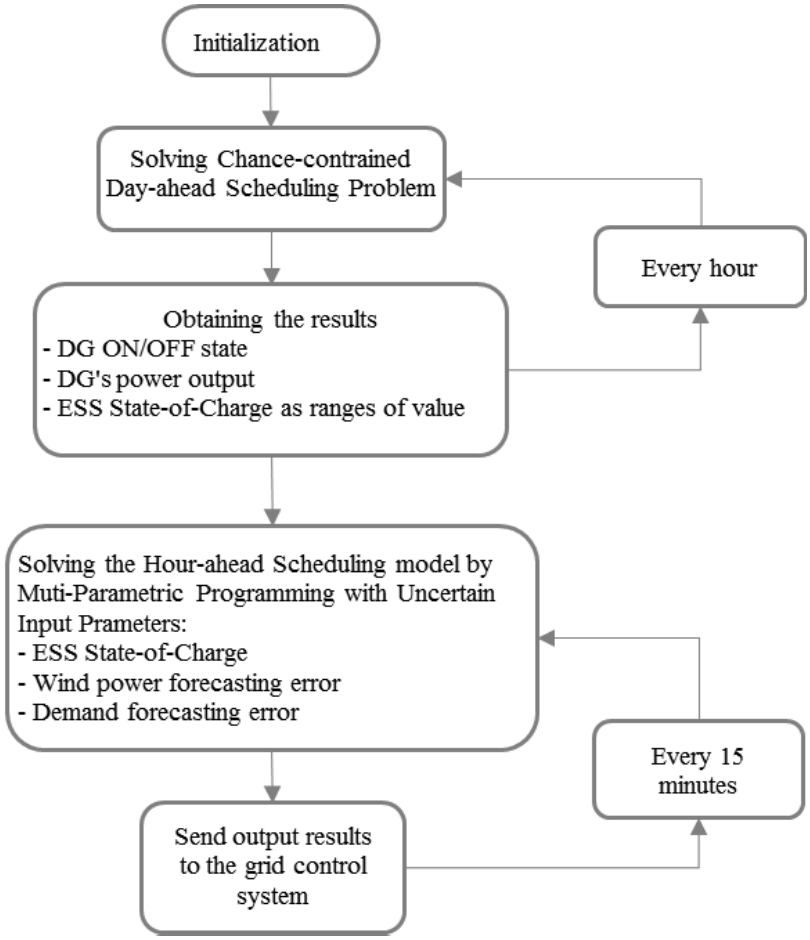


**Figure 4.3** The correlation between the day-ahead UC and short-term UC

Another method was used in STUC/RTUC model is Multi-Parametric Programming (MPP). This method finds the relationship between the output data and the uncertain input data. The results are flexible and close to the control problem. In fact, there are a few studies using this method to solve the short-term/real-time problem [97]

This research proposes a short-term scheduling model that can be considered as the second stage of the day-ahead scheduling problem presented in Chapter 3 and solved by Multi-Parametric Mixed Integer Linear Programming (mp-MILP). While the day-ahead UC is rescheduled every hour, the short-term schedule is repeated every 15 minutes and based on the one hour-ahead forecasting results (Figure 4.3). Besides considering the FFR provided by ESS, this model also takes into account the adjustment of the power output of DGs. Note that although the output of DGs was determined from the day-ahead UC problem in the previous chapter, this

adjustment is still necessary due to the difference between the long-term and short-term forecasts values of wind and demand.

## 4.2 Problem Description

### 4.2.1 Nomenclature

**Indices and Sets**

| | |
|---|---|
| $i \in I$ | Diesel generators |
| $t \in T$ | 15-minnute intervals in the considered one-hour interval, $T = \{1,2,3,4\}$ |
| $w \in W$ | Wind generators |
| $\xi$ | Random vector |

**Constants**

| | |
|---|---|
| $C$ | Operating cost of diesel generator ($/kWh) |
| $C_{SSc}$ | Charge cost of energy storage ($/kWh) |
| $C_{SSd}$ | Discharge cost of energy storage ($/kWh) |
| $P_{maxi}$ | Maximum power output of diesel generator *i* (kW) |
| $P_{mini}$ | Minimum power output of diesel generator *i* (kW) |
| $P_{Wmin}$ | The minimum power output of WG (kW) |
| $P_{SSmax}$ | Power rating of energy storage system (kW) |
| $E_{ssmax}$ | Capacity of energy storage system (kWh) |
| $\eta$ | Charging/discharging efficiency of energy storage system |
| $f_{norm}$ | Nominal frequency (Hz) |
| $f_{min}$ | Minimum frequency threshold (Hz) |
| $f_{db}$ | Dead band of governor (Hz) |
| $K$ | The system ramp rate which is determine from Chapter 3 (kW/s) |
| $t_d$ | The governor's dead time, which corresponds to the frequency dead band $f_{db}$ |
| $t_{nadir}$ | The time at nadir which is determined in Chapter 3 |

**Semi-constants**

| | |
|---|---|
| $P_{Wf}^{t}$ | Short-term forecast wind power at step *t* (kW) |

$P_{W-error\ max}^{t}$ The upper bound of the short-term forecast error of wind power at step $t$ (%)

$P_{W-error\ min}^{t}$ The lower bound of the short-term forecast error of wind power at step $t$ (%)

$P_{Df}^{t}$ Short-term forecast demand at step $t$ (kW)

$P_{D-error\ max}^{t}$ The upper bound of the short-term forecast error of demand at step $t$ (%)

$P_{D-error\ max}^{t}$ The lower bound of the short-term forecast error of demand at step $t$ (%)

$w_i$ ON/OFF state of diesel generator $i$ within the considered one-hour interval (binary)

$P_i$ Power output of diesel generator $i$ within the considered one-hour interval (kW)

$u_w$ ON/OFF state of wind turbine within the considered one-hour interval (binary)

$E_{SSmax}^{begin}$ Maximum energy stored in the energy storage system at the begin of the considered one-hour interval (kWh)

$E_{SSmin}^{begin}$ Minimum energy stored in the energy storage system at the begin of the considered one-hour interval (kWh)

$E_{SSmax}^{end}$ Maximum energy stored in the energy storage system at the end of the considered one-hour interval (kWh)

$E_{SSmin}^{end}$ Minimum energy stored in the energy storage system at the end of the considered one-hour interval (kWh)

**Uncertain Input Parameter**

$P_{W-error}^{t}$ Forecast error of wind power at step $t$ (kW)

$P_{D-error}^{t}$ Forecast error of demand at step $t$ (kW)

$E_{SS}^{t-1}$ Energy stored in the energy storage system at the begin of step $t$ (kWh)

**Variables**

$P_{DGs-adjust}^{t}$ The adjustment power provided by DGs at step $t$ (kW)

$P_{w}^{t}$ Actual wind power at step $t$ (kW)

$u_{SS}^{t}$ Charging state of energy storage system at step $t$ (binary)

$P_{SS}^{ch,t}$ Charge power of energy storage system at step $t$ (kW)

$P_{SS}^{disch,t}$ Discharge power of energy storage system at step $t$ (kW)

$P_{dispost}^{t}$ Discharge power of energy storage system after a contingency event at step $t$ (kW)

$E_{SS}^{t}$ Energy stored in the energy storage system at the end of step $t$ (kWh)

### 4.2.2 Mathematical Formulation

Figure 4.4 illustrates the short-term scheduling problem in this research. Note that the unit commitment and power output of each DG are predetermined after solving the chance-constrained day-ahead UC problem in Chapter 3 . Besides, the upper bound and lower bound of the energy stored at the end of each one-hour interval (or at the begin of next one-hour interval), which is also obtained by this day-ahead UC problem, are used as the input data. When implementing the short-term scheduling problem, the newest forecasting value of wind power and demand are updated. However, these forecasting results always have errors, which can be called the uncertainty in wind power and demand. Thus, the power imbalance may occur and an adjustment $P_{DGs-adjust}^{t}$ from DGs is necessary. In this model, the uncertain input parameters are the energy stored in the ESS( $E_{SS}^{t-1}$) at the begin of each 15-minute interval and the forecasting errors of wind and demand ($P_{W-error}^{t}$ and $P_{D-error}^{t}$). The results are the functions of ESS state ($P_{SS}^{ch,t}$, $P_{SS}^{disch,t}$, $E_{SS}^{t}$), the adjusted power $P_{DGs-adjust}^{t}$ and the WG power output $P_{w}^{t}$ at each step $t$ within the considered one-hour interval. This model will be implemented for each step $t$ separately.

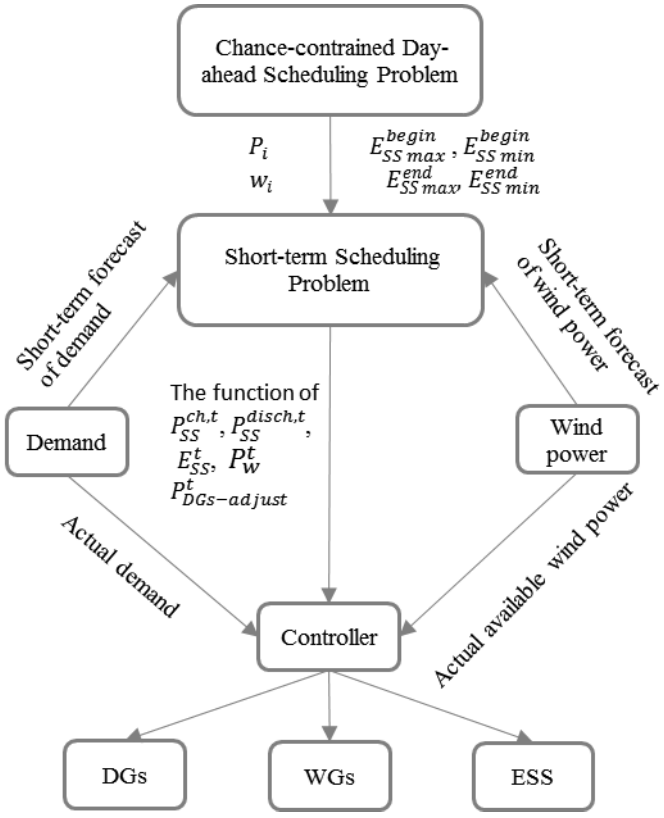


**Figure 4.4** Schematic illustrating the short-term scheduling problem

*1. Objective Function*

The objective function to be minimized comprises the operating cost including the ESS charge/discharge power and the absolute value of the adjustment provided by DGs. Particularly, this objective function makes sure that DGs power output is adjusted as little as possible. It can be explained that DGs power output is treated as the first-stage variable in the day-ahead UC formulation presented in Chapter 3 .

$$Minimize \left|CP_{DGs-adjust}^{t}\right| + C_{SSc}P_{SS}^{ch,t} - C_{SSd}P_{SS}^{disch,t} \tag{4-1}$$

*2. Constraints*

- **Active power balance constraint.** The total given active power output from the DGs $P_i$, the adjustment from DGs $P_{DGs-adjust}^{t}$, the wind plant $P_w^t$, and the storage system ($P_{SS}^{disch,t}$ and $P_{SS}^{ch,t}$) must equal the load $P_{Df}^{t}$ at any step *t*:

$$\sum_i P_i + P_{DGs-adjust}^{t} + P_w^t + P_{SS}^{disch,t} - P_{SS}^{ch,t} = P_{Df}^{t} + P_{D-error}^{t} \tag{4-2}$$

- **DG adjustment constraints.** This constraint ensures that the adjusted power is provided by the online DGs. No DG need to be startup to provide this adjustment

$$\sum_i (P_{\min i} - P_i) w_i^t \le P_{DGs-adjust}^{t} \le \sum_i (P_{\max i} - P_i) w_i^t \tag{4-3}$$

- **WG constraints**

$$u_w P_{Wmin} \le P_w^t \le u_w (P_{Wf}^{t} + P_{W-error}^{t})$$

- **Forecasting available wind power constraint.**

$$P_{W-error\ min}^{t} \le P_{W-error}^{t} \le P_{W-error\ min}^{t} \tag{4-4}$$

- **Forecasting demand constraint.**

$$P_{D-error\ min}^{t} \le P_{D-error}^{t} \le P_{D-error\ min}^{t} \tag{4-5}$$

- **ESS constraints.** The charging and discharging power of the ESS must be smaller than the actual power rating of the storage device $P_{SSmax}$. Besides, the energy stored in ESS is limited by the rated capacity $E_{ssmax}$. However, at the begin and the end of the considered one-hour period, this coefficient is limited by the lower bound and the upper bound determined in the chance constrained day-ahead UC problem. We have the following constraints:

$$\begin{cases} 0 \le P_{SS}^{ch,t} \le u_{SS}^{t} P_{SSmax} \\ 0 \le P_{SS}^{disch,t} \le (1 - u\ \ ) P_{SSmax} \end{cases} \tag{4-6}$$

$$E_{SS}^{t} = E_{SS}^{t-1} + 0.25 \times \eta P_{SS}^{ch,t} - 0.25 \times P_{SS}^{disch,t} / \eta \tag{4-7}$$

- With t=1

$$\begin{cases} E_{SS\,min}^{begin} \le E_{SS}^{t-1} = E_{SS}^{begin} \le E_{SS\,max}^{begin} \\ 0 \le E_{SS}^{t} \le E_{ssmax} \end{cases} \quad (4\text{-}8)$$

- With t=2 and 3

$$\begin{cases} 0 \le E_{SS}^{t-1} \le E_{ssmax} \\ 0 \le E_{SS}^{t} \le E_{ssmax} \end{cases} \quad (4\text{-}9)$$

- With t=4

$$\begin{cases} 0 \le E_{SS}^{t-1} \le E_{ssmax} \\ E_{SS\,min}^{end} \le E_{SS}^{t} \le E_{SS\,max}^{end} \end{cases} \quad (4\text{-}10)$$

- **Frequency nadir limit.** Continuing the research in Chapter 3 , to ensure that the frequency does not drop below the minimum allowable level after the loss of a DG $P_j$, the following constraint must be satisfied:

$$P_{dispost}^{t} - \left(P_{SS}^{disch,t} - P_{SS}^{ch,t}\right) = P_j - K(t_{nadir} - t_d) \quad (4\text{-}11)$$

- **Post-contingency energy storage capacity constraint.** After providing FFR within $\Delta t_{FFR}$, the remaining energy in the ESS must satisfy the following constraint:

$$0 \le E_{SS}^{t} - P_{dispost}^{t} \Delta t_{FFR} \le E_{SSmax} \quad (4\text{-}12)$$

### 4.2.3 Multi-Parametric Programming Framework

Particularly, MPP has received considerable attention in previous studies [97], [104]–[106] with widely application in control fields, however, using MPP in scheduling is still limited. Basically, MPP is implemented based on the concept of critical region, which is a part of the space of input parameters (Figure 4.5). In each CR, decision variables are defined as a function of input parameters. The authors of [107] presented a simple algorithm to determine CRs and solve mp-LP/MILP. Besides, an algorithm for a MILP is also presented in [108]. Based on [107], [108], we present the theory of MPP for MILP in a simple way as follow.

Firstly, to determine CRs, we consider a simple mp-LP problem as follow

$$\min_{x} \; z = c^T x \quad (4\text{-}13)$$

Subject: $Gx \le w + F\theta$

$\theta \in K$

Where $x$ are optimization variables; $\theta$ are parameters and $K$ is the region of parameter $\theta$

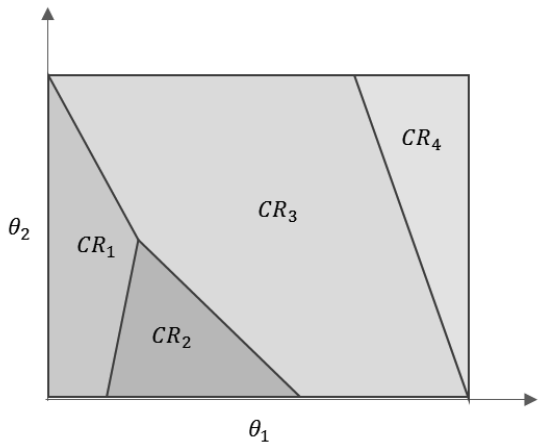


**Figure 4.5** The space of uncertain input parameters and critical regions

We denote $K^* = \{\theta \in K | \exists x \; satisfying \; Gx \leq w + F\theta\}$ is the region of parameter $\theta$ such that (4-13) is feasible.

Let $J = \{1 \div m\}$ be the set of constraint indices. Assuming that $x^*(\theta)$ and $z^*(\theta)$ as solution and optimal value of (4-13) with given $\theta$. It is easy to see that there is a set of constraints $A$ that is active at $x^*(\theta)$.

$$A = \{j \in J | G_j x^*(\theta) = w_j + F_j \theta \} \tag{4-14}$$

The critical region $CR_A$, which is related the set of constraints $A$, is defined as all value of $\theta$ such that all constraints that belong to set $A$ are active at the optimum of (4-13).

Problem (4-13) has dual formulation (4-15) with dual variables $y$

$$\underset{y}{\text{Max}} \;\; z = (w + F\theta)^T y \tag{4-15}$$

Subject

$$G^T y = c$$
$$y \leq 0$$

Choose an arbitrary value $\theta_0 \in K^*$and solve both primary and dual problems (4-13), (4-15) for $\theta = \theta_0$. Let $x_0^*$ and $y_0^*$ are optimal solution of primary and dual problem, respectively. We determine the $CR_{A(\theta_0)}$ as follow:

$$CR_{A(\theta_0)} = A = \{j \in J | G_j x_0^* = w_j + F_j \theta_0 \}$$

The value function in $CR_{A(\theta_0)}$ is defined by dual formulation (4-15) :

$$z^*(\theta) = (w + F\theta)^T y_0^* \tag{4-16}$$

Optimal solution $x^*$ is defined as follow.

$$G_j x^*(\theta) = w_j + F_j \theta \quad \text{with } j \in A \tag{4-17}$$

Now we consider a simple mp-MILP formulation as follow

$$\min_{z} \; z = c^T x + d^T b \tag{4-18}$$

Subject: $Gx + Hb \leq w + F\theta$

$\theta \in K; \; b \in \{0,1\}$

The authors of [108] proved that the problem (4-18) can be solved by the following steps:

- Step 1: Solve (4-18) considering $\theta$ as free variables. Let $b_0$ be the optimal integer solution.
- Step 2: Fixing $b = b_0$ and solve (4-18) as a mp-LP to find CRs and the optimal solution $x^*(\theta)$ and the optimal value $z^*(\theta)$ in each CR.
- Step 3: In each $CR_j$ obtained in step 2, we add an integer cut which is infeasible at the integer solution $b_0$ in step 1. Solve (4-18) for each $CR_j$ considering $\theta$ as free variables.
    - If in $CR_j$ , (4-18) is infeasible then the solution obtained in step 2 is the final solution.
    - If in $CR_j$ , (4-18) is feasible then we obtain new integer solutions of $b$. Solve step 2 with new integer solutions of $b$ to find new optimal value $z^*_{new}(\theta)$. Compare $z \quad (\theta)$ and old optimal value $z^*_{old}(\theta)$. If $z^*_{new}(\theta) < z^*_{old}(\theta)$, obtain new solution and new CR.
- Repeat step 2 and step 3 until no new solution of $b$ can be found.

## 4.3 Numerical Examples

In this chapter, we use the parameters and the results which obtained in Chapter 3 . Without loss of generality, we implement the short-term scheduling for the first 15-mintue interval of the third one-hour interval of the day-ahead UC model. At the time of this process, the newest forecast values of wind power and demand are updated. Assuming that the short-term forecast values of demand and wind power are as shown in Table 4.1. The optimization problem is solved by CPLEX version 12.6, the YALMIP toolbox and the Multi-Parametric Toolbox 3.0 [108].

**Table 4.1** The results obtained in the day-ahead UC problem and the newest forecast data

| | |
|---|---|
| **Diesel generator** | Three DGs are online with $P_i = 189.75$ kW |
| **ESS** | $E^{begin}_{SSmin} = 125.03$ kWh; $E^{begin}_{SSmax} = 568.78$ kWh |
| **Short-term wind power forecast** | $P^t_{Wf} = 402.15$ kW |
| **Short-term demand forecast** | $P^t_{Df} = 1073$ kW |

We analyze two cases of the short-term forecasting errors: **1)** within -5~5% for both demand and wind power; **2)** within -15~15% for both demand and wind power

Now we focus on the first case: the short-term forecasting errors are within -5~5% for both demand and wind power. With the input data illustrated in Table 4.1, we obtain 3 CRs illustrated in Figure 4.6. Table 4.2 present the function of these output data in detail. Figure 4.7 shows that the WG's power output, the ESS charge/discharge power and the DGs adjustment in case the short-term forecasting error of WG is zero. It can be seen that the results are suitable to the variation of demand and ESS energy: if demand is lower than forecasted value and energy stored in ESS is high, the power output of WG is kept at low level. In contrast, WG's power output increases in the opposite case: demand is higher than in forecasted value and ESS energy is lower than 200kWh. Besides, the power output of DGs is almost unchanged. However, in CR2, the load is much higher than the short-term forecast value while the energy stored in the ESS is quite low. On the other hand, the ESS must always keep an amount of energy for FFR in the case of N-1 contingency event. Thus, not only the entire available wind power used but also DGs have to generate an additional amount. The slice at the ESS' energy equal to 130 kW in Figure 4.8 shows more clearly the variability of DGs adjustment and WG output in CR2.

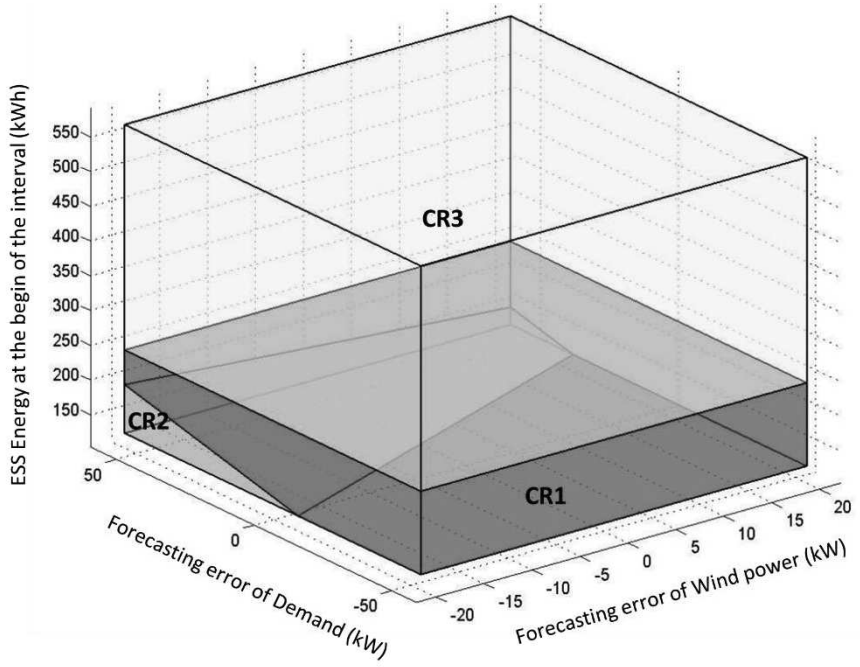


**Figure 4.6** Critical Regions in case the maximum forecasting errors are within -5~5%

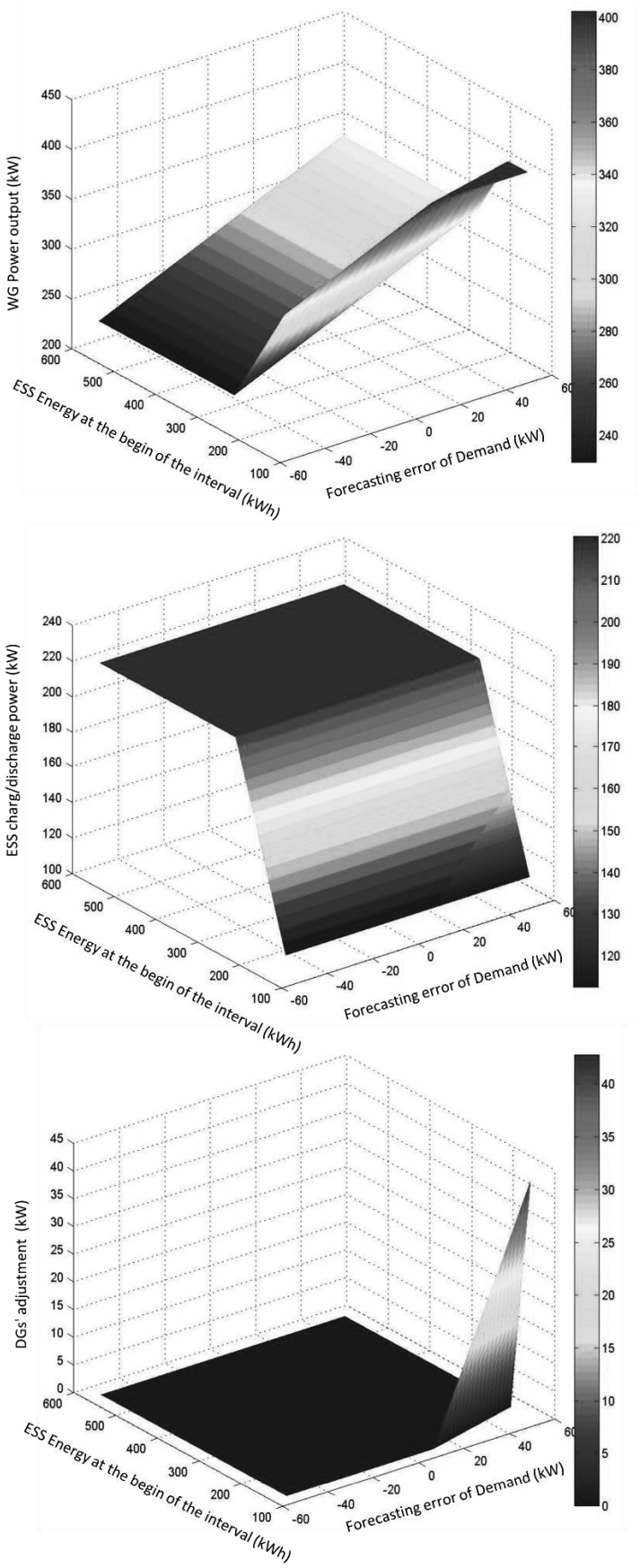


**Figure 4.7** The WG's power output, the ESS charge/discharge power and the DGs adjustment in case the short-term forecasting error of wind power is 0 kW.

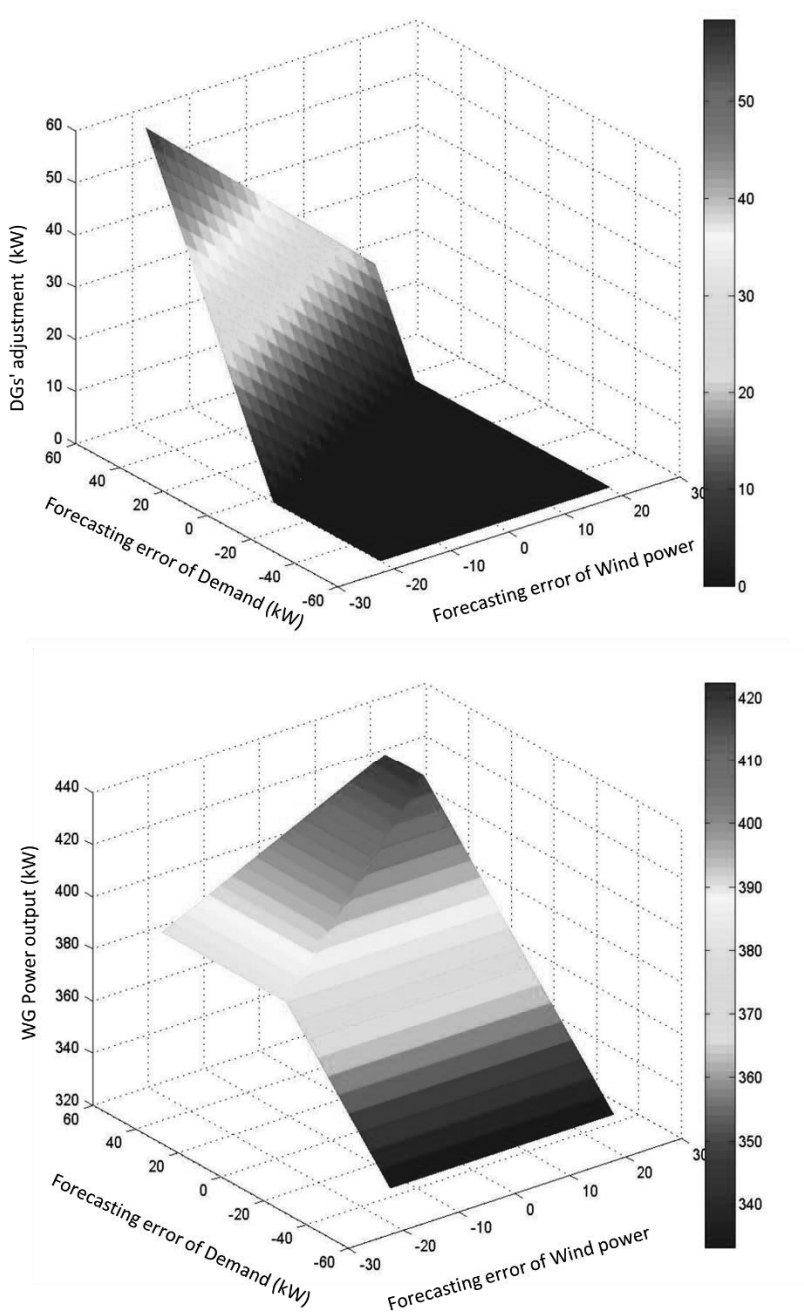


**Figure 4.8** The WG power output and the DGs' adjustment in case the energy stored in the ESS is 130 kW

**Table 4.2** The constraints of each CR and the function of the output data in case the maximum forecasting errors are within -5~5%

| | CR's Constraints | Output Data |
|---|---|---|
| **CR1** | $-20.1075 \leq P_{W-error} \leq 20.1075$<br>$-53.65 \leq P_{D-error} \leq 53.65$<br>$125.03 \leq E_{SS}^{begin} \leq 244.73$<br>$-0.597P_{W-error} + 0.597P_{D-error} - 0.537E_{SS}^{begin} \leq -60.61$ | $P_w = P_{D-error} - 0.9E_{SS}^{begin} + 503.75$ kW<br>$P_{SS}^{disch} = 0.9E_{SS}^{begin}$ kW;<br>$P_{SS}^{ch} = 0$ kW<br>$P_{DGs-adjust} = 0$ kW |
| **CR2** | $-20.1075 \leq P_{W-error} \leq 20.1075$<br>$P_{D-error} \leq 53.65$<br>$125.03 \leq E_{SS}^{begin}$<br>$0.597P_{W-error} - 0.597P_{D-error} + 0.537E_{SS}^{begin} \leq 60.61$ | $P_w = P_{W-error} + 402.15$ kW<br>$P_{SS}^{disch} = 0.9E_{SS}^{begin}$kW;<br>$P_{SS}^{ch} = 0$ kW<br>$P_{DGs-adjust} = -P_{W-error} + P_{D-error} - 0.9E_{SS}^{begin} + 101.60$ kW |
| **CR3** | $-20.1075 \leq P_{W-error} \leq 20.1075$<br>$-53.65 \leq P_{D-error} \leq 53.65$<br>$244.73 \leq E_{SS}^{begin} \leq 568.78$ | $P_w = P_{D-error} + 283.50$ kW<br>$P_{SS}^{disch} = 220.25$ kW;<br>$P_{SS}^{ch} = 0$ kW;<br>$P_{DGs-adjust} = 0$ kW |

In the second case, the short-term forecasting errors are assumed within a quite wide range (-15~15%). Similar to the first case, the results including CRs and the function of the power of ESS, WG and DGs in each CR are illustrated in Figure 4.9 and Table 4.3. It can be seen that the wider the range of uncertain input data, the more CRs. Besides, when comparing the CRs in Figure 4.6 and Figure 4.9, we can see that the CRs in the first case is a part of the CRs in the second case. For example, the CR1 in Figure 4.6 is a part of the CR3 in Figure 4.9. This show the flexibility of optimal model solving by MPP, we can use a wider range of uncertain input data to prevent unexpected situations such as the actual data has a big difference with the forecast data, which can happen in the case of WG and PV.

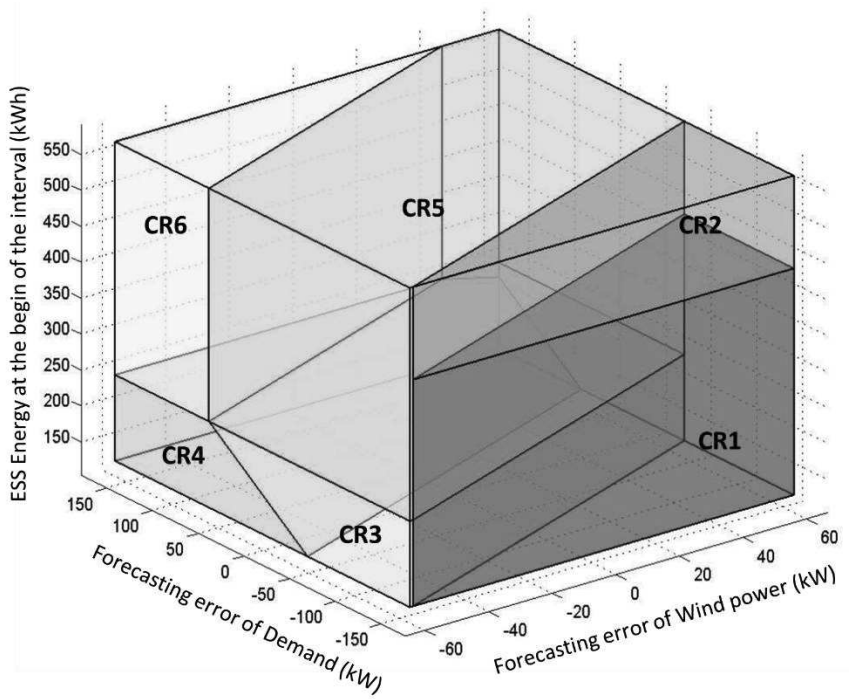


**Figure 4.9** Critical Regions in case the maximum forecasting errors are within -15~15%

**Table 4.3** The constraints of each CR and the function of the output data in case the maximum forecasting errors are within -15~15%

| | **CR's constraints** | **Output data** |
|---|---|---|
| **CR1** | $P_{W-error} \leq 60.3225$<br>$-160.95 \leq P_{D-error}$<br>$125.03 \leq E_{SS}^{begin} \leq 440$<br>$-0.707P_{W-error} + 0.707P_{D-error} \leq -71.84$ | $P_w = P_{D-error} + 503.75$ kW<br>$P_{SS}^{disch} = 0$ kW;<br>$P_{SS}^{ch} = 400$ kW;<br>$P_{DGs-adjust} = 0$ kW |
| **CR2** | $P_{W-error} \leq 60.3225$<br>$-160.95 \leq P_{D-error}$<br>$440 \leq E_{SS}^{begin} \leq 568.78$<br>$-0.707P_{W-error} + 0.707P_{D-error} \leq -71.84$ | $P_w = P_{D-error} + 503.75$ kW<br>$P_{SS}^{disch} = 0$ kW;<br>$P_{SS}^{ch} = -1.11E_{SS}^{begin} + 888.89$ kW;<br>$P_{DGs-adjust} = 0$ kW |
| **CR3** | $-60.3225 \leq P_{W-error} \leq 60.3225$<br>$-160.95 \leq P_{D-error} \leq 160.95$<br>$125.03 \leq E_{SS}^{begin} \leq 244.73$ | $P_w = P_{D-error} - 0.9E_{SS}^{begin} + 503.75$ kW<br>$P_{SS}^{disch} = 0.9E_{SS}^{begin}$ kW; |

| | | |
|---|---|---|
| | $0.707P_{W-error} - 0.707P_{D-error} \leq 71.84$<br>$-0.597P_{W-error} + 0.597P_{D-error} - 0.537E_{SS}^{begin} \leq -60.61$ | $P_{SS}^{ch} = 0$ kW<br>$P_{DGs-adjust} = 0$ kW |
| **CR4** | $-60.3225 \leq P_{W-error} \leq 60.3225$<br>$P_{D-error} \leq 160.95$<br>$125.03 \leq E_{SS}^{begin} \leq 244.73$<br>$0.597P_{W-error} - 0.597P_{D-error} + 0.537E_{SS}^{begin} \leq 60.61$ | $P_w = P_{W-error} + 402.15$ kW<br>$P_{SS}^{disch} = 0.9E_{SS}^{begin}$kW;<br>$P_{SS}^{ch} = 0$ kW<br>$P_{DGs-adjust} = -P_{W-error} + P_{D-error} - 0.9E_{SS}^{begin} + 101.60$ kW |
| **CR5** | $-60.3225 \leq P_{W-error} \leq 60.3225$<br>$-160.95 \leq P_{D-error} \leq 160.95$<br>$244.73 \leq E_{SS}^{begin} \leq 568.78$<br>$0.707P_{W-error} - 0.707P_{D-error} \leq 71.84$<br>$-P_{W-error} + P_{D-error} \leq 118.6490$ | $P_w = P_{D-error} + 283.50$ kW<br>$P_{SS}^{disch} = 220.25$ kW;<br>$P_{SS}^{ch} = 0$ kW;<br>$P_{DGs-adjust} = 0$ kW |
| **CR6** | $60.3225 \leq P_{W-error}$<br>$P_{D-error} \leq 160.95$<br>$244.73 \leq E_{SS}^{begin} \leq 568.78$<br>$-P_{W-error} + P_{D-error} \leq 118.6490$ | $P_w = P_{W-error} + 402.15$ kW<br>$P_{SS}^{disch} = 220.25$ kW;<br>$P_{SS}^{ch} = 0$ kW<br>$P_{DGs-adjust} = -P_{W-error} + P_{D-error} - 118.65$ kW |

## 4.4 Summary

In this chapter, an optimal short-term scheduling problem concerning the application of ESS for FFR is considered and analyzed in detail. The proposed model can be treated as the second stage of the optimal day-ahead UC problem in Chapter 3 . The mp-MLIP algorithm is used to solve this model. The adjustment from DGs, the ESS charge/discharge power, and the WG's power output are presented as functions of not only the short-term forecasting error of wind power and demand but also the energy stored in ESS at the begin of each time interval. This model ensures that the power balance when the short-term forecast results are different from the long-term forecast value. Although in some value of uncertain data, an adjustment from DGs is required, this

model still ensures that DGs must change their power output as little as possible. This is important in operating not only a small island power system but also a large-scale grid.

# Chapter 5 Probabilistic Dynamic Power Flow: A Method to Evaluate the Frequency Disturbance Caused by Forecast Errors and Decide the ESS Behavior

## 5.1 Introduction

In small islands, the hybrid diesel-wind generator is a typical configuration of power systems. Besides, an ESS is installed to maximize the utilization of wind power and reduce diesel fuel costs. The high penetration level of RES and the uncertainty of both RES and demand make the operation of these grids face many technical challenges. An important challenge is to ensure that the system frequency is always within the continuous operating band. Report [109] shows that in the European Generator Connection Code requirement, the frequency must be in the range of 49.0-51.0Hz while European Standard EN 50160 standard requires the frequency must be within 49.5-50.5Hz for 95% of time. On the other hand, the authors of [110]–[112] show that each country/region has a typical frequency standard. While the continuous frequency range in Great Britain or European countries is the interval of 49.5–50.5 Hz, other countries require a narrower nominal frequency band, such as 49.8–50.2 Hz in China or 49.9–50.1 Hz in Italy. Some countries have two different standards for mainland and island, for example, in Australia mainland, an interval of 49.75–50.25 Hz is required while this interval is 49–51Hz for island [113].

In Part III, we implemented long-term/short-term optimal scheduling problems considering the role of ESS in FFR. This means the power output of DGs, RES or ESS is predetermined to ensure all constraints related power balance, frequency, etc. However, although the uncertainty of RES and demand is taken into account these problems, a small power imbalance in real-time operation due to forecast errors may happen and leads to a small frequency variation. So that, a real time regulation process is necessary (Figure 4.1). In detail, depending on the size of the difference between the forecast value and the real-time data, the system frequency may be out of the continuous operating band. In this case, a small regulation from ESS or DGs is necessary to restore frequency.

Normally, the DGs' governor response immediately starts if the frequency deviation is higher than the dead-band (15–20 mHz). Besides, there are studies focus on the primary frequency response from ESS [25], [29], [49], [80], in which ESS' dynamic behavior is modeled as a generator. However, we notice that if the power imbalance is small enough, the frequency can be

arrested before reaching the thresholds with only frequency regulation from DGs. Consequently, the ESS does not need to adjust its output or change its charge/discharge state. Now we have a problem: How to determine that the steady-state frequency with only DGs' frequency regulation is outside or still within the continuous operating band? This will decide the behavior of the ESS. Actually, the steady-state frequency can be calculated by using the primary frequency regulation formula directly [114]. However, this formula does not consider the system configuration such as transmission/distribution line's capacity.

In this chapter, we propose a probabilistic approach to evaluate the steady-state frequency after a small power imbalance due to forecasting errors. This approach not only consider the system configuration but also have a very short computing time. Thus, we can give a decision and send a control signal to the ESS. The main idea of this approach is probabilistic dynamic power flow (PDPF) which consider the static power-frequency characteristic of generators and demand. The Stochastic Response Surface Method (SRSM) is applied to deal with the uncertain parameters in PDPF and compute the probabilistic distribution of the frequency. This method is based on polynomial chaos expansion to approximate the output data with input random data following any distribution. In literature, SRSM is applied in several studies and show that it is computationally efficient [115], [116]. The authors of [116] also show that SRSM can be applied to a control problem because its computing time in this study is only 100-200ms.

## 5.2 Proposed Methodology

### 5.2.1 Dynamic Power Flow Model

In an interconnected large-scale power system, any power imbalance caused by the sudden changes of load or forecasting errors of RES can be compensated quickly. Besides, these power imbalances are small in comparison to the total capacity of the grid. Thus, the system frequency is assumed to be constant in the traditional load flow model. By contrast, in an isolated grid, the instance imbalance between production and consumption due to forecasting errors can lead to a significant frequency variation. So that, power flow calculation must consider the system frequency. This model is called dynamic power flow (DPF) and presented below.

After a power disturbance happens, generators that have reserve capacity are all able to adjust the active and reactive power based on their own modulation characteristics. Besides, the demands also change their consumption accordingly. In addition, the response of RES is ignored.

Following [117], [118], the power output of each generator is adjusted by primary frequency response.

$$P_{Gi} = P_{GNi} - K_{Gi}(f - f_{norm}) \qquad for\ i \in G \tag{5-1}$$

where $f_{norm}$ is rated frequency; $f$ is actual frequency; $P_{Gi}$ and $P_{GNi}$ are the $i^{th}$ generator's power output corresponding to $f$ and $f_{norm}$; $K_{Gi}$ is the frequency regulation coefficient of the $i^{th}$ generator; and $G$ is group of generator buses.

Besides, active load of power system varies as the following equation:

$$P_{Dj} = P_{DNj} + K_{Di}(f - f_{norm}) \qquad for\ j \in D \tag{5-2}$$

where $P_{Dj}$ and $P_{DNj}$are the $j^{th}$ load's active power corresponding to $f$ and $f_{norm}$; $K_{Di}$is the frequency regulation coefficient of the$j^{th}$ load; and $D$ is group of load buses.

In dynamic power flow model, the injection power function at bus *i* can be written as follow:

$$\begin{aligned} P_i &= P_{GNi} - K_{Gi}(f - f_{norm}) - (P_{DNj} + K_{Di}(f - f_{norm})) \\ &= V_i \sum_{j=1}^{n} V_j(G_{ij}\cos\theta_{ij} - B_{ij}\sin\theta_{ij}) \end{aligned} \tag{5-3}$$

$$Q_i = V_i \sum_{j=1}^{n} V_j(G_{ij}\sin\theta_{ij} - B_{ij}\cos\theta_{ij}) \tag{5-4}$$

where $n$ is number of buses; $V_i$and $V_j$ are voltage amplitude of bus *i* and *j* respectively; $G_{ij}$ and $B_{ij}$ are conductance and susceptance between bus *i* and bus *j* respectively; $\theta_{ij}$ is the voltage angle difference between bus *i* and bus *j*.

Assuming bus $n$ is slack bus, the correction equation is:

$$\begin{bmatrix} \mathbf{\Delta P} \\ \mathbf{\Delta Q} \\ \mathbf{\Delta P_n} \end{bmatrix} = \begin{bmatrix} \mathbf{J_1} & \mathbf{J_2} & \mathbf{C} \\ \mathbf{J_3} & \mathbf{J_4} & \mathbf{0} \\ \mathbf{H_n} & \mathbf{0} & \mathbf{C_n} \end{bmatrix} \begin{bmatrix} \mathbf{\Delta\theta} \\ \mathbf{\Delta V} \\ \mathbf{\Delta f} \end{bmatrix} \tag{5-5}$$

where:

**$J_1$, $J_2$, $J_3$, $J_4$**: Submatrices of Jacobian matrix in traditional load flow model.

**$H_n$**: vector of the partial derivatives of injection power of slack bus corresponding to voltage angle and can be calculated as follow:

$$H_{nj} = \frac{\partial \Delta P_n}{\partial \theta_j} = V_n V_j\left(G_{nj}\sin\theta_{nj} - B_{nj}\cos\theta_{nj}\right) \qquad for\ j = 1, 2, 3, \dots, n-1 \tag{5-6}$$

**C**, **$C_n$**: column vector and a diagonal element correspond to generator and load's response when the system frequency changes.

$$C_i = \frac{\partial P_i}{\partial f} = \begin{cases} -K_{Gi} - K_{Di}\ for\ generator\ buses \\ -K_{Di}\ for\ load\ buses \end{cases} \qquad for\ i = 1, 2, 3, \dots, n \tag{5-7}$$

The state variables including voltage amplitudes, voltage angles and system frequency are determined by solving (5-5).

### 5.2.2 Stochastic Response Surface Method

*1. Mathematical Formulation of Stochastic Response Surface Method*

Stochastic Response Surface Method (SRSM) was first introduced by S. Isukapalli in 1998 and applied to uncertainty problems in environment and biological system [119]–[121]. This is a method used to approximate an output response when the input parameter is uncertain. Assume that the input parameter $x$ is uncertain and with given value of $x$, the output response $y$ is determined as $y = f(x)$. The above references proved that any uncertain input parameter $x$ can be represented as a function of a standard random variables $\xi$. Table 5.1 presents the transformation function of some typical distribution functions. On the other hand, any uncertain response $y$ of system can be expressed by a Hermite polynomial chaos expansion of standard random variables. Thus, instead of calculating the response $y$ directly from input data $x$, we use intermediate parameters that are a set of standard random variables $\xi$ (Figure 5.1). The advantage of SRSM is that it can model system with uncertain input following both normal distribution, non-normal distribution or empirical distribution. Hence, handling real uncertain data can be easier and more accurate.

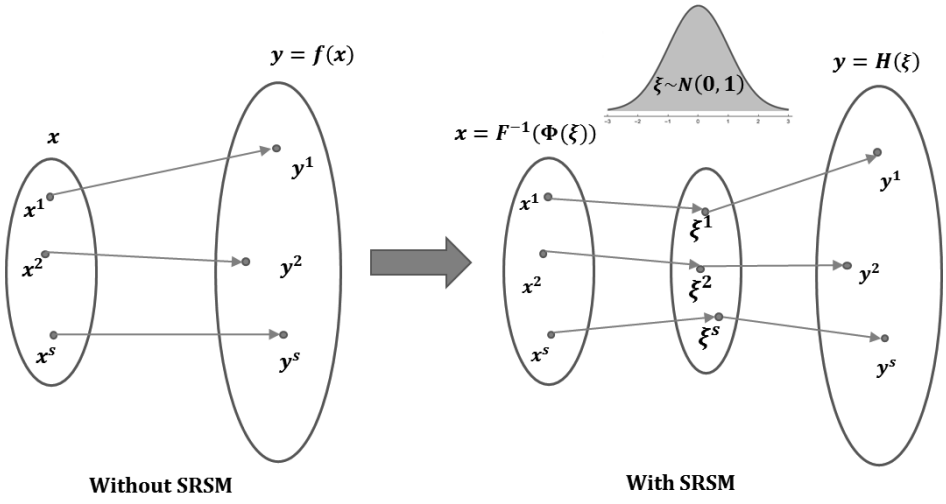


**Figure 5.1** Description of the idea of the SRSM in case there is one uncertain input data and one output response

The basic formulation of SRSM is written in detail as following:

- **Inputs:**

$$x_i = F_i^{-1}\big(\Phi(\xi_i)\big) \qquad for\ i = 1, 2, 3, \dots, n \tag{5-8}$$

where:

$n$: The number of random input variables $x$.

$\xi$: Standard random variable with zero mean and unit variance.

$\Phi(\xi)$: The cumulative probability function of $\xi$.

$F_i$: The cumulative probability function of random variable $x_i$.

In case input parameter $x_i$ follows a typical distribution such as normal distribution or uniform distribution, we can transform from $x_i$ to $\xi_i$ and vice versa by using the transformation function in Table 5.1.

- **Response:**

$$y = H(\xi) = a_0 + \sum_{j_1=1}^{n} a_{j_1} H_1(\xi_{j_1}) + \sum_{j_1=1}^{n} \sum_{j_2=1}^{j_1} a_{j_1 j_2} H_2(\xi_{j_1}, \xi_{j_2}) + \sum_{j_1=1}^{n} \sum_{j_2=1}^{j_1} \sum_{j_3=1}^{j_2} a_{j_1 j_2 j_3} H_3(\xi_{j_1}, \xi_{j_2}, \xi_{j_3}) + \cdots \quad (5\text{-}9)$$

where:

$a_0, a_{j_1}, a_{j_1 j_2}, a_{j_1 j_2 j_3}$: The unknown coefficients.

$H_m$: The $m^{th}$ order of multidimensional probabilists' Hermite polynomial chaos expansion is formulated as follow:

$$H_m(\xi_{j_1}, \xi_{j_2}, \dots, \xi_{j_n}) = (-1)^m e^{\frac{1}{2}\xi^T \xi} \frac{\partial^n}{\partial \xi_{j_1} \partial \xi_{j_2} \dots \partial \xi_{j_n}} e^{\frac{1}{2}\xi^T \xi} \quad (5\text{-}10)$$

Taking one-dimensional Hermite polynomial as an example, the first five expansions are:

$$H_0(\xi) = 1;\ H_1(\xi) = \xi;\ H_2(\xi) = \xi^2 - 1;\ H_3(\xi) = \xi^3 - 3\xi;$$
$$H_4(\xi) = \xi^4 - 6\xi^2 + 3;\ H_5(\xi) = \xi^5 - 10\xi^3 + 15\xi; \dots \quad (5\text{-}11)$$

The accuracy of this method depends on the highest order used in Hermite polynomial chaos expansion. However, when the highest order increases, the number of unknown coefficients also increase; so estimating coefficients will be more difficult. Follow the result in [121], the 2-order or 3-order have high accuracy and can be adopted.

The Hermite polynomial chaos expansion of the second order and third order are presented by (5-12) and (5-13) respectively:

$$y = H(\xi) = a_0 + \sum_{i=1}^{n} a_i \xi_i + \sum_{i=1}^{n} a_{ii}(\xi_i^2 - 1) + \sum_{i=1}^{n-1} \sum_{j>i}^{n} a_{ij} \xi_i \xi_j \quad (5\text{-}12)$$

$$y = H(\xi) = a_0 + \sum_{i=1}^{n} a_i \xi_i + \sum_{i=1}^{n} a_{ii}\left(\xi_i^2 - 1\right) + \sum_{i=1}^{n-1}\sum_{j>i}^{n} a_{ij}\xi_i\xi_j + \sum_{i=1}^{n} a_{iii}\left(\xi_i^3 - 3\xi_i\right) + \sum_{i=1}^{n}\sum_{j=1}^{n} a_{ijj}\left(\xi_i\xi_j^2 - \xi_i\right) + \sum_{i=1}^{n-2}\sum_{j>i}^{n-1}\sum_{k>j}^{n} a_{ijk}\xi_i\xi_j\xi_k \quad (5\text{-}13)$$

**Table 5.1** Relationship between uncertain parameter and standard random variable [121]

| **Distribution type of uncertain input parameter $x$** | **Transformation function from a standard random variable $\xi$** |
|---|---|
| Uniform: $\mathcal{U}(a, b)$ | $a + (b - a)\Phi(\xi)$ |
| Normal Distribution: $\mathcal{N}(\mu, \sigma^2)$ | $\mu + \sigma\xi$ |
| Lognormal Distribution: $Lognormal(\mu, \sigma^2)$ | $exp(\mu + \sigma\xi)$ |
| Gamma Distribution: $\Gamma(a, b)$ | $ab\left(\xi\sqrt{\frac{1}{9a}} + 1 - \frac{1}{9a}\right)^3$ |

*2. Implementation and Application of the SRSM*

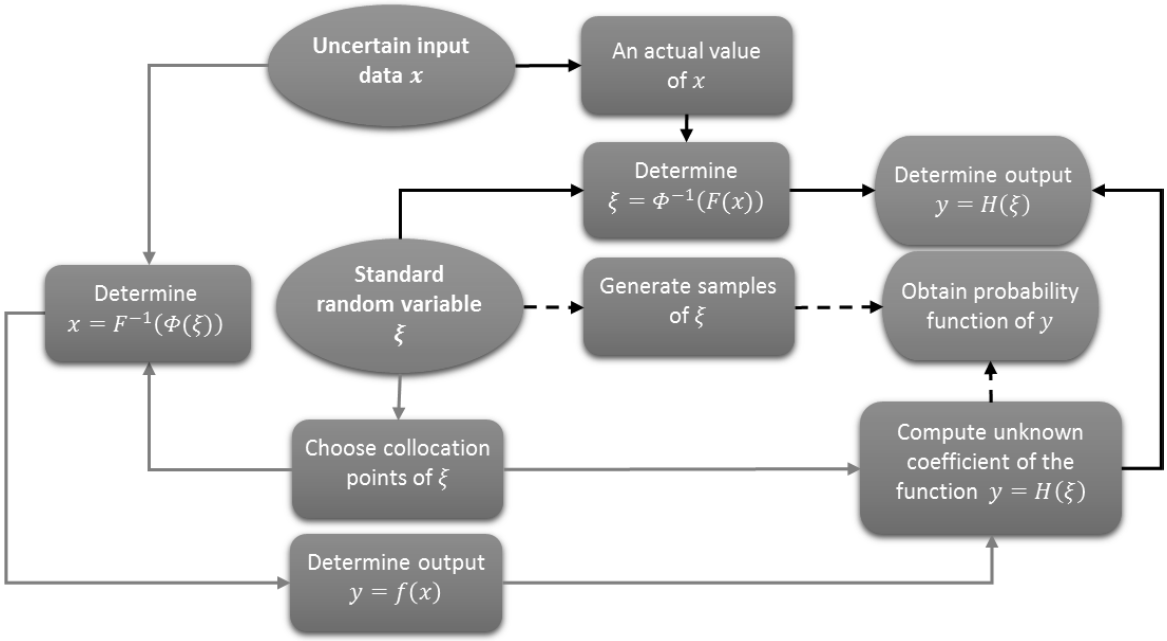


**Figure 5.2** Description diagram of the SRSM

In order to understand the SRSM in detail, let see Figure 5.2. The blue arrows in this figure describe how to determine coefficients of the function $y = H(\xi)$. This process begins by selecting some collocation points, which are combination of different values of $\xi_i$. Using Efficient Collocation Method presented in [121], these collocation points are selected by combining zero

and the root of one higher order one-dimensional Hermite expansion given by (5-11). Depending on whether we choose the 2-order or 3-order expansion for the output response $y$, the roots are determined by solving equation $H_3(\xi) = \xi^3 - 3\xi = 0$ or $H_4(\xi) = \xi^4 - 6\xi^2 + 3 = 0$. On the other hand, reference [121] shows that the number of collocation point should be at least two times of the number of unknown coefficients. This ensures that we can capture response y in high probability region.

Note that each standard random variable $\xi_i$ is corresponding to an uncertain input parameter $x_i$ . In next step, the collocations points are transformed into the samples of original variables $x_i$ by (5-8), and then we calculate the corresponding values of response *y* directly by the function $y = f(x)$. With the given collocation points of $\xi_i$ and the corresponding values *y*, we can determine the function $y = H(\xi)$ by solving equations (5-12) or (5-13) depending on the chosen order of Hermite polynomial chaos expansion.

After obtaining the function $y = H(\xi)$, we can use it with two applications. The first application is analyzing statistical characteristics of the output response *y* due to the uncertainty of the input parameter by obtaining the probability function of *y*. This process is described by the black dashed arrows in Figure 5.2. The second application is to calculate the output parameter *y* while ignoring the relationship between *y* and *x*. This is implemented by transforming from *x* to a value of $\xi$ and find $y = H(\xi)$ (the black solid arrows in Figure 5.2). This process is faster than using the function $y = f(x)$.

### 5.2.3 Probabilistic Dynamic Power Flow and Assessment of the Steady-State Frequency after a Small Power Imbalance Due to Forecasting Errors

In fact, the probabilistic dynamic power flow (PDPF) is a combination of the DPF model in section 5.2.1 and the SRSM approach presented in section 5.2.2. With random input parameters such as load or wind power, the PDPF is implemented as shown in Figure 5.3. Based in two applications of the SRSM, which presented in the previous section, the PDPF can be used to:

- Obtaining the probability function of the steady-state frequency with the given probabilistic forecast results of RES and demand. Consequently, we can evaluate the probability that the nominal frequency band is exceeded.
- Determining the steady-state frequency quickly after a small power imbalance due to forecasting errors, thereby deciding whether the ESS should be involved in frequency regulation.

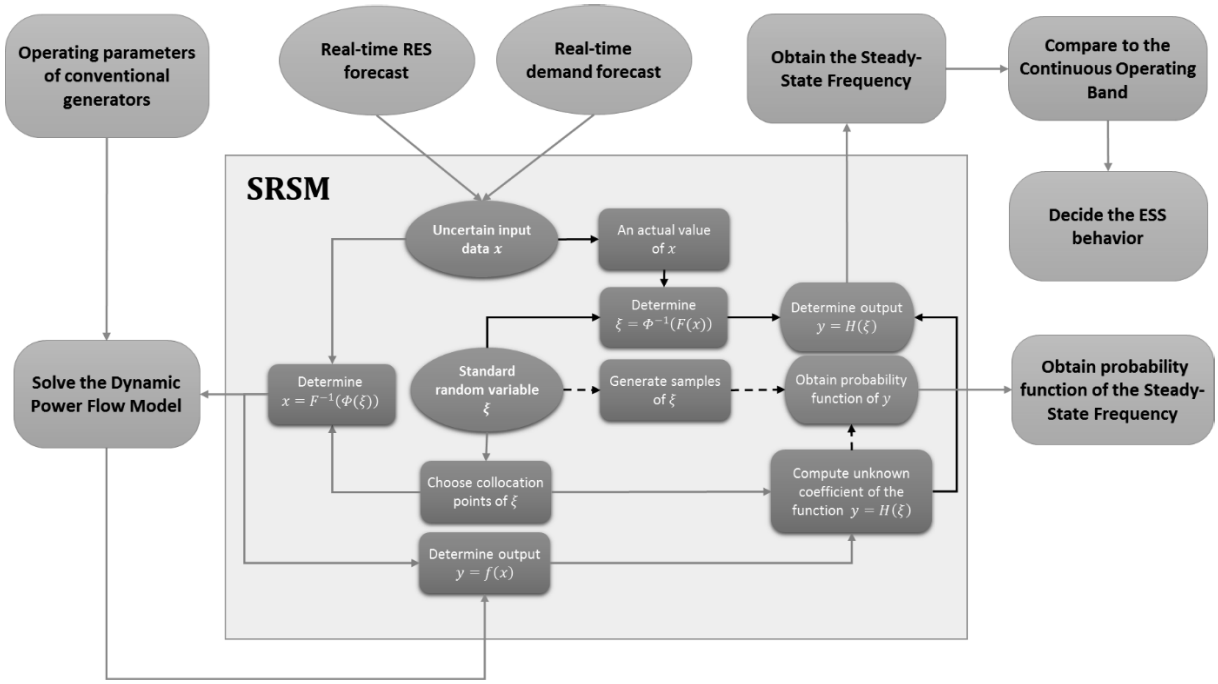


**Figure 5.3** Description of the PDPF and the application in assessment of the steady-state frequency

## 5.3 Numerical Application

In this section, the proposed method is applied to 39-bus New England test system [122]. The one-line diagram of this system is shown in Figure 5.4. Without losing generality, we assume that generators connected to bus 32 and 33 are WGs. So that, the penetration level of WG in this system is approximate 20%. The conventional generators are assumed to have the droop factor of 5%. The power output of WGs and the demand connected to bus 27 have forecasting errors which follow a normal distribution function with zero mean and standard deviation of 0.05. This means the maximum errors are approximately 15% in correspondence to the confidence interval of 99.7%. Tests are implemented by MatPower toolbox [123] in the MATLAB on a PC with 2.6GHz Intel® Core ™ i5-3320M and 4GB RAM.

Figure 5.5 presents the density function of the system frequency in case the forecasting errors of the WGs and 27$^{th}$-bus demand are within -15%∼15%. The results are obtained by simulating SRSM two thousand times within approximately 14 seconds. On the other hand, using the second application of the SRSM, we can find the system frequency with given forecasting value of the WGs. It takes only 744ms to implement these steps to obtain two thousand value of the frequency which is shown in Figure 5.6. This means that the required computing time of each value is only 0.3720 ms. In contrast, to find the steady-state frequency directly by DPF model, a computing time of 282ms is required (Table 5.2).

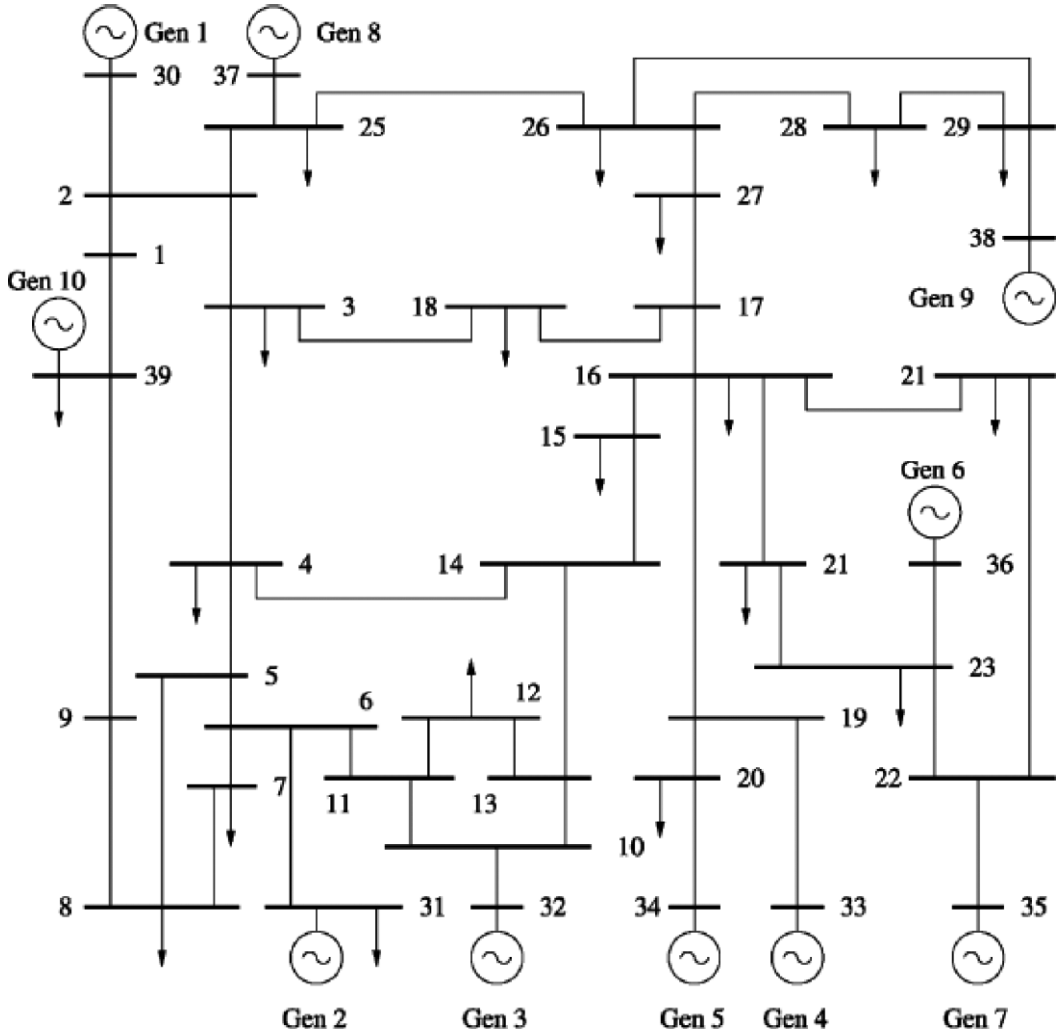


**Figure 5.4** The 39-bus New England test system's one-line diagram [124]

Noting that this chapter does not pay attention to the amount of charge/discharge power of the ESS but only focuses on answering the question: Does the ESS need to change status or charge/discharge power to maintain the frequency when there is a small power imbalance. Figure 5.7 shows the steady-state frequency and ESS behavior with two hundred samples of forecast errors. There are two requirements of the system frequency are considered: 49.5-50.5 Hz and 49.8-50.2 Hz. The ESS behavior is 1 in case this device must increase discharging power or reduce charging power due to the frequency smaller than the lower threshold, and vice versa if the frequency exceeds the higher threshold. It is easy to see that in the case of the frequency standard of 49.5-50.5 Hz under normal operations, the frequency regulation from conventional generators is enough to maintain the system. In contrast, if the grid requires a narrower frequency band, such as 49.8-50.2Hz, the ESS need to adjust the discharging/charging power to reduce the power imbalance. The ESS behavior in two cases of the frequency standard can be shown from Figure 5.7.

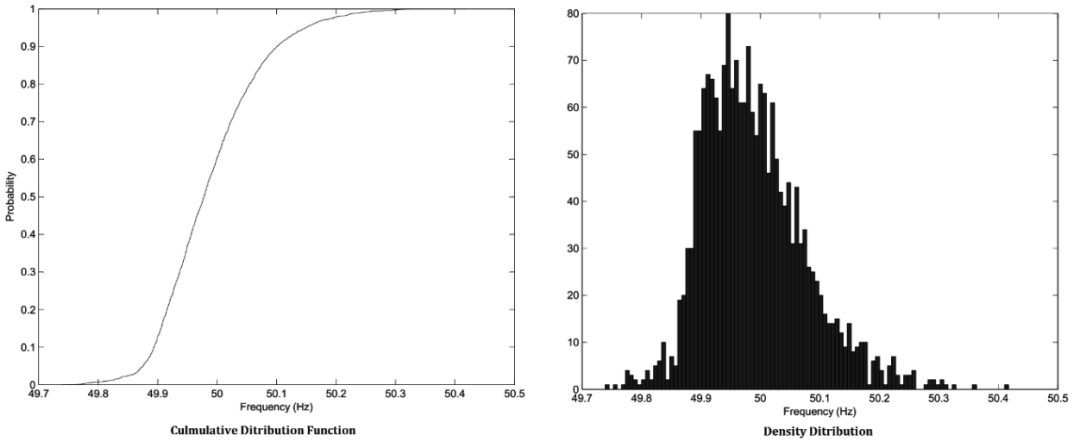


**Figure** 5.5 The system frequency in the case the penetration level of WGs is 20%

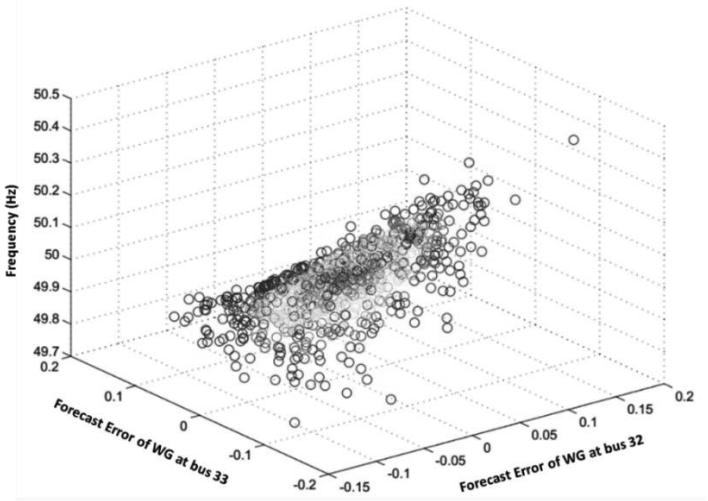


**Figure 5.6** The dependence of frequency on the forecasting error when the penetration level of WGs is 20%

**Table 5.2** Comparison the computing time between 2 cases: SRSM and DPF

| | **Solving DPF directly** | **Using the SRSM** |
|---|---|---|
| **Computing time (ms)** | 282 | 0.3720 |

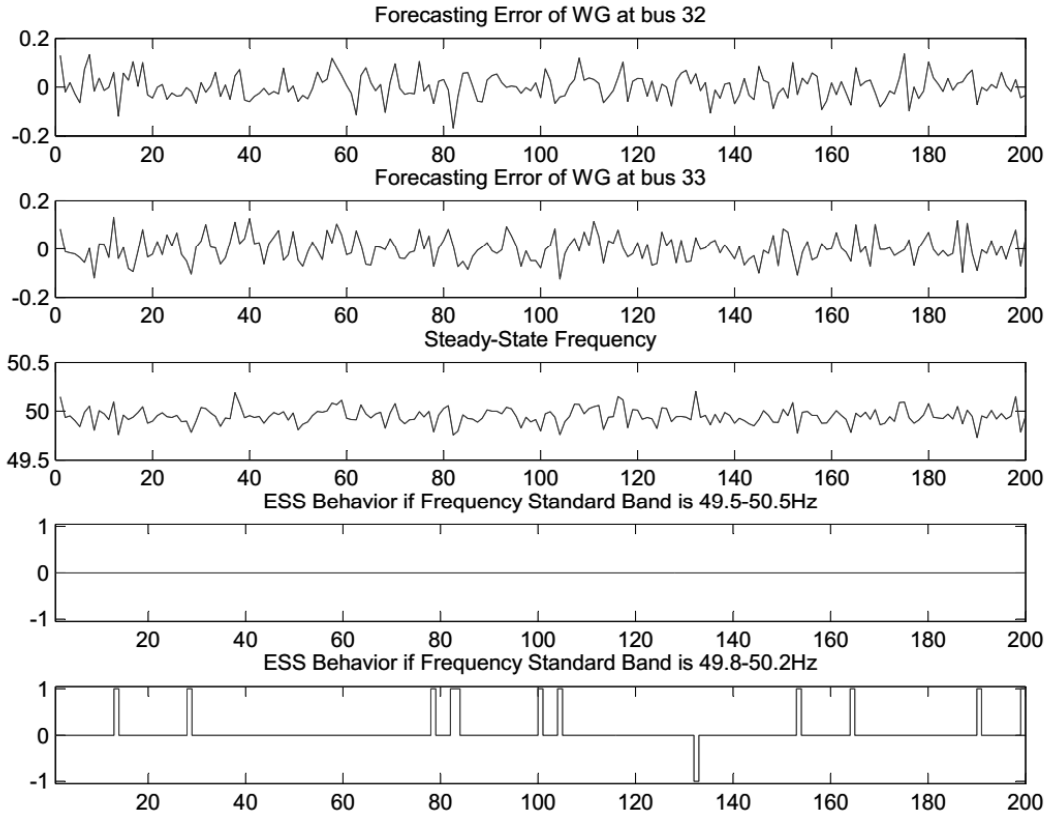


**Figure 5.7** ESS behavior depend on requirements of the system frequency in the case the penetration level of WGs is 20%

Now we increase the level of WG in this system by assuming that the generators are connected to bus 34 and 35 are WGs, consequently, the WP level is 40%. Figure 5.8 and Figure 5.9 show that even in the cases of a quite wide continuous frequency band (49.5-50.5Hz), there is still some value of frequency out of the operating band and let the ESS must respond.

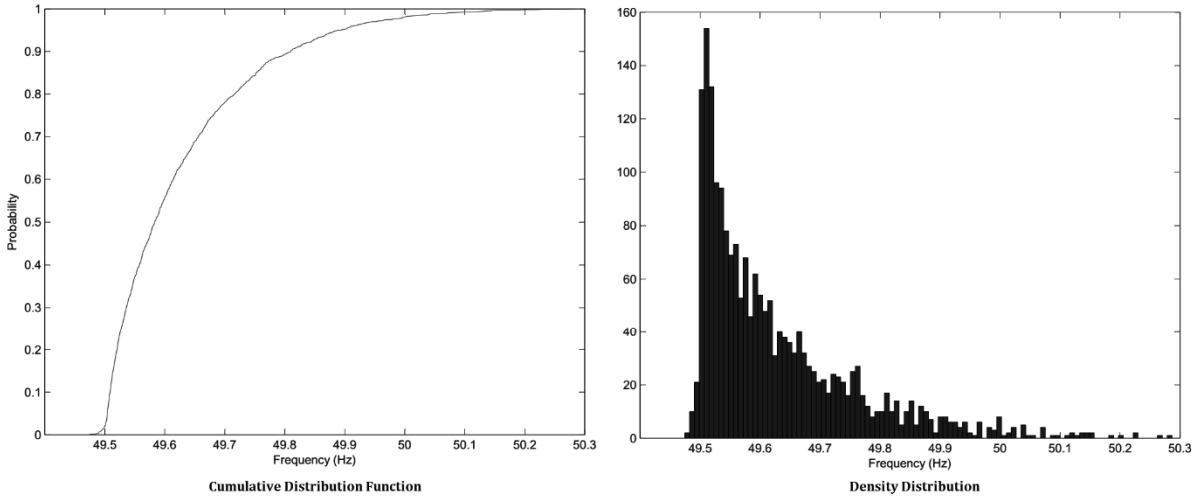


**Figure 5.8** The system frequency in the case the penetration level of WGs is 40%

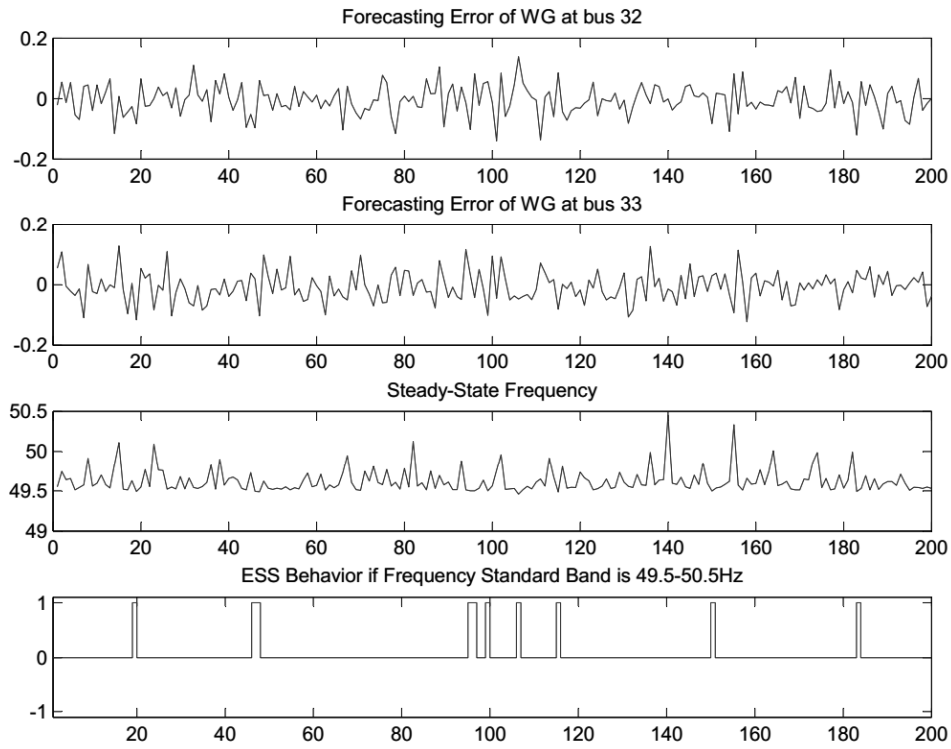


**Figure 5.9** ESS behavior depend on forecasting error of WGs in the case the penetration level of WGs is 40%

## 5.4 Summary

This chapter presented a probabilistic power flow model to evaluate the steady-state frequency after a small power disturbance due to forecasting errors of RES or demand. The first application of this method is obtaining the probability function of the steady-state frequency and then evaluating the probability that the nominal frequency band is exceeded. The second application is determining the steady-state frequency quickly after a small power imbalance due to forecasting errors of RES and demand. Because this method is significant faster than implementing the DPF directly, we can calculate the system frequency immediately after the real-time data. Consequently, we can decide whether the ESS needs to adjust its discharging/charging power to maintain the frequency. The results in this chapter show the efficient of this method. On the other hand, we can use this method to evaluate other parameter of the power system such as voltage, thereby apply the results to control field.

# Chapter 6 Conclusions and Future Works

The main goal of this thesis is to study and develop an island power system including DG, WP, and ESS with stable, sustainable end economic performance. This chapter highlights the main contributions of this thesis and outlines the most promising avenues for further study.

## 6.1 General Summary and Conclusions

This work solves 2 main issues of the island power system which are: 1) The sizing optimization of ESS in the system; 2) the optimal day-ahead scheduling of the system considering the frequency criteria after N-1 contingency. The ESS, which is employed to keep power balance and take advantage of wind power, also provide FFR. Besides, we also solve two issues: 3) a short-term scheduling model, which can be considered as pre-controlled model, find the power output of WG and the adjustment of DGs as functions of uncertain parameters; 4) a probabilistic dynamic power flow which helps evaluate the system frequency after a small power imbalance, and then make a decision for the ESS behavior.

In Chapter 2 , we proposed a two-stage stochastic model to find the optimal sizing of ESS in an island power system. In this problem, the uncertainty in wind speed and load growth factor are considered. A scenario reduction approach, which is a combination of moment matching and k-means algorithm, is presented. The results show that the scenarios after reducing process still keep the original scenarios' statistical properties. The impact of the project's lifetime, spinning reserve and the minimum number of online DGs on the optimal size of ESS is also analyzed.

In Chapter 3 , we proposed a two-stage chance-constrained day-ahead scheduling problem. In this model, the ESS, which is employed to keep power balance and take advantage of wind power, is used to provide FFR to ensure that the frequency criteria are met after the sudden loss of a generator. The results show the effectiveness of this method: the quality of the system frequency is ensured while the operating cost does not increase. Besides, the effects of the ESS size and its response time on the frequency nadir is analyzed and show that a larger ESS is required in the case of slower response.

Chapter 4 present a short-term scheduling model, which solve the second stage problem of the day-ahead UC model presented in Chapter 3 . In this problem, the FFR from the ESS in N-1 contingency event is still considered. An adjustment from DGs is used to prevent power imbalance because the WGs and the ESS cannot compensate for the difference between the short-term and long-term forecast results of wind and demand. A multiparametric mixed integer linear

programming is applied to solve this problem. The output data including the ESS charge/ discharge power, the DGs adjustment, and the WG's output are described as functions of uncertain input data. The results show that DGs do not need to change their power output in most of the cases. This is important in operating not only a small island power system but also a large-scale grid.

Chapter 5 present a probabilistic approach to evaluate the steady-state frequency after a small power disturbance due to forecasting errors of RES or demand. Based on this probabilistic approach, we propose a method to determine the steady-state frequency quickly, and then decide whether the ESS needs to change its discharging/charging power to maintain the frequency. The results show that this method is significantly faster than implementing the DPF directly.

In conclusion, the thesis provides new solutions to design and operate a hybrid wind-diesel power system with ESS for a stable, sustainable and economic performance. The thesis also contributes to broadening the application of ESS in frequency service in a power system with high penetration of RES, especially island power system.

## 6.2 Future Works

During this thesis, there are several issues and challenges identified for further optimization and research.

The first interesting problem is the optimal sizing model in Chapter 2 , which was implemented to determine the ESS sizing while the DG and WG sizing are known. Actually, this model can be expanded to identify both sizes of DG as well as WG. However, this increases the number of variables in the optimization model and makes solving this problem more complicated. Besides, in Chapter 2 the scenarios of the wind speed in each hour is assumed to be independent to the wind speed in the previous or next hour. In other words, we did not consider the wind speed's transition matrix**.** The correlation relationship between RES and demand is also ignored although it is an important factor, especially in the case of PV. Thus, a new optimization model is needed to take into account these issues.

The second investigation is required is the variation of the ESS discharge power over the FFR duration. In Chapter 3 , the ESS discharge power after contingency event is treated as constant. However, in actual operation, it should be reduced after the DGs' primary response fully active to make sure the system stability and we need to determine how it changes. This study can be implemented in both optimal planning and control aspects.

The third study must be considered is the short-term optimal planning problem. Although in Chapter 4 , the output data was determined as a function of uncertain input data and can be

treated as a pre-control law, the results are still limited. Besides, to apply these functions to control field, this model should consider the power system configuration. Therefore, it is necessary to further study this model.

Finally, although the research in this thesis was implemented for a small island power system, they can be expanded and applied to any isolated power system with high penetration level of RES. Thus, we can further study and develop these optimization models in operating microgrids or Virtual Power Plants.

# Reference


[1] P. Blechinger, C. Cader, P. Bertheau, H. Huyskens, C. Breyer, and R. Seguin, "GLOBAL PV AND WIND POWER POTENTIAL OF SMALL ISLAND HYBRID MINI-GRIDS Motivation and Purpose Results: Renewable Energy Storage, PV and Wind Power Potential."

[2] O. Norojono, A. Maxwell, J. M. Trainor, W. Y. Lee, S. H. Haider, and F. Ramos, "PACIFIC ENERGY UPDATE CONTENTs," 2018. [Online]. Available: https://www.adb.org/sites/default/files/institutional-document/425871/pacific-energy-update-2018.pdf. [Accessed April 03, 2019].

[3] A. Chauhan and R. P. Saini, "A review on Integrated Renewable Energy System based power generation for stand-alone applications: Configurations, storage options, sizing methodologies and control," *Renew. Sustain. Energy Rev.*, vol. 38, pp. 99–120, Oct. 2014.

[4] Q. Fu, A. Hamidi, A. Nasiri, V. Bhavaraju, S. B. Krstic, and P. Theisen, "The Role of Energy Storage in a Microgrid Concept: Examining the opportunities and promise of microgrids.," *IEEE Electrif. Mag.*, vol. 1, no. 2, pp. 21–29, Dec. 2013.

[5] I. N. Moghaddam and B. Chowdhury, "Optimal sizing of Hybrid Energy Storage Systems to mitigate wind power fluctuations," in *2016 IEEE Power and Energy Society General Meeting (PESGM)*, 2016, pp. 1–5.

[6] J. P. Fossati, A. Galarza, A. Martín-Villate, and L. Fontán, "A method for optimal sizing energy storage systems for microgrids," *Renew. Energy*, vol. 77, pp. 539–549, May 2015.

[7] T. Ma, H. Yang, and L. Lu, "Feasibility study and economic analysis of pumped hydro storage and battery storage for a renewable energy powered island," *Energy Convers. Manag.*, 2014.

[8] D. Quintero Pulido *et al.*, "Characterization of Storage Sizing for an Off-Grid House in the US and the Netherlands," *Energies*, vol. 11, no. 2, p. 265, Jan. 2018.

[9] M.-S. Lu, C.-L. Chang, W.-J. Lee, and L. Wang, "Combining the Wind Power Generation System with Energy Storage Equipments," in *2008 IEEE Industry Applications Society Annual Meeting*, 2008, pp. 1–6.

[10] J. Hamilton, M. Negnevitsky, and X. Wang, "Economic Rationalization of Energy Storage under Low Load Diesel Application," *Energy Procedia*, vol. 110, pp. 65–70, 2017.

[11] G. O. Suvire, M. G. Molina, and P. E. Mercado, "Improving the Integration of Wind Power Generation Into AC Microgrids Using Flywheel Energy Storage," *IEEE Trans. Smart Grid*, vol. 3, no. 4, pp. 1945–1954, 2012.

[12] J. V. Paatero and P. D. Lund, "Effect of energy storage on variations in wind power," *Wind Energy*, vol. 8, no. 4, pp. 421–441, Oct. 2005.

[13] J. Hamilton, A. Tavakoli, M. Negnevitsky, and X. Wang, "Investigation of no load diesel technology in isolated power systems," in *2016 IEEE Power and Energy Society General Meeting (PESGM)*, 2016, pp. 1–5.

[14] F. Díaz-González, A. Sumper, O. Gomis-Bellmunt, and R. Villafáfila-Robles, "A review of energy storage technologies for wind power applications," *Renew. Sustain. Energy Rev.*, vol. 16, no. 4, pp. 2154–2171, May 2012.

[15] C. Abbey, W. Li, and G. Joos, "An Online Control Algorithm for Application of a Hybrid ESS to a Wind–Diesel System," *IEEE Trans. Ind. Electron.*, vol. 57, no. 12, pp. 3896–3904, 2010.

[16] E. Lobato, L. Sigrist, and L. Rouco, "Use of energy storage systems for peak shaving in the Spanish Canary Islands," in *2013 IEEE Power & Energy Society General Meeting*, 2013, pp. 1–5.

[17] J. P. Barton and D. G. Infield, "Energy storage and its use with intermittent renewable energy," *IEEE Trans. Energy Convers.*, vol. 19, no. 2, pp. 441–448, Jun. 2004.

[18] M. Yue and X. Wang, "Grid Inertial Response-Based Probabilistic Determination of Energy Storage System Capacity Under High Solar Penetration," *IEEE Trans. Sustain. Energy*, vol. 6, no. 3, pp. 1039–1049, 2015.

[19] X. Luo, J. Wang, M. Dooner, and J. Clarke, "Overview of current development in electrical energy storage technologies and the application potential in power system operation," *Appl. Energy*, vol. 137, pp. 511–536, Jan. 2015.

[20] J. Eyer and G. Corey, "SANDIA REPORT Energy Storage for the Electricity Grid: Benefits and Market Potential Assessment Guide A Study for the DOE Energy Storage Systems Program," 2010. [Online]. Available: https://www.sandia.gov/ess-ssl/publications/SAND2010-0815.pdf. [Accessed February 16, 2019].

[21] D. Ipsakis *et al.*, "Energy management in a stand-alone power system for the production of electrical energy with long term hydrogen storage," *Comput. Aided Chem. Eng.*, vol. 25, pp. 1125–1130, Jan. 2008.

[22] K. ZHOU, "Optimal energy management strategy and system sizing method for stand-alone photovoltaic-hydrogen systems," *Int. J. Hydrogen Energy*, vol. 33, no. 2, pp. 477–489, Jan. 2008.

[23] M. Castañeda, A. Cano, F. Jurado, H. Sánchez, and L. M. Fernández, "Sizing optimization, dynamic modeling and energy management strategies of a stand-alone PV/hydrogen/battery-based hybrid system," *Int. J. Hydrogen Energy*, vol. 38, no. 10, pp. 3830–3845, Apr. 2013.

[24] M. R. Aghamohammadi and H. Abdolahinia, "A new approach for optimal sizing of battery energy storage system for primary frequency control of islanded Microgrid," *Int. J. Electr. Power Energy Syst.*, vol. 54, pp. 325–333, Jan. 2014.

[25] G. Delille, B. François, S. Member, and G. Malarange, "Dynamic Frequency Control Support by Energy Storage to Reduce the Impact of Wind and Solar Generation on Isolated Power System's Inertia," *IEEE Trans. Sustain. ENERGY*, vol. 3, no. 4, 2012.

[26] X. Tang, X. Hu, N. Li, W. Deng, and G. Zhang, "A novel frequency and voltage control method for islanded microgrid based on multienergy storages," *IEEE Trans. Smart Grid*, vol. 7, no. 1, pp. 410–419, Jan. 2016.

[27] C. E. Murillo-Sanchez, R. D. Zimmerman, C. Lindsay Anderson, and R. J. Thomas, "Secure Planning and Operations of Systems With Stochastic Sources, Energy Storage, and Active Demand," *IEEE Trans. Smart Grid*, vol. 4, no. 4, pp. 2220–2229, Dec. 2013.

[28] M. R. Aghamohammadi and H. Abdolahinia, "A new approach for optimal sizing of battery energy storage system for primary frequency control of islanded Microgrid," *Int. J. Electr. Power Energy Syst.*, vol. 54, pp. 325–333, Jan. 2014.

[29] G. Delille, B. Francois, and G. Malarange, "Dynamic frequency control support: A virtual inertia provided by distributed energy storage to isolated power systems," in *2010 IEEE PES Innovative Smart Grid Technologies Conference Europe (ISGT Europe)*, 2010, pp. 1–8.

[30] L. Sigrist, E. Lobato, and L. Rouco, "Energy storage systems providing primary reserve and peak shaving in small isolated power systems: An economic assessment," *Int. J. Electr. Power Energy Syst.*, vol. 53, pp. 675–683, 2013.

[31] Y. Wen, W. Li, G. Huang, and X. Liu, "Frequency Dynamics Constrained Unit Commitment With Battery Energy Storage," *IEEE Trans. Power Syst.*, vol. 31, no. 6, pp. 5115–5125, Nov. 2016.

[32] A. Oudalov, D. Chartouni, and C. Ohler, "Optimizing a Battery Energy Storage System for Primary Frequency Control," *IEEE Trans. Power Syst.*, vol. 22, no. 3, pp. 1259–1266, Aug. 2007.

[33] A. Oudalov, R. Cherkaoui, and A. Beguin, "Sizing and Optimal Operation of Battery Energy Storage System for Peak Shaving Application," in *2007 IEEE Lausanne Power Tech*, 2007, pp. 621–625.

[34] G. Merei, C. Berger, and D. U. Sauer, "Optimization of an off-grid hybrid PV–Wind–Diesel system with different battery technologies using genetic algorithm," *Sol. Energy*, vol. 97, pp. 460–473, Nov. 2013.

[35] R. Belfkira, L. Zhang, and G. Barakat, "Optimal sizing study of hybrid wind/PV/diesel power generation unit," *Sol. Energy*, vol. 85, no. 1, pp. 100–110, Jan. 2011.

[36] Y. V. Makarov, P. Du, M. C. W. Kintner-Meyer, C. Jin, and H. F. Illian, "Sizing Energy Storage to Accommodate High Penetration of Variable Energy Resources," *IEEE Trans. Sustain. Energy*, vol. 3, no. 1, pp. 34–40, Jan. 2012.

[37] E. Koutroulis, D. Kolokotsa, A. Potirakis, and K. Kalaitzakis, "Methodology for optimal sizing

of stand-alone photovoltaic/wind-generator systems using genetic algorithms," *Sol. Energy*, vol. 80, no. 9, pp. 1072–1088, Sep. 2006.

[38] K. Baker, G. Hug, and X. Li, "Energy Storage Sizing Taking Into Account Forecast Uncertainties and Receding Horizon Operation," *IEEE Trans. Sustain. Energy*, vol. 8, no. 1, pp. 331–340, Jan. 2017.

[39] IEEE Standards Coordinating Committee 21., IEEE-SA Standards Board., and Institute of Electrical and Electronics Engineers., *IEEE recommended practice for sizing lead-acid batteries for stand-alone photovoltaic (PV) systems*. Institute of Electrical and Electronics Engineers, 2007.

[40] E. D. Hatziargyriou, "Operation and Control of Wind Farms in Non-Interconnected Power Systems,"2011.[Online].Available: http://orbit.dtu.dk/files/5678103/Operation_and_control_of_wind_farms_in_non_interconnected_power_systems.pdf. [Accessed February 16, 2019].

[41] H. Ahmadi and H. Ghasemi, "Security-Constrained Unit Commitment With Linearized System Frequency Limit Constraints," *IEEE Trans. Power Syst.*, vol. 29, no. 4, pp. 1536–1545, Jul. 2014.

[42] F. Teng, V. Trovato, and G. Strbac, "Stochastic Scheduling With Inertia-Dependent Fast Frequency Response Requirements," *IEEE Trans. Power Syst.*, vol. 31, no. 2, pp. 1557–1566, Mar. 2016.

[43] Jae Won Lee, Seung Wan Kim, Yong Hyun Song, Sunkyo Kim, and Yong Tae Yoon, "Economic benefit of energy storage system for frequency regulation," in *2016 IEEE Power and Energy Conference at Illinois (PECI)*, 2016, pp. 1–5.

[44] V. Knap, S. K. Chaudhary, D.-I. Stroe, M. Swierczynski, B.-I. Craciun, and R. Teodorescu, "Sizing of an Energy Storage System for Grid Inertial Response and Primary Frequency Reserve," *IEEE Trans. Power Syst.*, vol. 31, no. 5, pp. 3447–3456, Sep. 2016.

[45] D. M. Greenwood, K. Y. Lim, C. Patsios, P. F. Lyons, Y. S. Lim, and P. C. Taylor, "Frequency response services designed for energy storage," *Appl. Energy*, vol. 203, pp. 115–127, Oct. 2017.

[46] Yen-Yu Lee and R. Baldick, "A frequency-constrained stochastic economic dispatch model," in *2013 IEEE Power & Energy Society General Meeting*, 2013, pp. 1–1.

[47] F. Ceja-Gomez, S. S. Qadri, and F. D. Galiana, "Under-Frequency Load Shedding Via Integer Programming," *IEEE Trans. Power Syst.*, vol. 27, no. 3, pp. 1387–1394, 2012.

[48] Q. Hong *et al.*, "Fast frequency response for effective frequency control in power systems with low inertia," *J. Eng.*, vol. 2019, no. 16, pp. 1696–1702, Mar. 2019.

[49] P. Mercier, R. Cherkaoui, and A. Oudalov, "Optimizing a Battery Energy Storage System for Frequency Control Application in an Isolated Power System," *IEEE Trans. Power Syst.*, vol.

24, no. 3, pp. 1469–1477, Aug. 2009.

[50] C. Abbey and G. Joos, "A Stochastic Optimization Approach to Rating of Energy Storage Systems in Wind-Diesel Isolated Grids," *IEEE Trans. Power Syst.*, vol. 24, no. 1, pp. 418–426, Feb. 2009.

[51] P. Yang and A. Nehorai, "Joint Optimization of Hybrid Energy Storage and Generation Capacity With Renewable Energy," *IEEE Trans. Smart Grid*, vol. 5, no. 4, pp. 1566–1574, 2014.

[52] M. Korpaas, A. T. Holen, and R. Hildrum, "Operation and sizing of energy storage for wind power plants in a market system," *Int. J. Electr. Power Energy Syst.*, vol. 25, no. 8, pp. 599–606, Oct. 2003.

[53] R. S. Garcia and D. Weisser, "A wind–diesel system with hydrogen storage: Joint optimisation of design and dispatch," *Renew. Energy*, vol. 31, no. 14, pp. 2296–2320, 2006.

[54] E. Hajipour, M. Bozorg, and M. Fotuhi-Firuzabad, "Stochastic Capacity Expansion Planning of Remote Microgrids With Wind Farms and Energy Storage," *IEEE Trans. Sustain. Energy*, vol. 6, no. 2, pp. 491–498, Apr. 2015.

[55] R. Billinton and R. Karki, "Capacity expansion of small isolated power systems using PV and wind energy," *IEEE Trans. Power Syst.*, vol. 16, no. 4, pp. 892–897, 2001.

[56] N. Growe-Kuska, H. Heitsch, and W. Romisch, "Scenario reduction and scenario tree construction for power management problems," in *2003 IEEE Bologna Power Tech Conference Proceedings,* vol. 3, pp. 152–158.

[57] H. Heitsch and W. Römisch, "Scenario Reduction Algorithms in Stochastic Programming," *Comput. Optim. Appl.*, vol. 24, no. 2/3, pp. 187–206, 2003.

[58] H. Pranevicius and K. Sutiene, "Scenario tree generation by clustering the simulated data paths," in *Proceedings 21st European Conference on Modelling and Simulation ECMS 2007*, 2007, pp. 203–208.

[59] N. Nguyen-Hong and H. Nguyen-Duc, "Optimal sizing of energy storage devices in wind-diesel systems considering load growth uncertainty," in *2016 IEEE International Conference on Sustainable Energy Technologies (ICSET)*, 2016, pp. 54–59.

[60] X. Ji, S. Zhu, S. Wang, and S. Zhang, "A stochastic linear goal programming approach to multistage portfolio management based on scenario generation via linear programming," *IIE Trans.*, vol. 37, no. 10, pp. 957–969, Oct. 2005.

[61] D. Xu, Z. Chen, and L. Yang, "Scenario tree generation approaches using K-means and LP moment matching methods," *J. Comput. Appl. Math.*, vol. 236, no. 17, pp. 4561–4579, Nov. 2012.

[62] J. van Campenhout and T. Cover, "Maximum entropy and conditional probability," *IEEE Trans. Inf. Theory*, vol. 27, no. 4, pp. 483–489, Jul. 1981.

[63] W. Ximing, "Calculation of maximum entropy densities with application to income distribution," *J. Econom.*, vol. 115, no. 2, pp. 347–354, Aug. 2003.

[64] K. Tanaka and A. A. Toda, "Discrete approximations of continuous distributions by maximum entropy," *Econ. Lett.*, vol. 118, no. 3, pp. 445–450, Mar. 2013.

[65] L. E. Farmer and A. A. Toda, "Discretizing Stochastic Processes with Exact Conditional Moments," *SSRN Electron. J.*, Oct. 2015.

[66] J. Riesz and J. Palermo, "INTERNATIONAL REVIEW OF FREQUENCY CONTROL ADAPTATION," 2016. [Online]. Available: https://www.aemo.com.au/-/media/Files/Electricity/NEM/Security_and_Reliability/Reports/2016/FPSS---International-Review-of-Frequency-Control.pdf. [Accessed January 29, 2019].

[67] "NERC | 2013 Special Reliability Assessment: Performance of Variable Resources During and After System Disturbance | Performance of Distributed Energy Resources During and After System Disturbance Voltage and Frequency Ride-Through Requirements-DRAFT," 2013. [Online]. Available: https://www.nerc.com/comm/PC/Integration of Variable Generation Task Force I1/IVGTF17_PC_FinalDraft_December_clean.pdf. [Accessed January 09, 2019].

[68] E. Orlando *et al.*, "Use of Frequency Response Metrics to Assess the Planning and Operating Requirements for Reliable Integration of Variable Renewable Generation," 2010. [Online]. Available:https://www.ferc.gov/industries/electric/indus-act/reliability/frequencyresponsemetrics-report.pdf. [Accessed January 29, 2019].

[69] "System Operator TASC Report TASC 033 report," 2014. [Online]. Available: https://www.transpower.co.nz/sites/default/files/bulk-upload/documents/TASC 033 report.pdf. [Accessed January 31, 2019].

[70] P. Mancarella *et al.*, "Power system security assessment of the future National Electricity Market,"2017.[Online].Available: https://www.energy.gov.au/sites/default/files/independent-review-future-nem-power-system-security-assessment.pdf. [Accessed January 28, 2019].

[71] "FAST FREQUENCY RESPONSE IN THE NEM," 2017. [Online]. Available: https://www.aemo.com.au/-/media/Files/Electricity/NEM/Security_and_Reliability/Reports/2017/FFR-Working-Paper---Final.pdf. [Accessed January 31, 2019].

[72] P. Kundur, *Power System Stability and Control*. EPRI Power Systems Engineering Series, 1994.

[73] M. H. J. Bollen, *Integration of distributed generation in the power system*. Wiley, 2011.

[74] D. Stenclik, "Integrated Grid Planning Symposium State of IGP Technology," 2017. [Online]. Available:https://www.hawaiianelectric.com/documents/clean_energy_hawaii/integrat

ed_grid_planning/igp_symposium/8_1_derek_stenclik_presented_by_bob_zavadil.pdf. [Accessed January 31, 2019].

[75] D. Lew *et al.*, "Technology Capabilities for Fast Frequency Response," 2017. [Online]. Available:https://www.aemo.com.au/-/media/Files/Electricity/NEM/Security_and_Reliability/Reports/2017/2017-03-10-GE-FFR-Advisory-Report-Final---2017-3-9.pdf. [Accessed January 03, 2019].

[76] "RoCoF Alternative Solutions Technology Assessment High level assessment of frequency measurement and FFR type technologies and the relation with the present status for the reliable detection of high RoCoF events in a adequate time frame," 2015. [Online]. Available: http://www.eirgridgroup.com/site-files/library/EirGrid/RoCoF-Alternative-Solutions-Technology-Assessment-Phase-1-DNV-GL-Report_.pdf. [Accessed January 03, 2019].

[77] P. V. Brogan, R. J. Best, D. J. Morrow, K. McKinley, and M. L. Kubik, "Effect of BESS Response on Frequency and RoCoF During Underfrequency Transients," *IEEE Trans. Power Syst.*, vol. 34, no. 1, pp. 575–583, Jan. 2019.

[78] P. Tielens and D. Van Hertem, "Receding Horizon Control of Wind Power to Provide Frequency Regulation," *IEEE Trans. Power Syst.*, vol. 32, no. 4, pp. 2663–2672, Jul. 2017.

[79] G. Delille, B. Francois, and G. Malarange, "Dynamic Frequency Control Support by Energy Storage to Reduce the Impact of Wind and Solar Generation on Isolated Power System's Inertia," *IEEE Trans. Sustain. Energy*, vol. 3, no. 4, pp. 931–939, Oct. 2012.

[80] M. Cheng, S. S. Sami, and J. Wu, "Benefits of using virtual energy storage system for power system frequency response," *Appl. Energy*, vol. 194, pp. 376–385, May 2017.

[81] H. Chavez, R. Baldick, and S. Sharma, "Governor Rate-Constrained OPF for Primary Frequency Control Adequacy," *IEEE Trans. Power Syst.*, vol. 29, no. 3, pp. 1473–1480, May 2014.

[82] Q. P. Zheng, J. Wang, and A. L. Liu, "Stochastic Optimization for Unit Commitment—A Review," *IEEE Trans. Power Syst.*, vol. 30, no. 4, pp. 1913–1924, Jul. 2015.

[83] M. Tahanan, W. van Ackooij, A. Frangioni, and F. Lacalandra, "Large-scale Unit Commitment under uncertainty," *4OR*, vol. 13, no. 2, pp. 115–171, Jun. 2015.

[84] W. Van Ackooij, "Chance Constrained Programming : with applications in Energy Management." Other. Ecole Centrale Paris, 2013. English. NNT : 2013ECAP0071. tel-00978519.

[85] B. K. Pagnoncelli, · S Ahmed, · A Shapiro, S. Ahmed, and A. Shapiro, "Sample Average Approximation Method for Chance Constrained Programming: Theory and Applications," *J Optim Theory Appl*, vol. 142, pp. 399–416, 2009.

[86] S. Ahmed, A. Shapiro, and H. M. Stewart, "Solving Chance-Constrained Stochastic Programs

via Sampling and Integer Programming," *INFORMS | isbn*, 2008.

[87] Q. Wang, Y. Guan, and J. Wang, "A Chance-Constrained Two-Stage Stochastic Program for Unit Commitment With Uncertain Wind Power Output," *IEEE Trans. Power Syst.*, vol. 27, no. 1, pp. 206–215, Feb. 2012.

[88] C. Zhao, Q. Wang, J. Wang, and Y. Guan, "Expected Value and Chance Constrained Stochastic Unit Commitment Ensuring Wind Power Utilization," *IEEE Trans. Power Syst.*, vol. 29, no. 6, pp. 2696–2705, Nov. 2014.

[89] D. Pozo and J. Contreras, "A Chance-Constrained Unit Commitment With an $n-K$ Security Criterion and Significant Wind Generation," *IEEE Trans. Power Syst.*, vol. 28, no. 3, pp. 2842–2851, Aug. 2013.

[90] I. Egido, F. Fernandez-Bernal, P. Centeno, and L. Rouco, "Maximum Frequency Deviation Calculation in Small Isolated Power Systems," *IEEE Trans. Power Syst.*, vol. 24, no. 4, pp. 1731–1738, Nov. 2009.

[91] J. Lofberg, "YALMIP : a toolbox for modeling and optimization in MATLAB," in *2004 IEEE International Conference on Robotics and Automation (IEEE Cat. No.04CH37508)*, pp. 284–289.

[92] Y. An and B. Zeng, "Exploring the Modeling Capacity of Two-Stage Robust Optimization: Variants of Robust Unit Commitment Model," *IEEE Trans. Power Syst.*, vol. 30, no. 1, pp. 109–122, Jan. 2015.

[93] B. Zeng and L. Zhao, "Solving two-stage robust optimization problems using a column-and-constraint generation method," *Oper. Res. Lett.*, vol. 41, no. 5, pp. 457–461, Sep. 2013.

[94] L. Zhao and B. Zeng, "An Exact Algorithm for Two-stage Robust Optimization with Mixed Integer Recourse Problems," 2012. [Online]. Available: https://pdfs.semanticscholar.org/6b15/8459656b321a0791cc9df4a09af161c8f5e2.pdf. [Accessed February 19, 2019].

[95] M. Tahanan *et al.*, "Large-scale Unit Commitment under uncertainty," *4OR,* vol. 13, pp. 115–171, 2015.

[96] P. Yun, Y. Ren, Y. Xue, "Energy-Storage Optimization Strategy for Reducing Wind Power Fluctuation via Markov Prediction and PSO Method," *Energies*, vol. 11, no. 12, p. 3393, Dec. 2018.

[97] G. M. Kopanos and E. N. Pistikopoulos, "Reactive Scheduling by a Multiparametric Programming Rolling Horizon Framework: A Case of a Network of Combined Heat and Power Units," *Ind. Eng. Chem. Res.*, vol. 53, no. 11, pp. 4366–4386, Mar. 2014.

[98] L. Han *et al.*, "Multi-Time Scale Rolling Economic Dispatch for Wind/Storage Power System Based on Forecast Error Feature Extraction," *Energies*, vol. 11, no. 8, p. 2124, Aug. 2018.

[99] J. Silvente, G. M. Kopanos, E. N. Pistikopoulos, and A. Espuña, "A rolling horizon

optimization framework for the simultaneous energy supply and demand planning in microgrids," *Appl. Energy*, vol. 155, pp. 485–501, Oct. 2015.

[100] S. S. Soman, H. Zareipour, O. Malik, and P. Mandal, "A review of wind power and wind speed forecasting methods with different time horizons," in *North American Power Symposium 2010*, 2010, pp. 1–8.

[101] Y. V Makarov *et al.*, "Wind Energy Management System EMS Integration Project Incorporating Wind Generation and Load Forecast Uncertainties into Power Grid Operations,"2010.[Online].Available: https://www.pnnl.gov/main/publications/external/technical_reports/PNNL-19189.pdf. [Accessed February 03, 2019].

[102] A. Tuohy, E. Denny, and M. O'Malley, "Rolling Unit Commitment for Systems with Significant Installed Wind Capacity," in *2007 IEEE Lausanne Power Tech*, 2007, pp. 1380–1385.

[103] Y. Huo *et al.*, "Optimal Real-Time Scheduling of Wind Integrated Power System Presented with Storage and Wind Forecast Uncertainties," *Energies*, vol. 8, no. 2, pp. 1080–1100, Feb. 2015.

[104] L. Jenkins, "Parametric Mixed Integer Programming: An Application to Solid Waste Management," *Manage. Sci.*, vol. 28, no. 11, pp. 1270–1284, Nov. 1982.

[105] J. A. and and E. N. Pistikopoulos*, "A Multiparametric Programming Approach for Linear Process Engineering Problems under Uncertainty," *Ind. Eng. Chem. Res.*, vol. 36, no. 3, pp. 717–728, Mar. 1997.

[106] M.-S. Chern and R.-H. Jan, "Parametric Programming Applied to Reliability Optimization Problems," *IEEE Trans. Reliab.*, vol. R-34, no. 2, pp. 165–170, Jun. 1985.

[107] F. Borrelli, A. Bemporad, and M. Morari, *Predictive Control for Linear and Hybrid Systems*. Cambridge University Press, 2017.

[108] M. Herceg, M. Kvasnica, C. N. Jones, and M. Morari, "Multi-Parametric Toolbox 3.0," in *2013 European Control Conference (ECC)*, 2013, pp. 502–510.

[109] "Frequency Quality, phase 2," 2017. [Online]. Available: https://www.fingrid.fi/globalassets/dokumentit/fi/yhtio/tki-toiminta/raportit/20170608-fq2-report-v1.2.pdf. [Accessed April 06, 2019].

[110] A. Etxegarai Madina, "Compliance verification methodology for renewable generation integration. Application to island power grids," Ph.D dissertation, University of the Basque Country - Editorial Service (UPV/EHU), Jul. 2015.

[111] E. Robles, M. Haro-Larrode, M. Santos-Mugica, A. Etxegarai, and E. Tedeschi, "Comparative analysis of European grid codes relevant to offshore renewable energy installations," *Renew. Sustain. Energy Rev.*, vol. 102, pp. 171–185, Mar. 2019.

[112] X. Luo *et al.*, "Review of Voltage and Frequency Grid Code Specifications for Electrical Energy Storage Applications," *Energies*, vol. 11, no. 5, p. 1070, Apr. 2018.

[113] G. Jardine, G. Maltabarow, and G. Willis, "Tasmanian Frequency Operating Standard Review,"2008.[Online].Available: https://www.aemc.gov.au/sites/default/files/content/0c7a3cbd-2627-400e-a1b7-e25af8364cd7/Final-Report.pdf. [Accessed April 09, 2019].

[114] P. (Prabha) Kundur, N. J. Balu, and M. G. Lauby, *Power system stability and control*. McGraw-Hill, 1994.

[115] Haibo Bao, H. Wei, and Xiaoxuan Guo, "Stochastic response surface method addressing correlated wind power for probabilistic evaluation of voltage stability," in *2016 IEEE PES Asia-Pacific Power and Energy Engineering Conference (APPEEC)*, 2016, pp. 1660–1664.

[116] Y. Zhou, Y. Li, W. Liu, D. Yu, Z. Li, and J. Liu, "The Stochastic Response Surface Method for Small-Signal Stability Study of Power System With Probabilistic Uncertainties in Correlated Photovoltaic and Loads," *IEEE Trans. Power Syst.*, vol. 32, no. 6, pp. 4551–4559, Nov. 2017.

[117] Y. O-ura, F. Ishiguro, M. Okamura, K. Uemura, and S. Hayashi, "A new power flow model and solution method┤Including load and generator characteristics and effects of system control devices," *IEEE Trans. Power Appar. Syst.*, vol. 94, no. 3, pp. 1042–1050, May 2007.

[118] Y. Duan and B. Zhang, "An improved fast decoupled power flow model considering static power-frequency characteristic of power systems with large-scale wind power," *IEEJ Trans. Electr. Electron. Eng.*, vol. 9, no. 2, pp. 151–157, Mar. 2014.

[119] S. S. Isukapalli, A. Roy, and P. G. Georgopoulos, "Stochastic response surface methods (SRSMs) for uncertainty propagation: application to environmental and biological systems.," *Risk Anal.*, vol. 18, no. 3, pp. 351–63, Jun. 1998.

[120] S. S. Isukapalli, S. Balakrishnan, and P. G. Georgopoulos, "Computationally efficient uncertainty propagation and reduction using the stochastic response surface method," in *2004 43rd IEEE Conference on Decision and Control (CDC) (IEEE Cat. No.04CH37601)*, 2004, p. 2237–2243 Vol.2.

[121] S. S. Isukapalli, "UNCERTAINTY ANALYSIS OF TRANSPORT-TRANSFORMATION MODELS," Ph.D dissertation, Graduate School—New Brunswick Rutgers, The State University of New Jersey,1999.[Online].Available: http://citeseerx.ist.psu.edu/viewdoc/download?doi=10.1.1.473.402&rep=rep1&type=pdf. [Accessed April 12, 2019].

[122] M. A. Pai, *Energy Function Analysis for Power System Stability*, Norwell, MA, USA:Kluwer, 1989.

[123] R. D. Zimmerman, C. E. Murillo-Sanchez, and and R. J. Thomas, "Matpower: Steady State

Operations, Planning and Analysis Tools for Power Systems Research and Education," *IEEE Trans. Power Syst.*, vol. 26, no. 1, 2011.

[124] Ting Dai and Liyan Qu, "Real-time optimal participation of wind power in an electricity market," in *IEEE PES Innovative Smart Grid Technologies*, 2012, pp. 1–6.

# Acknowledgement

Undertaking this Ph.D has been a truly unforgettable experience for me. During this course, I received great support and encouragement from many people. I would like to give many thanks to all of these people.

First of all, I would like to express my deepest appreciation to my supervisor, Professor Nakanishi Yosuke (Waseda University) for all the support and encouragement that he has given me during the PhD course. He is a great teacher with a warm, tolerant heart, who can patiently listen to my bad English and give me the freedom to work and study. He also always told me "if there is anything you need, don't hesitate to ask me", thus helping me feel confident in my work.

I would like to express my sincere thanks to all members in Lab Power System and Environment, Graduate School of Environment and Energy Engineering, Waseda University. Thanks to Mr. Iwamura and Mr. Zhou for talking, sharing experience, and sometimes interesting stories. Thanks to Ms. Hanaoka, she not only supported me all administrative issues but also a great friend of mine. Thanks to all the members of the lab for every help and conversation together. The laboratory has been a source of friendship and collaboration. I also want to thank Mr. Ryo and Mr. Hu Zuo, they were my first friends in Japan and helped me a lot.

I would like to thank my colleagues at the Department of Electrical Systems, School of Electrical Engineering, Hanoi University of Science and Technology for taking over my work, supporting me to study abroad for a long time. They also encouraged me and gave me some advice whenever I have difficulty studying.

I would like to thank Japan International Cooperation Agency (JICA) for financial support (AUN-Seed / Net Scholarship) in the PhD course.

Finally, I would like to say a heartfelt thanks to my family for always encouraging me to follow my dream. Thanks to Dr. Huy Nguyen-Duc, who is my husband, my teacher and my colleague, for teaching me a lot of things. I thank my son, his smile is always my greatest encouragement. I would like to thank my parents and my parents-in-law for their support and help me take care of my son during my stay in Japan. Thanks to my sister for being with me, listening to me whenever I'm stressed, from the Master course to the Ph.D. course. Thank you for everything.